Molecular identification and electrophysiological characterization of the volume-regulated anion channel VRAC

Inaugural-Dissertation to obtain the academic degree
Doctor rerum naturalium (Dr. rer. nat.)

submitted to the Department of Biology, Chemistry and Pharmacy
of Freie Universität Berlin

by
Florian Ullrich
from Jena

2016

This work was prepared from July 1, 2012 to September 16, 2016 under the supervision of Prof. Dr. Dr. Thomas J. Jentsch at the Max-Delbrück-Centrum für Molekulare Medizin (MDC) and the Leibniz-Institut für Molekulare Pharmakologie (FMP) in Berlin.

1st Reviewer: **Prof. Dr. Dr. Thomas J. Jentsch**
Department Physiology and Pathology of Ion Transport
Max-Delbrück-Centrum für Molekulare Medizin (MDC) and Leibniz-Institut für Molekulare Pharmakologie (FMP), Berlin

2nd Reviewer: **Prof. Dr. Stephan J. Sigrist**
Institute of Biology
Department of Biology, Chemistry and Pharmacy
Freie Universität Berlin

Date of defense: January 6, 2017

PREFACE

Part of this work has been published in the following peer-reviewed journal articles:

ULLRICH, F., REINCKE, S.M., VOSS, F.K., STAUBER, T., AND JENTSCH, T.J. (2016). Inactivation and Anion Selectivity of Volume-regulated Anion Channels (VRACs) Depend on C-terminal Residues of the First Extracellular Loop. *J. Biol. Chem.* **291,** 17040–17048. DOI: http://dx.doi.org/10.1074/jbc.M116.739342

VOSS, F.K., ULLRICH, F., MÜNCH, J., LAZAROW, K., LUTTER, D., MAH, N., ANDRADE-NAVARRO, M.A., VON KRIES, J.P., STAUBER, T., AND JENTSCH, T.J. (2014). Identification of LRRC8 heteromers as an essential component of the volume-regulated anion channel VRAC. *Science* **344**, 634–638. DOI: http://dx.doi.org/10.1126/science.1252826

PLANELLS-CASES, R., LUTTER, D., GUYADER, C., GERHARDS, N.M., ULLRICH, F., ELGER, D.A., KUCUKOSMANOGLU, A., XU, G., VOSS, F.K., REINCKE, S.M., STAUBER, T., BLOMEN, V.A., VIS, D.J., WESSELS, L.F., BRUMMELKAMP, T.R., BORST, P., ROTTENBERG, S., AND JENTSCH, T.J. (2015). Subunit composition of VRAC channels determines substrate specificity and cellular resistance to Pt-based anti-cancer drugs. *EMBO J.* **34**, 2993–3008. DOI: http://dx.doi.org/10.15252/embj.201592409

JENTSCH, T.J., LUTTER, D., PLANELLS-CASES, R., ULLRICH, F., AND VOSS, F.K. (2016). VRAC: Molecular identification as LRRC8 heteromers with differential functions (Review). *Pflügers Arch.* **468**, 385–393. DOI: http://dx.doi.org/10.1007/s00424-015-1766-5

Part of the experiments shown in this work was performed in collaboration with or exclusively by Felizia K. Voss, Tobias Stauber, S. Momsen Reincke and Jonas Münch.

Detailed contributions: F.K.V. and T.S. established and conducted the siRNA screen (Figure 7), cloned LRRC8 genes (Table 8), purified and validated LRRC8 antibodies (Table 10), and performed immunostainings and microscopy (Figure 9). Knockout cell lines were generated and validated in collaboration with F.K.V. and T.S. (Figure 10, Tables 4–5 and 7). F.K.V. conducted qRT-PCR experiments (Figure 14, Table 11). F.K.V., T.S. and S.M.R. generated some of the LRRC8 mutants and chimeras. J.M. and S.M.R. contributed to patch clamp experiments. The parts of section 5.2 (Methods) that describe procedures performed exclusively by F.K.V. and T.S. (sections 5.2.1.2, 5.2.1.3, and 5.2.3) are based on Voss et al. (2014) and Voss (2015).

TABLE OF CONTENTS

LIST OF FIGURES

LIST OF TABLES

LIST OF ABBREVIATIONS

ADP	adenosine diphosphate
AE2	Anion exchange protein 2
AMP	adenosine monophosphate
ATP	adenosine triphosphate
AVD	apoptotic volume decrease
BlaS	blasticidin S
bp	base pair
CaCC	Ca^{2+}-activated Cl^- channel
CALHM1	calcium homeostasis modulator 1
CaM	calmodulin
cAMP	cyclic adenosine monophosphate
cDNA	copy DNA, reverse-transcribed mRNA
CFTR	Cystic fibrosis transmembrane conductance regulator
cGMP	cyclic guanosine monophosphate
CRISPR	clustered regularly interspaced short palindromic repeats
cryo-EM	cryo-electron microscopy
C-terminal	carboxy-terminal
DIDS	4,4'-diisothiocyanatostilbene-2,2'-disulfonic acid
DNA	deoxyribonucleic acid
dNTP	deoxyribonucleoside triphosphate
ECL	extracellular loop
ER	endoplasmic reticulum
EST	expressed sequence tag
FLIPR	fluorometric imaging plate reader
GDP	guanosine diphosphate
GMP	guanosine monophosphate
GPCR	G-protein coupled receptor
GTP	guanosine triphosphate
h	hour(s)
HEK293 cells	human embryonic kidney 293 cells
HEPES	4-(2-hydroxyethyl)-1-piperazineethanesulfonic acid
KCC	K^+-Cl^--co-transporter
kDa	kilodalton
LRR	leucine-rich repeat
LRRD	leucine-rich repeat domain
LRRC8	leucine-rich repeat-containing 8
min	minute(s)
NFA	niflumic acid
NKCC	Na^+-K^+-$2Cl^-$-co-transporter
NMDG	N-methyl-D-glucamine
N-terminal	amino-terminal
P	p-value
PBS	phosphate-buffered saline
PCR	polymerase chain reaction

Pt	platinum
qRT-PCR	quantitative real-time PCR
RFP	red fluorescent protein
RNA	ribonucleic acid
RRID	Research Resource Identifier
RT-PCR	reverse transcriptase PCR
RVD	regulatory volume decrease
RVI	regulatory volume increase
SEM	standard error of the mean
SDS	sodium dodecyl sulfate
ss	steady state
TM	transmembrane
VRAC	volume-regulated anion channel
VSOAC	volume-sensitive organic osmolyte/anion channel
VSOR	volume-sensitive outwardly rectifying anion channel
WT	wild type
YFP	yellow fluorescent protein

SI units and SI prefixes are used according to the International System of Units. Nomenclature and symbolism for amino acids and peptides follows the guidelines of the IUPAC-IUB Joint Commission on Biochemical Nomenclature (JCBN): “Nomenclature and symbolism for amino acids and peptides. Recommendations 1983.”

ABSTRACT

The volume-regulated anion channel (VRAC) is ubiquitously expressed in vertebrate cells and is a key component of the cellular volume regulation machinery. The characteristic current mediated by VRAC termed volume-activated chloride current ($I_{Cl,vol}$) has been first described in the late 1980s, but despite several attempts, the underlying protein(s) could not be identified. A large body of work suggests that in addition to its role in volume regulation, VRAC may be important in various other physiological and pathophysiological processes including cell proliferation and migration, apoptosis, gliotransmission, ischemic brain edema and cancer.

A genome-wide siRNA screen identified the plasma membrane protein LRRC8A that is distantly related to pannexins as an essential component of VRAC. Disruption of the *LRRC8A* gene in mammalian cells led to a loss of endogenous $I_{Cl,vol}$. LRRC8A formed heteromers with the four other LRRC8 family proteins LRRC8B-LRRC8E, which required LRRC8A to reach the plasma membrane. Functional VRACs were only detected in the presence of LRRC8A and at least one other LRRC8 isoform. Kinetics of the characteristic voltage-dependent inactivation of $I_{Cl,vol}$ depended on the LRRC8 subunit composition, suggesting that the VRAC pore is formed by LRRC8 heteromers. Regulatory volume decrease (RVD) and swelling-induced efflux of the important cellular osmolyte taurine also required LRRC8 heteromers.

A chimeric approach identified part of the first extracellular loop adjacent to the second transmembrane domain of LRRC8 proteins as a major determinant of the differential inactivation properties. Mutation of two amino acid residues, Lys98 and Asp100 in LRRC8A and equivalent residues in LRRC8C and -E, were found to strongly alter kinetics and steady state extent of $I_{Cl,vol}$ inactivation. Charge reversal of the conserved Lys98 also led to a reduction of the characteristic $I^- > Cl^-$ selectivity that was more pronounced when mutations were introduced into both the obligatory LRRC8A and the co-expressed isoform, thus suggesting that this region contributes to the conduction pathway of VRACs, probably forming the extracellular opening of their pore.

I conclude that LRRC8 heteromers are the pore-forming entities of a distinct new class of ion channels. Our findings pave the way for further research on the physiological and pathophysiological roles and the structure-function relationship of VRACs.

ZUSAMMENFASSUNG

Der Volumen-regulierte Anionenkanal (volume-regulated anion channel, VRAC) ist ubiqitär exprimiert und stellt eine Schlüsselkomponente der zellulären Maschinerie für Volumenregulation dar. Der charakteristische VRAC-vermittelte Strom, genannt Volumen-aktivierter Chloridstrom ($I_{Cl,vol}$), wurde bereits in den späten 1980er Jahren beschrieben. Das zugrundeliegende Protein konnte jedoch bisher nicht identifiziert werden. Zahlreiche Studien deuten darauf hin, dass VRAC neben seiner Rolle in der Volumenregulation ebenfalls bei verschiedenen anderen physiologischen und pathophysiologischen Prozessen von Bedeutung ist, so zum Beispiel bei der Zellproliferation und -migration, Apoptose, Gliotransmission, Schlaganfall und Krebs.

Durch einen genomweiten siRNA-Screen konnte das entfernt mit Pannexinen verwandte Plasmamembranprotein LRRC8A als essentielle Komponente von VRAC identifiziert werden. Deaktivierung des *LRRC8A*-Gens führte zum Verlust des endogenen $I_{Cl,vol}$. LRRC8A bildete Heteromere mit den vier anderen Proteinen der LRRC8-Familie (LRRC8B-LRRC8E), welche LRRC8A benötigten um zur Plasmamembran zu gelangen. VRAC-Funktionalität konnte nur in Gegenwart von LRRC8A und mindestens einer anderen LRRC8-Isoform nachgewiesen werden. Die Kinetik der charakteristischen spannungsabhängigen Inaktivierung von $I_{Cl,vol}$ wurde von der LRRC8-Zusammensetzung bestimmt. Dies legt nahe, dass die VRAC-Pore durch LRRC8-Heteromere gebildet wird. Die regulatorische Zellvolumenreduktion sowie der schwellinduzierte Efflux des wichtigen zellulären Osmolyts Taurin hingen ebenfalls von LRRC8-Heteromeren ab.

Ein chimärischer Ansatz wurde gewählt, um molekulare Determinanten der unterschiedlichen Inaktivierungseigenschaften verschiedener VRACs zu identifizieren. Diese konnten bis auf das C-terminale Drittel des ersten extrazellulären Loops von LRRC8-Proteinen eingegrenzt werden. Die Mutation zweier Aminosäurereste in diesem Bereich, Lys98 und Asp100 in LRRC8A und äquivalente Reste in LRRC8C und -E, führte zu stark veränderter Kinetik und Sättigung der Inaktivierung von $I_{Cl,vol}$. Ladungsumkehrende Mutationen des konservierten Lys98 führten zudem zu einer Verringerung der charakteristischen $I^- > Cl^-$ Selektivität, die größer war wenn Mutationen sowohl in das obligatorische LRRC8A als auch in die koexprimierte LRRC8-Isoform eingeführt wurden. Dies deutet darauf hin, dass dieser Bereich strukturell zur extrazellulären VRAC-Pore beiträgt.

Es wird geschlussfolgert, dass LRRC8-Heteromere die porenbildenden Einheiten einer neuen Klasse von Ionenkanälen sind. Unsere Ergebnisse ebnen den Weg für die weitere Erforschung der physiologischen und pathophysiologischen Rollen sowie der Struktur-Funktionsbeziehung von VRACs.

1. INTRODUCTION

1.1. Mechanisms of cellular volume regulation

Metazoan cells, lacking a rigid cell wall, shrink or swell in response to anisotonic challenges since the lipid bilayer forming the cell membrane is permeable to water, which can therefore follow its concentration gradient. In most cells, dedicated water channels, the aquaporins, further increase water permeability and accelerate cell volume changes (Verkman, 2011).

While the osmolarity of the extracellular fluids in multicellular organisms is generally tightly regulated to prevent excessive volume perturbations, some cells are exposed to extracellular osmotic challenges because of their localization, for example in the kidney medulla or the gastrointestinal tract. Furthermore, pathological states such as cerebral ischemia, diabetes, renal failure, congestive heart failure or hepatic cirrhosis may lead to changes in plasma ion concentrations and osmolarity. Under physiological conditions, cell volume challenges mostly originate from disturbances in intracellular osmolarity. These may arise during processes like epithelial transport, prolonged neuronal activity, or the breakdown of nutrients during metabolism.

Cell volume alterations can be harmful for several reasons. Swelling is considered especially dangerous because it may lead to cell lysis. Bilayers formed from phospholipids typically found in cell membranes can only sustain an expansion of around 3% before rupturing, leaving limited room for volume increase (Nichol and Hutter, 1996). However, cells generally have sufficient amounts of extra plasma membrane in the form of invaginations and intracellular reserves to increase their surface area several-fold in response to hypotonic challenges (Groulx et al., 2006). Thus, bursting is only observed upon extreme swelling. Lesser perturbations of cellular volume can be considered pathological for various other reasons. As the cytosol is crowded with macromolecules, even small changes in cellular water content drastically affect the concentration of cellular constituents, thus altering metabolic processes, protein folding, enzymatic activities and signaling pathways (Ellis, 2001). The cell shape, which is vital for the function of many specialized cell types, may be altered. In swelling cells, the cytoskeleton is mechanically stressed, affecting processes like vesicle trafficking, while shrinkage can disrupt cell-cell contacts. In multicellular organisms, widespread swelling or shrinkage can affect organ size and function as well as tissue integrity. Therefore, mechanisms to rapidly and accurately regulate cellular volume are paramount to the sustainability of all metazoan organisms. Elaborate molecular machineries have evolved to fulfill this task.

The regulatory processes that are activated in response to cell shrinkage or swelling are termed regulatory volume increase (RVI) and regulatory volume decrease (RVD), respectively. Both processes utilize existing concentration gradients for Na^+, K^+, Cl^- and organic osmolytes through the activation of plasma membrane channels and transporters to quickly counteract osmotic imbalances (Hoffmann et al., 2009).

Main players in RVI are Na^+-K^+-$2Cl^-$-co-transporters (NKCCs), Na^+/H^+-exchangers of the NHE family and Na^+-coupled osmolyte transporters (Figure 1). NKCCs use Na^+ and Cl^- concentration gradients to mediate the electroneutral uptake of K^+. The steep Na^+ gradient is also utilized for the uptake of organic substrates such as the physiologically important osmolyte taurine. NHEs mediate further electroneutral shrinkage-stimulated Na^+ influx, while parallel exchange of intracellular HCO_3^- for Cl^- through anion exchangers (AEs) ensures the stability of the cytosolic pH. The osmolytes taken up through these mechanisms are then followed by water, causing an increase in volume (Hoffmann et al., 2009).

As RVD cannot make use of the Na^+ concentration gradient, it relies on the extrusion of KCl and intracellular organic osmolytes which are followed by water, leading to a volume reduction. The main effectors involved are K^+ channels, K^+-Cl^--co-transporters (KCCs) and the volume-regulated anion channel (VRAC, Figure 1). KCCs couple efflux of K^+ along its steep outward concentration gradient to Cl^- extrusion, resulting in a net loss of KCl. Due to the high basal K^+ conductance, K^+ also leaves the cell in an uncoupled manner. However, the K^+ efflux alone is limited since it hyperpolarizes the membrane potential, thereby quickly depleting its driving force. Since hyperpolarization drives chloride extrusion which in turn leads to depolarization, opening of VRAC balances the opposed electrical effects and allows rapid electroneutral loss of KCl. Thus, VRAC is the rate-limiting effector in RVD. In addition to its permeability for anions, VRAC is also thought to conduct small organic molecules like taurine, thereby further contributing to osmolyte extrusion.

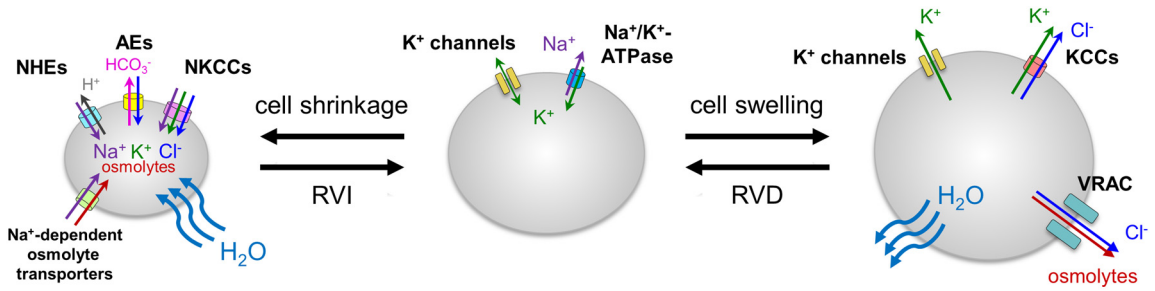

Figure 1 | Schematic overview of effectors in RVI and RVD
See text for details.

1.2. The volume-regulated anion channel VRAC

As discussed before, RVD as a tightly regulated process relies on a swelling-activated Cl^- conductance for electroneutral net loss of KCl. This conductance was first described in the late 1970s and early 1980s using microelectrodes and radioactive flux measurements (Grinstein et al., 1982; Hoffmann, 1978). Shortly after the advent of the patch clamp technique, the corresponding Cl^- currents could first be recorded in T lymphocytes and Intestine 407 cells[1] (Cahalan and Lewis, 1988; Hazama and Okada, 1988). Its ubiquitous expression and easy experimental accessibility led to a surge of interest in this characteristic current, termed $I_{Cl,swell}$ or $I_{Cl,vol}$ for swelling- or volume-activated Cl^- current, in the 1990s. $I_{Cl,vol}$ exhibited very similar properties in diverse cell types, suggesting that it is mediated by a distinct channel type termed VRAC. However, despite major efforts the underlying channel protein(s) could not be identified thus far.

Here, the literature on basic properties of VRAC, including its electrophysiological fingerprint, pharmacology, mechanisms of activation and proposed roles in physiological and pathophysiological processes will be summarized. Furthermore, the long search for proteins underlying VRAC and obstacles on the way to its final identification will be reviewed.

1.2.1. Biophysical properties

Several Cl^- channels have been described to be sensitive to changes in cell volume. These include bestrophins (Fischmeister and Hartzell, 2005) and CLC family channels like ClC-2 (Gründer et al., 1992). Members of the anoctamin/TMEM16 family of Ca^{2+}-activated Cl^- channels have also been referred to as swelling-activated chloride channels by others (Kunzelmann, 2015). Whereas anoctamins may indeed be activated indirectly through a swelling-induced raise in $[Ca^{2+}]_i$, it is important to distinguish them and other swelling-sensitive Cl^- channels from VRAC. The term VRAC strictly refers to the channel mediating $I_{Cl,vol}$, a current defined by characteristics which differ notably from those of currents mediated by other anion channels.

$I_{Cl,vol}$ shows no or only little activity under basal conditions and is slowly activated by hypotonic swelling (Figure 2A-C), decreases in intracellular ionic strength or several isovolumic stimuli which will be discussed in depth in section 1.2.3. Currents mediated by VRAC are weakly outwardly rectifying (Figure 2A,C,D), hence its alternative name volume-sensitive outwardly rectifying (VSOR) anion channel (Akita and Okada, 2014;

[1] It is now known that Intestine 407 cells were actually derived from a HeLa contamination and are thus authentic HeLa cells. There is no evidence that they contain genetic information from any other cell type (Masters, 2002).

Okada, 1997). This is in stark contrast to other anion channels like the inwardly rectifying ClC-2 (Gründer et al., 1992), bestrophins with a linear I-V-relationship (Hartzell et al., 2008) or anoctamins with a steep outward rectification at low $[Ca^{2+}]_i$ and linearity at high $[Ca^{2+}]_i$ (Grubb et al., 2013; Juul et al., 2014; Pifferi et al., 2009; Schroeder et al., 2008).

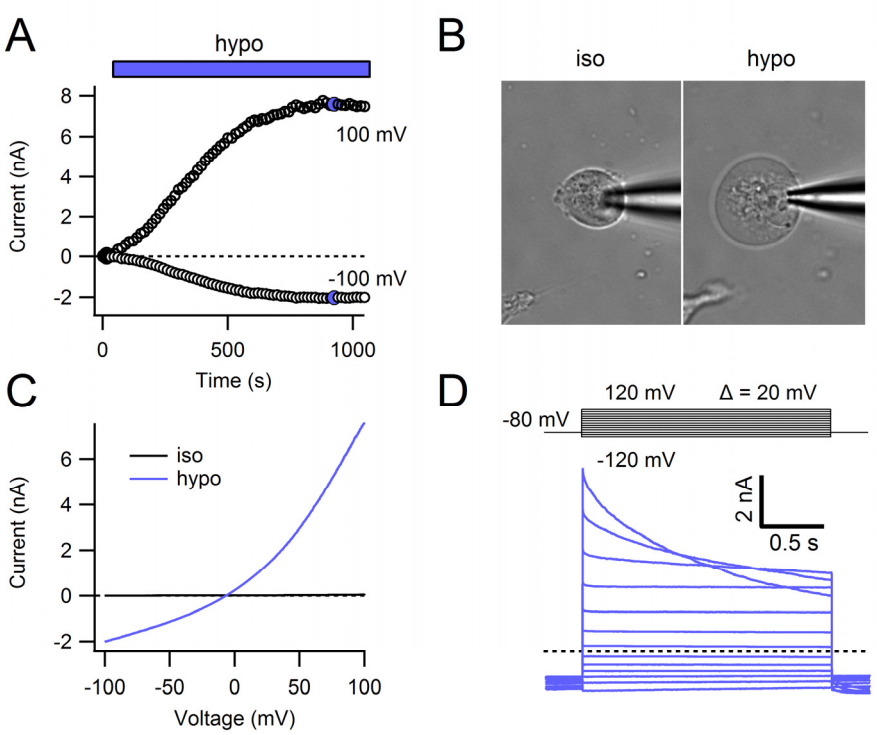

Figure 2 | Properties of the swelling-activated anion current $I_{Cl,vol}$
(A) Time course of the activation of $I_{Cl,vol}$ upon perfusion of a HEK293 cell patched in the whole-cell configuration with hypotonic saline as indicated. Maximal and minimal currents elicited by a 2.6-s voltage ramp from −100 to 100 mV are plotted. **(B)** Activation of $I_{Cl,vol}$ is accompanied by visible cell swelling. **(C)** Ramp currents at the indicated time points in A. Note the mild outward rectification of $I_{Cl,vol}$. **(D)** Currents from the same cell elicited by the voltage protocol shown above. Note the pronounced inactivation at potentials >80 mV. The dashed line indicates zero current.

Another property that is exclusive for VRAC among anion channels is its pronounced inactivation at cytosol-positive potentials (Figure 2D), which will be discussed in more detail in section 1.2.1.2. In contrast, ClC-2, bestrophins and anoctamins do not inactivate (Grubb et al., 2013; Hartzell et al., 2008; Makara et al., 2003; Pifferi et al., 2009; Schroeder et al., 2008). A further characteristic of VRAC is its virtual exclusion of cations and its $I^- > Br^- > Cl^-$ anion selectivity sequence (Okada, 1997), which will be discussed in depth in the next section. While some anion channels, including bestrophins and anoctamins share the characteristic $I^- > Br^- > Cl^-$ selectivity (Hartzell et al., 2008; Huang et al., 2012), others are distinct in this respect: CFTR exhibits $Br^- > Cl^- > I^-$ selectivity and $Cl^- > Br^- > I^-$ selectivity is characteristic for CLC family channels (Jentsch, 2015; Sheppard and Welsh, 1999).

1.2.1.1. Permeation properties

A negligible cation permeability ($P_{Na/K}/P_{Cl} > 0.05$) was found for $I_{Cl,vol}$ in several different cell lines, suggesting that VRAC currents accessible to electrophysiological techniques are carried almost exclusively by anions (Gosling et al., 1995; Kubo and Okada, 1992; Lewis et al., 1993; Meyer and Korbmacher, 1996; Worrell et al., 1989). As determined from shifts in the reversal potential of $I_{Cl,vol}$ upon anion substitution, the permeability sequence among halides is as follows: $I^- > NO_3^- > Br^- > Cl^- > F^-$ (Akita and Okada, 2014; Nilius and Droogmans, 2003; Nilius et al., 1997). Thus, VRAC prefers larger anions over smaller ones. This sequence corresponds to an Eisenmann type I sequence as observed in channels with low affinity binding sites, where the dehydration of ions required for pore entry is the rate-limiting step of permeation (Eisenman, 1961). Such a weak discrimination among halides suggests that VRAC might be permeable for larger anions or even uncharged substrates.

Indeed, VRAC has been proposed to conduct small organic osmolytes known to be released during RVD alongside chloride in many cell types, hence its alternative name VSOAC (volume-stimulated organic osmolyte/anion channel; Strange and Jackson, 1995). Possible substrates include amino acids and their derivatives (e.g., aspartate, glycine, taurine), polyols (e.g., *myo*-inositol) and methylamines (e.g., ethanolamine). Several groups have shown that these substances can leave the cell through a swelling-activated pathway and that time courses and pharmacological profiles of $I_{Cl,vol}$ and the swelling-activated organic osmolyte efflux overlap closely (Hall et al., 1996; Jackson and Strange, 1993; Kirk and Kirk, 1993; Manolopoulos et al., 1997a; Sánchez-Olea et al., 1996). More direct evidence for VRAC conducting organic osmolytes came from bi-ionic selectivity measurements in the whole-cell patch clamp configuration, where significant currents for glycine, gluconate, aspartate, glutamate and anionic taurine could be recorded, yielding relative permeabilities (P_X/P_{Cl}) between 0.1 and 0.6 (Boese et al., 1996a; Jackson and Strange, 1993; Jackson et al., 1996; Kirk and Strange, 1998; Manolopoulos et al., 1997a; Roy, 1995). Other reports, however, presented contradictory findings arguing for an organic osmolyte efflux pathway different from VRAC/VSOAC (Lambert and Hoffmann, 1994; Shennan et al., 1994; Stutzin et al., 1999), igniting a debate that is still ongoing (Hoffmann et al., 2009; Shennan, 2008).

Moreover, there is evidence that VRAC conducts ATP (Blum et al., 2010; Burow et al., 2015; Hisadome et al., 2002; Koyama et al., 2001) and the antioxidative tripeptide glutathione (Sabirov et al., 2013). Bicarbonate (HCO_3^-), physiologically important as part of the pH buffering system in the body, was shown to permeate the channel as well (Nilius et al., 1998; Verdon et al., 1995). Finally, a decrease in water permeability upon pharmacological inhibition of $I_{Cl,vol}$ suggested that VRAC also transports water and may

thus complement aquaporins as the major pathway for physiological water fluxes (Nilius, 2004).

The well described permeability sequence quantitatively deduced from shifts in reversal potentials in bi-ionic measurements (Figure 3A) has been used to estimate the pore size of VRAC (Nilius et al., 1999a). Fitting the P_X/P_{Cl} of a range of different anions (X) permeating VRAC to their Stoke's diameter yielded a pore diameter of 1.1 nm (Figure 3B). Calixarenes, organic cyclic oligomers of distinctive molecular sizes, have been used to further probe the pore diameter and geometry of VRAC. Whereas 4-sulphonic-calix[4]arene permeated VRAC, the slightly larger 4-sulphonic-calix[6]arene only exerted a voltage-dependent blocking effect (Droogmans et al., 1998, 1999). Thus, the VRAC pore was estimated to measure approximately 1.1 x 1.7 nm, compatible with the passage of large substrates such as amino acids or ATP. Another study, using differently sized polyethylene glycols to probe the VRAC pore, arrived at an estimated pore diameter of 1.26 nm (Ternovsky et al., 2004).

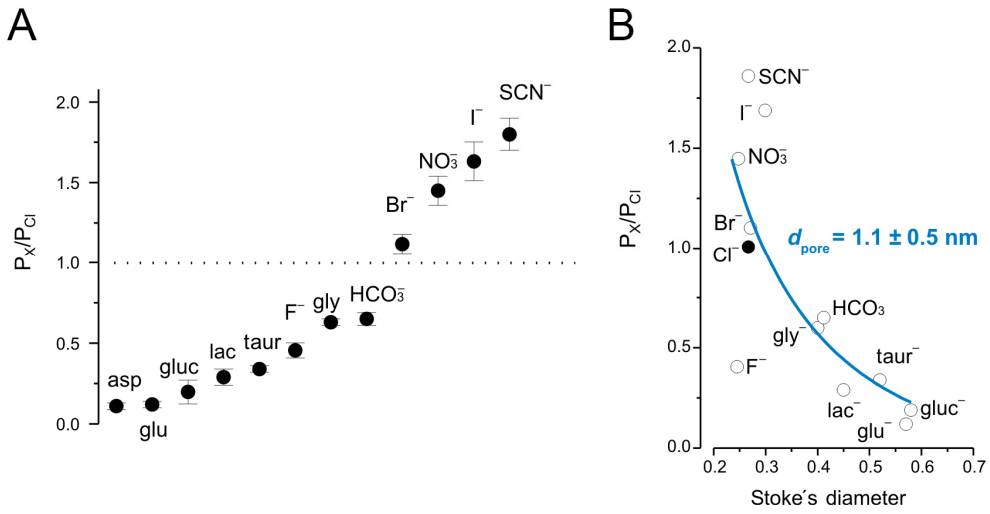

Figure 3 | Permeation properties of VRAC
(A) Permeability ratios calculated from the shifts in E_{rev} upon substitution of Cl^- with the indicated anions (asp, aspartate; glu, glutamate; gluc, gluconate; lact, lactate; taur, taurine; gly, glycine; HCO_3^-, bicarbonate; SCN^-, thiocyanate). **(B)** Stoke's diameters of the anions used for Cl^- substitution plotted against their permeability relative to Cl^-. The diameter of the open VRAC pore was estimated from the excluded volume model (blue line). Figure and caption is modified from Nilius and Droogmans, 2003. For experimental details, also see Nilius et al., 1999a.

1.2.1.2. Voltage-dependent properties

One of the most striking properties of $I_{Cl,vol}$ is its characteristic current inactivation (Akita and Okada, 2014; Nilius et al., 1997; Okada, 1997). At inside-positive potentials above a certain threshold that differs between cell lines and tissues, VRAC currents decrease slowly. More positive voltages accelerate the current decay, which saturates on

a timescale of tens of milliseconds at sufficiently strong depolarizations. Inactivation is not complete but rather saturates at around 10–20% of the initial peak current. However, the remaining current might at least partially differ from $I_{Cl,vol}$ since swelling also activates leak currents that are especially prominent at highly depolarized voltages where inactivation is most pronounced. The time course of inactivation could be fitted by double exponentials in some (Jackson and Strange, 1995a; Voets et al., 1997a), but not all cell types (Voss et al., 2014), suggesting a kinetically complex process. Negative potentials facilitate recovery from inactivation which occurs more rapidly at more hyperpolarized potentials (Nilius et al., 1997; Okada, 1997). Steady state inactivation, a process observed in some voltage-gated channels, has been reported for $I_{Cl,vol}$ (Braun and Schulman, 1996), but was later found to be an artifact caused by insufficient recovery periods in the voltage clamp protocol used (Voets et al., 1997a).

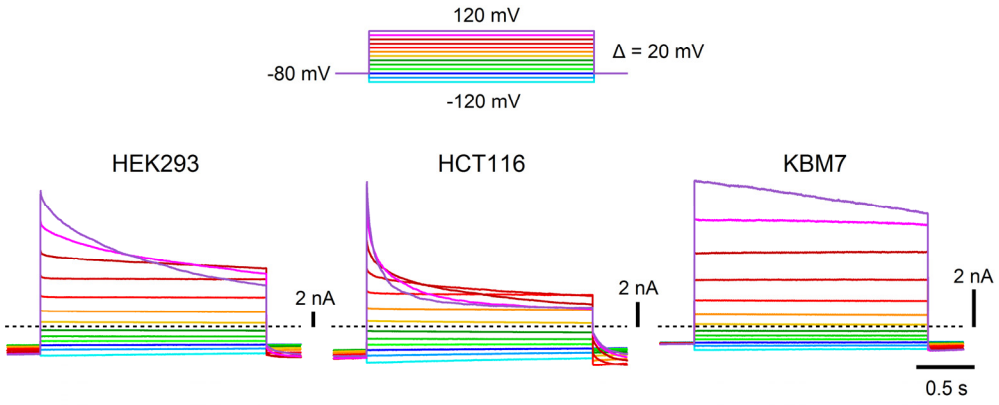

Figure 4 | Voltage-dependent inactivation of $I_{Cl,vol}$
$I_{Cl,vol}$ was evoked in different cell types by hypotonic swelling in the whole-cell patch clamp configuration. Currents in response to the voltage clamp protocol shown above were recorded under identical conditions. The dashed lines indicate zero current. Note the pronounced inactivation in HEK293 and HCT116 cells, which is almost absent in KBM7 cells. KBM7 cells have been classified as non-inactivating in Table 1 since weak inactivation only becomes apparent at 120 mV, a voltage only rarely used in the other reports.

As mentioned before, inactivation can differ drastically when comparing $I_{Cl,vol}$ from different cells types. In Table 1, results from an in-depth review of the literature describing $I_{Cl,vol}$ in different cell lines or tissues are shown. Generally, $I_{Cl,vol}$ inactivation is observed in most cell types. Epithelial cells show pronounced fast inactivation that is often already evident at around 40–50 mV. $I_{Cl,vol}$ of neuronal and endothelial cells also inactivates, albeit with significantly slower kinetics and at more depolarized voltages. Currents from blood cells, skate hepatocytes and some glial cells did not inactivate at voltages up to 100 mV. It has been discussed whether VRAC in these cells is really entirely non-inactivating or if the threshold voltage for inactivation is simply higher

(Okada, 1997). It has to be noted, however, that recording conditions, voltage clamp protocols and factors like cell size, current amplitude, series resistance, space clamp, or the size of confounding background currents may have differed drastically between reports.

Table 1 | $I_{Cl,vol}$ inactivation kinetics in different cell lines and tissues
Inactivation kinetics of $I_{Cl,vol}$ were compared between several studies containing appropriate current traces. Currents were classified as non-inactivating if no inactivation was obvious at voltages ≥80 mV. Only studies using intracellular ATP and permissive intracellular Ca^{2+} concentrations were considered.

Cells	Origin	Type	Inactivation	References
HCT116	human, colon	epithelial	very fast	(Voss et al., 2014)
T_{84}	human, colon	epithelial	very fast	(Worrell et al., 1989)
HeLa	human, cervical cancer	epithelial	fast	(Shimizu et al., 2004)
Intestine 407	human, identical to HeLa	epithelial	fast	(Kubo and Okada, 1992)
HEK293	human, embryonic kidney	epithelial	fast	(Ando-Akatsuka et al., 2002; Hernández-Carballo et al., 2010)
IMCD	rat, inner meduallary collecting duct	epithelial	fast	(Boese et al., 1996b)
ROS 17/2.8	rat, osteosarcoma	osteoblast-like	fast	(Gosling et al., 1995)
C_6 cells	rat, glioma	neuronal	fast	(Solc and Wine, 1991)
cortical neurons	mouse, cortex, primary culture	neuronal	slow	(Inoue and Okada, 2007; Inoue et al., 2005)
hypothalamic neurons	rat, arginine-vasopressin neurons (AVN), primary culture	neuronal	slow	(Sato et al., 2011)
sympathetic neurons	rat, superior cervical ganglia, isolated	neuronal	slow	(Leaney et al., 1997)
parotid acinar cells	rat, parotid glands, dissociated	exocrine	slow	(Arreola et al., 1995)
umbilical vein endothelial cells	human, primary culture	endothelial	slow	(Nilius et al., 1994a)
pulmonary artery endothelial cells	bovine, primary culture	endothelial	very slow	(Szücs et al., 1996a)
artery smooth muscle cells	canine, primary culture	smooth muscle	very slow	(Wang et al., 2004)
astrocytes	mouse, cortical, primary culture	glial	very slow	(Akita and Okada, 2011; Akita et al., 2011; Liu et al., 2009)
microglia	rat, primary culture	glial	absent	(Ducharme et al., 2007; Schlichter et al., 2011)
hepatocytes	skate, primary culture	hepatocyte	absent	(Jackson et al., 1996)
neutrophils	human, primary culture	hematocyte	absent	(Stoddard et al., 1993)
KBM7	human, chronic myelogenous leukemia	hematocyte	absent	(Planells-Cases et al., 2015)
HL-60	human, promyelocytic leukemia	hematocyte	absent	(Hernández-Carballo et al., 2010)
T-lymphocytes	human, primary culture	hematocyte	absent	(Schumacher et al., 1995)
T/B-lymphocytes	mouse, primary culture	hematocyte	absent	(Lewis et al., 1993)

To explain the pronounced differences between reported inactivation kinetics, it has been proposed that VRACs might be composed of distinct isoforms in different cell types (Nilius et al., 1997). Yet, it is also conceivable that $I_{Cl,vol}$ inactivation is completely or partially determined by environmental differences, such as membrane lipid distribution, cytoskeleton integrity or composition of extracellular and intracellular solutions. Indeed, several factors that impact inactivation kinetics have been described.

High concentrations of divalent cations in the extracellular bath solution facilitated inactivation with their efficacy decreasing in the order $Mg^{2+} > Ca^{2+} > Sr^{2+} > Ba^{2+}$ (Anderson et al., 1995; Braun and Schulman, 1996; Voets et al., 1997a). A mechanism has been proposed in which the influx of Cl^- at depolarized potentials forces bivalent cations into a blocking site within the pore (Anderson et al., 1995). However, this seems unlikely as it would require movement of cations against a strong electrochemical gradient (Nilius et al., 1997; Okada, 1997). It was alternatively suggested that bivalent cations may bind to extracellular sites on the channel protein thereby altering its gating properties (Nilius et al., 1997). More acidic extracellular pH also sped up $I_{Cl,vol}$ inactivation as observed in several cell lines (Hernández-Carballo et al., 2010; Jackson and Strange, 1995a; Voets et al., 1997a). Low pH has been proposed to act in a similar fashion as bivalent cations by protonation of extracellular site(s) on VRAC (Hernández-Carballo et al., 2010; Nilius et al., 1997; Voets et al., 1997a).

Another factor influencing $I_{Cl,vol}$ inactivation is the concentration and nature of permeant anions. It has been shown that reduction of extracellular Cl^- accelerates inactivation (Voets et al., 1997a). Furthermore, anion substitution led to a facilitation of inactivation in the case of less permeant anions (gluconate) and a slower inactivation in the case of more permeant anions (SCN^-, I^-, NO_3^-), with the extent of the respective effects closely following the permeability sequence of $I_{Cl,vol}$ for these anions (Voets et al., 1997a). Similar observations have also been made by others (Braun and Schulman, 1996; Hernández-Carballo et al., 2010; Meyer and Korbmacher, 1996). Thus, VRAC seems to be less prone to inactivation the more permeation events take place. This hypothesis is further supported by the effect of channel blockers, many of which accelerate inactivation and shift its voltage-dependence to less positive potentials (Gosling et al., 1995; Kubo and Okada, 1992; Meyer and Korbmacher, 1996; Voets et al., 1997a). However, there are exceptions: ATP, which blocks $I_{Cl,vol}$ in a voltage-dependent manner, almost completely prevented inactivation in the remaining current (Jackson and Strange, 1995a; Tsumura et al., 1996).

In conclusion, multiple factors including pH and the ion composition of intra- and extracellular solutions alter $I_{Cl,vol}$ inactivation. The voltage clamp protocol is also of high importance, as short hyperpolarizing pre-pulses will recover VRACs already inactivated

by prior depolarizations and investigators not using such pre-pulses might severely underestimate inactivation (Gosling et al., 1995). The large dependence of inactivation on experimental parameters is illustrated by an example which Yasunobu Okada described in his 1997 review on VRAC: Several groups have reported very different inactivation kinetics of $I_{Cl,vol}$ in B lymphocytes, yielding threshold voltages of 50 mV (McDonald et al., 1992), 70 mV (Kitano et al., 1992) and 80 mV (Levitan and Garber, 1995), while another group found non-inactivating currents up to 100 mV (Lewis et al., 1993). Thus, care should be taken when considering the results shown in Table 1. Notwithstanding, there are major differences in inactivation kinetics between different cell types that cannot solely be explained by differences in experimental conditions and thus hint at a natural diversity of VRACs.

1.2.1.3. Single channel properties

VRAC single channel recordings have proven difficult for several reasons. First, channels must be activated in sufficient quantity by cell swelling. Several groups have succeeded in recording single VRACs in cell-attached patches made on swollen cells (Jackson and Strange, 1995a; Voets et al., 1997a), but no active channels were detected when cells were not pre-swollen, but swollen after on-cell patches had been established (Akita and Okada, 2014). Furthermore, pre-swelling does not activate VRAC sufficiently to be detected at a high enough frequency in on-cell patches in many cell types, even when VRAC activation in the whole-cell configuration is appreciable (unpublished observation). These problems, together with the poor voltage control in the cell-attached configuration, could be overcome by double-patch recordings, in which a cell is first patched in the whole-cell configuration, swollen and again patched on-cell with a second electrode (Inoue et al., 2005; Okada et al., 1994). The cytosolic composition is clamped via dialysis from the pipette solution and VRAC activation can be confirmed through observation of whole-cell currents. The membrane voltage of the on-cell patch can also be conveniently controlled through the whole-cell patch electrode. Whereas this approach increases the quality of recordings and the probability to observe VRAC activity in a given patch, on-cell patch stability is a major issue. Thus, it is not surprising that only few groups have ever succeeded in performing such recordings.

Another major obstacle that many studies fail to overcome is the convincing confirmation of recorded single channel events as VRAC-dependent. Because the molecular identity of VRAC remained enigmatic, it could neither be overexpressed nor knocked down. Thus, single channel approaches had to rely on endogenous currents which are very prone to contamination by other conductances such as Ca^{2+}-activated Cl^- channels, the maxi-anion channel, or even cation channels. Since VRAC rapidly runs down in excised patches from most cells, it is not well accessible to perfusion techniques

required for the confirmation of the pharmacological profile and ion selectivity of the single channel currents (Akita and Okada, 2014).

Notwithstanding these difficulties, some studies stand out by providing compelling evidence that the presented single channel activities are indeed mediated by VRAC. Jackson and Strange were able to observe a 'flickering block' of single channels in outside-out patches by extracellular ATP at inside-positive potentials, as predicted from the voltage-dependent block it exerted on macroscopic VRAC currents (Jackson and Strange, 1995a). Furthermore, Voets et al., and also Jackson and Strange could show that ensemble currents from several jumps upon steps to inside-positive potentials exhibited similar inactivation kinetics as whole-cell $I_{Cl,vol}$ (Figure 5A), and single channels recovered at inside-negative potentials as is characteristic for VRAC (Figure 5B; Strange and Jackson, 1995; Voets et al., 1997a).

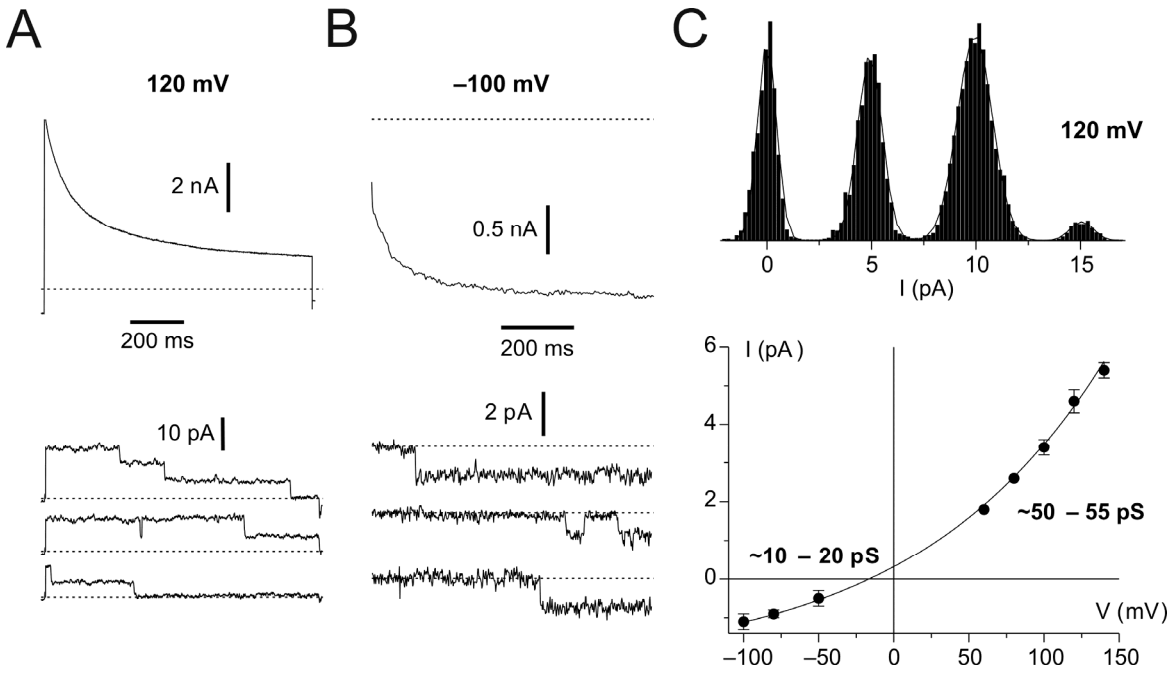

Figure 5 | Single channel properties of VRAC
(A) Swelling-activated currents of a BC_3H1 myoblast cell upon a voltage step from −80 to 120 mV. Dashed lines indicate zero current. Note the inactivation. Bottom traces are single channel currents from an outside-out patch obtained from the same cell using the same voltage protocol **(B)** Current from the same cell as in A, in response to a step from 80 to −100 mV. Bottom traces are corresponding single channel recordings after patch excision. **(C)** Amplitude histograms from single channel openings in an outside-out patch pulled from a swollen cell which was held at −80 mV and stepped to 120 mV. The histogram was fitted by four Gaussian functions. The single channel amplitude was approximately 5 pA. Plotted below is the entire single channel current-voltage relationship from those experiments (BC_3H1 cells). Figure and caption is modified from Nilius and Droogmans, 2003. For experimental details, also see Voets et al., 1997a.

The few high-quality papers on this topic converge on a VRAC single channel conductance of 50–80 pS at positive and 10–20 pS at negative membrane potentials (Jackson and Strange, 1995a; Nilius et al., 1997; Okada et al., 1994; Voets et al., 1997a). This puts the channel in the intermediate conductance range and further distinguishes it from other chloride channels such as bestrophins (2–8 pS, Hartzell et al., 2008), anoctamins (3–4 pS, Adomaviciene et al., 2013), ClCs (<1–40 pS, Jentsch, 2008, 2015), or CFTR (6–10 pS, Sheppard and Welsh, 1999). The rectification of the single channel currents resembles that of the macroscopic currents which implies that the mild voltage-dependence of VRAC is a property of its pore and not the result of a voltage-dependent gating mechanism (Figure 5C). As mentioned above, inactivation and subsequent recovery of single channels was observed for swelling-activated currents by several groups (Jackson and Strange, 1995a; Okada et al., 1994; Voets et al., 1997a). Thus, inactivation of macroscopic VRAC currents seems to reflect a reduction in single channel open probability over time.

The results from direct single channel measurements were further corroborated by non-stationary noise analysis of currents from whole-cell and outside-out patches from C_6 glioma cells, where the unitary conductance was estimated at 55 pS (Jackson and Strange, 1995b). However, stationary noise analysis of the same currents yielded a unitary conductance of just 1 pS. The stationary variation of the noise analysis method relies on the assumption that channel activation occurs in the form of a graded increase in the open probability of a fixed number of channels with a fixed unitary conductance. The authors concluded that this must not be the case for VRAC, hence the severe underestimation of unitary conductance. They rather proposed that VRACs must activate by an increase of the number of active channels with a constantly high open probability (Jackson and Strange, 1995b).

1.2.2. Pharmacological properties

Another attribute frequently used to distinguish $I_{Cl,vol}$ from other currents and to study its physiological role is its characteristic pharmacological profile. However, no specific inhibitor of VRAC is known as of yet, severely hampering these approaches.

One of the more specific agents is the ethacrynic-acid derivative DCPIB (4-(2-butyl-6,7-dichlor-2-cyclopentyl-indan-1-on-5-yl) oxybutyric acid), which potently inhibited $I_{Cl,vol}$ in several cell lines and tissues at low micromolar concentrations, while not affecting other major Cl^- currents (Abdullaev et al., 2006; Akita et al., 2011; Decher et al., 2001; Harrigan et al., 2008; Liu et al., 2009; Schlichter et al., 2011). Yet, blocking effects of DCPIB on connexin hemichannels, the glutamate transporter GLT-1 (Bowens et al., 2013) and the gastric H^+,K^+-ATPase (Fujii et al., 2015) as well as an enhancement of TREK-mediated K^+ currents by DCPIB have been reported (Minieri et al., 2013).

NS3728, an acidic di-aryl urea, was described as a rather potent and specific inhibitor of $I_{Cl,vol}$ (Hélix et al., 2003; Klausen et al., 2007; Pedersen et al., 2015). However, it also inhibited Ca^{2+}-activated chloride currents (Klausen et al., 2007; Sauter et al., 2015).

The natural bisphenol phloretin has also been shown to be relatively selective for VRAC, inhibiting it in epithelial cells, neurons and astrocytes at micromolar concentrations while leaving Ca^{2+}-activated Cl^- currents unaffected (Abdullaev et al., 2006; Fan et al., 2001; Inoue et al., 2005). Yet, phloretin also affects several other transporters, cation channels and aquaporins (Fan et al., 2001).

The steroid derivative carbenoxolone is widely used as an experimental blocker of gap junctions as well as connexin and pannexin hemichannels (Bruzzone et al., 2005; Juszczak and Swiergiel, 2009), but it has also been reported to block $I_{Cl,vol}$ (Akita and Okada, 2014; Benfenati et al.; Ye et al., 2009). Carbenoxolone is also applied clinically for the treatment of gastric ulcers and other types of inflammation since it potently inhibits 11β-hydroxysteroid dehydrogenase, an enzyme involved in glucocorticoid metabolism (Connors, 2012).

Another drug in frequent clinical use that also blocks $I_{Cl,vol}$ is the common antidepressant fluoxetine (also known by the trade name Prozac), a selective serotonin-reuptake inhibitor. It inhibited VRAC in a reversible, pH-dependent manner but was rather unspecific amongst anion channels as it also affected Ca^{2+}-activated Cl^- currents and CFTR (Maertens et al., 1999).

Interestingly, the estrogen receptor agonist/antagonist tamoxifen exerted cell type specific effects (Okada, 1997). On one hand, it produced potent block of $I_{Cl,vol}$ in, amongst others, fibroblasts (Ehring et al., 1994), astrocytes (Abdullaev et al., 2006; Liu et al., 2009), macrophages (Burow et al., 2015), cardiac (Duan et al., 1997a; Vandenberg et al., 1994), endothelial (Nilius et al., 1994b), epithelial (Hélix et al., 2003), kidney collecting duct (Meyer and Korbmacher, 1996), pancreatic duct (Verdon et al., 1995), as well as eye and lens-derived cells (Wu et al., 1996; Zhang and Jacob, 1996; Zhang et al., 1994). On the other hand, no or only little block could be observed in neurons of the central nervous system or neuron-derived cells (Harvey et al., 2010; Inoue and Okada, 2007; Inoue et al., 2005; Zhang et al., 2011). Furthermore, tamoxifen also affected voltage-gated K^+ and Na^+ channels (Dick et al., 2001; Smitherman and Sontheimer, 2001). Tamoxifen, as well as 1,9-dideoxyforskolin, verapamil, nifedipine and quinidine block both, $I_{Cl,vol}$ and P-glycoprotein-mediated drug transport with similar potencies, leading to the proposal of P-glycoprotein as a component of VRAC, which will be discussed further in 1.2.5 (Gill et al., 1992; Mintenig et al., 1993; Valverde et al., 1992, 1993).

VRAC is also inhibited by conventional non-specific anion channel blockers such as DIDS (4,4'-diisothiocyano-2,2'-stilbenedisulfonic acid), DBDS (4,4'-dibenzamido-2,2'-stilbenedisulfonic acid), DNDS (4,4′-diamino-2,2′-stilbenedisulfonic acid), and SITS (4-acetamido-4'-isothio-cyanato-2,2'-stilbenedisulfonic acid), which exert a voltage-dependent block (Jentsch et al., 2002; Nilius et al., 1997; Okada, 1997). Differences in DIDS-sensitivity for $I_{Cl,vol}$ and swelling-induced taurine fluxes have been described (Lambert and Hoffmann, 1994; Pedersen et al., 1998). Other unspecific anion channel inhibitors, including NPPB (5-nitro-2-(3-phenylpropylamino)benzoic acid), IAA-94 (indanyloxy acetic acid 94) and NFA (niflumic acid) gave low-affinity blocking effects that were voltage-independent (Akita and Okada, 2014; Nilius et al., 1997). Notably, NFA can be used at low concentrations (around 100 µM), where it potently inhibits Ca^{2+}-activated Cl^- currents but does not affect $I_{Cl,vol}$, to discern these ubiquitous currents (Abdullaev et al., 2006; Pedersen et al., 1998). Other anion channel or transporter blockers that also affect VRAC are NPA (N-phenylanthracillic acid), DPC (diphenylamine-2-carboxylate), MK-196 (3',5-dichlorodiphenylaminocarboxy acid), gossypol, MK-447 (2-aminomethyl-4-t-butyl-6-iodophenol hydrochloride), and furosemide (Nilius et al., 1997; Okada, 1997).

Extracellular ATP in the Mg^{2+}-free form inhibited $I_{Cl,vol}$ in a voltage-dependent manner (Jackson and Strange, 1995a; Nilius et al., 1994a; Tsumura et al., 1996). Flickering observed in outside-out patches upon ATP addition suggested an open-channel block mechanism (Jackson and Strange, 1995a).

Surprisingly, the alkaloids quinine and quinidine, which have been shown to block K^+ channels (Grinstein and Foskett, 1990) also potently inhibited $I_{Cl,vol}$ in a pH-dependent manner, suggesting that the uncharged form of these compounds is the active one (Voets et al., 1996a).

The polyunsaturated fatty acid arachidonic acid, which is present in part of the phospholipids of cell membranes and also serves as a lipid second messenger, has been found to be a potent blocker of $I_{Cl,vol}$ (Gosling et al., 1996; Kubo and Okada, 1992; Nilius et al., 1994b). Furthermore, inhibitors of enzymes involved in phospholipid breakdown, such as phospholipase A_2 or lipoxygenases have been demonstrated to inhibit VRAC (Fatherazi et al., 1994; Gosling et al., 1996; Nilius et al., 1994a).

1.2.3. Mechanisms of activation and regulation

The mechanism by which VRAC opens in response to hypotonic swelling remains largely enigmatic. A multitude of stimuli, signaling pathways, second messengers and modulators have been found to influence or induce VRAC activation to some extent, the most prominent of which will be discussed in this section. However, only few of these could be convincingly shown to be universally required for $I_{Cl,vol}$. It has to be assumed that many others are either artifacts or cell type specific regulation mechanisms of often

questionable physiological relevance (Akita and Okada, 2014; Pedersen et al., 2015). Generally, VRAC seems to be very sensitive to many kinds of manipulations of the cellular homeostasis, including overexpression of unrelated proteins, activation of growth- or apoptosis-related signaling pathways, changes in the growth substrate or increases in metabolic activity. This sensitivity may have led to the great variety of published mechanisms of activation or regulation of VRAC and the many wrong molecular candidates (see section 1.2.5).

One of the central questions is if VRAC itself is able to sense volume changes or accompanying phenomena or if it relies on an extrinsic sensor which could be coupled to the channel either directly or via a signal transduction cascade. The current knowledge about $I_{Cl,vol}$ activation, which will be outlined in some detail below, is compatible with both mechanisms and further research is required to identify a common activation mechanism for VRAC.

INTRACELLULAR IONIC STRENGTH. The notion of a 'volume regulated' channel has been challenged because it was shown that VRAC can be activated isovolumically by a reduction in intracellular ionic strength (Cannon et al., 1998; Nilius et al., 1998; Sabirov et al., 2000; Voets et al., 1999). $I_{Cl,vol}$ amplitudes and the time course of activation correlated better with ionic strength than with cell volume, and swelling induced by a hypertonic intracellular solution of high ionic strength even inhibited VRAC (Voets et al., 1999). Furthermore, single VRACs could be activated in on-cell patches when cells were permeabilized and ionic strength was subsequently reduced, demonstrating a direct relationship between VRAC gating and intracellular ionic strength (Sabirov et al., 2000). It was thus concluded that VRAC activation is not triggered directly by cell volume changes, but indirectly by the resulting changes in ion concentrations.

MECHANICAL STRETCH OR TENSION. Mechanical activation of VRAC through membrane stretch or shear stress has been discussed (Nilius and Droogmans, 2001; Nilius et al., 1997; Okada, 1997). Notably, $I_{Cl,vol}$ could be induced by application of positive pressure through the patch pipette (Hagiwara et al., 1992; Lewis et al., 1993; Nilius et al., 1994a; Zhang and Jacob, 1997). However, it has been argued that osmotic swelling might not actually induce membrane stretch, as cells have great amounts of membrane invaginations which may unfold during volume increase (Okada, 1997). Direct shear stress activated small Cl^- currents in endothelial cells, but no hallmarks of $I_{Cl,vol}$ were reported for them and sensitivity to low concentrations of niflumic acid rather indicates that they may be mediated by calcium-activated chloride channels (Barakat et al., 1999; Nakao et al., 1999). Another study provided evidence that VRAC is not directly activated by shear stress, but that shear stress enhances VRAC activation induced by osmotic challenges in a biphasic manner (Romanenko et al., 2002).

INTRACELLULAR ATP. Activation of $I_{Cl,vol}$ depends on the presence of intracellular ATP at physiological concentrations (Jackson et al., 1994; Oike et al., 1994; Oiki et al., 1994). Hydrolysis of ATP is probably not required for $I_{Cl,vol}$, since substitution for the non-hydrolysable homologues ATPγS, AMP-PNP and AMP-PCP, as well as ADP and GTP still permitted its activation (Jackson et al., 1994; Oike et al., 1994). The Mg-bound form of ATP, however, was not sufficient for VRAC activation and high intracellular concentrations of free Mg^{2+} inhibited the current, probably by binding to free ATP (Oiki et al., 1994). It has been proposed that the ATP-dependence might prevent the loss of osmolytes through VRAC in energy-deprived cells (Nilius et al., 1997).

AUTOCRINE AND PARACRINE SIGNALING. An early study proposed that cell swelling causes release of ATP and that the subsequent autocrine activation of purinergic P2Y receptors is an obligatory step in the signaling cascade leading to the opening of VRAC (Wang et al., 1996). While such a non-permissive role of ATP release in VRAC activation could not be confirmed (Okada et al., 2001), numerous following studies provided evidence that stimulation of P2Y receptors in astrocytes leads to a limited isovolumic activation of VRAC (Akita et al., 2011; Darby et al., 2003; Mongin and Kimelberg, 2005; Takano et al., 2005). Moreover, signaling through several other G-protein-coupled receptors has been shown to similarly activate astrocytic VRAC (Fisher et al., 2008, 2010; Franco et al., 2008).

INTRACELLULAR CALCIUM AND EXOCYTOSIS. Whereas cell swelling is often accompanied by a rise in $[Ca^{2+}]_i$, $I_{Cl,vol}$ is generally assumed not to be Ca^{2+}-dependent in the classical sense (Kubo and Okada, 1992; Nilius et al., 1994a, 1997; Strange et al., 1996). However, similar to the ATP dependence, full activation of $I_{Cl,vol}$ required permissive Ca^{2+} concentrations in endothelial cells (≥50 nM free Ca^{2+}) while higher concentrations did not affect the current (Nilius et al., 1997; Szücs et al., 1996b). Yet, others reported that $I_{Cl,vol}$ could still be elicited when intracellular Ca^{2+} was chelated by large amounts of BAPTA (1,2-bis(o-aminophenoxy)ethane-N,N,N',N'-tetraacetic acid, Kubo and Okada, 1992). The possible requirement of permissive amounts of Ca^{2+} has been invoked as an argument for a previously proposed mechanism of VRAC activation, in which active channels reside in intracellular vesicles which fuse with the plasma membrane (a Ca^{2+}-dependent process) only upon cell swelling (Jackson and Strange, 1995a; Strange et al., 1996). This would fit to the observation that single channels apparently do not activate through a gradual increase in open probability, but rather an increase in the number of active channels (see section 1.2.1.3). Such a mechanism would require that the membrane capacitance increases during $I_{Cl,vol}$ activation because of the increase in plasma membrane surface upon exocytic insertion of vesicle

membranes. However, no capacitance increase coinciding with $I_{Cl,vol}$ activation has been observed (Graf et al., 1995; Heinke et al., 1997; Ross et al., 1994).

PROTEIN PHOSPHORYLATION. Various reports linked tyrosine phosphorylation upon hypotonic challenges to the activation of VRAC. The tyrosine kinase inhibitors genistein, tyrphostin B46 and tyrphostin A25 prevented VRAC activation (Bryan-Sisneros et al., 2000; Sorota, 1995; Tilly et al., 1993; Voets et al., 1998), while the tyrosine phosphatase inhibitors Na_3VO_4 and dephostatin potentiated it (Tilly et al., 1993; Voets et al., 1998). Swelling also led to an increase in protein tyrosine phosphorylation in cardiac myocytes, which was not blocked by any pharmacological agent except for tyrosine kinase inhibitors (Sadoshima et al., 1996). Since tyrosine phosphorylation was the first detectable reaction to swelling it was hypothesized that it might happen upstream of VRAC activation (Nilius et al., 1997; Sadoshima et al., 1996; Tilly et al., 1993). However, it remains unknown if the target of tyrosine phosphorylation is another upstream regulator or VRAC itself (Nilius and Droogmans, 2003). While it is also not yet clear which tyrosine kinase is specifically responsible for the hypotonicity-induced phosphorylation, evidence has pointed towards the Src family (Lepple-Wienhues et al., 1998).

GTP-BINDING PROTEINS. VRAC could be activated by intracellular GTPγS, a non-hydrolysable GTP analog, even in the absence of cell volume perturbations (Doroshenko, 1991; Doroshenko and Neher, 1992; Mitchell et al., 1997; Nilius et al., 1994a). This suggests a role of GTP binding proteins in the signal transduction leading to $I_{Cl,vol}$ activation. However, no effect of GTPγS was found in several other studies (Ackerman et al., 1994; Botchkin and Matthews, 1993; Strange et al., 1996). Pharmacological inhibition of RhoA, a small Rho family GTPase, and one of its targets, Rho kinase, led to a decrease in $I_{Cl,vol}$ (Nilius et al., 1999b; Pedersen et al., 2002). One of the targets of Rho kinase is the myosin light chain phosphatase. Consistently, interference with myosin light chain phosphorylation also modulated VRAC activation (Nilius et al., 2000). Overexpression of constitutively active forms of proteins involved in Rho signaling, however, did not increase $I_{Cl,vol}$ (Carton et al., 2002). Therefore, it has been inferred that the role of Rho signaling in VRAC activation is permissive at best.

CYTOSKELETON, CAVEOLAE AND INTEGRINS. When VRAC is activated classically via cell swelling, current densities seem to depend on the 'nativity' of cells, and were much higher in cultured cells (Nilius et al., 1997) than in freshly isolated cells and in cells of primary cultures (Nilius et al., 1994a, 1994c; Suh et al., 1999). These observations could hint at an involvement of the cytoskeleton, which is differently arranged in cells within native tissue and which could act as a sensor for the extent of cell shape and volume changes. A role of actin as a stabilizing factor for membrane invaginations, the unfolding

of which might facilitate $I_{Cl,vol}$ activation, has been proposed (Okada, 1997). Pharmacologically induced F-actin depolarization mildly enhanced VRAC's sensitivity to volume changes (Levitan and Garber, 1995; Morishima et al., 2000; Okada, 1997). However, other studies found no or even inhibitory effects of cytoskeletal modifiers on $I_{Cl,vol}$ (Oike et al., 1994; Pedersen et al., 2001). Further investigation of the role of cytoskeleton components pointed to a role of caveolae, distinct membrane domains abundant in endothelial cells and adipocytes with key roles in signal transduction processes and endocytosis (Anderson, 1998). Interference with the binding of annexin II, an actin-membrane-linker protein involved in caveolae formation, to its intracellular ligand p11 resulted in decreased $I_{Cl,vol}$ amplitudes (Nilius et al., 1996). Interestingly, the annexin II-p11 complex also dissociates at very low intracellular Ca^{2+} concentrations at which no VRAC activation occurs, thus pointing to a possible explanation for the low amounts of Ca^{2+} required for $I_{Cl,vol}$ (Nilius et al., 1997). The expression of caveolin 1, a principal scaffold protein of caveolae, also correlated well with $I_{Cl,vol}$ current densities (Trouet et al., 1999). Cancer cell lines lacking caveolin 1 displayed very low $I_{Cl,vol}$ which could be restored to normal levels by transient caveolin 1 overexpression. Furthermore, expression of a dominant-negative caveolin 1 as well as artificial targeting of the c-Src tyrosine kinase to caveolae strongly inhibited VRAC (Trouet et al., 2001a, 2001b). It has thus been hypothesized that VRACs might cluster to caveolae, which could provide a microdomain for their activation (Nilius and Droogmans, 2001). Integrins, adhesion molecules connecting extracellular matrix or cell-cell contacts to intracellular signaling complexes and the cytoskeleton, have also been linked to VRAC activation. A complex signaling pathway involving FAK, Src, EGF receptor, PI3K, Rac, NADPH oxidase and ROS was proposed to couple integrin stretch to the induction of a current partially resembling $I_{Cl,vol}$, but evidence for a general role of such a pathway remains very limited (Browe and Baumgarten, 2003, 2004, 2006). Notably, one of the studies by Browe and Baumgarten also implicated the angiotensin II type 1 receptor (AT1R) as part of the mechanosensory machinery leading to VRAC activation (Browe and Baumgarten, 2004). Indeed, angiotensin-independent activation of AT1R by mechanical stress has been demonstrated (Zou et al., 2004).

MEMBRANE LIPIDS. Membrane cholesterol depletion has been shown to potentiate or even induce $I_{Cl,vol}$ in several cell types (Klausen et al., 2006; Levitan et al., 2000; Romanenko et al., 2004). Cholesterol determines membrane elasticity, which has been implied in the gating of other ion channels (Lundbaek et al., 2004). The finding that incorporation of polyunsaturated fatty acids, which also affect membrane elasticity, increased $I_{Cl,vol}$ is in agreement with a membrane elasticity-modulated gating mechanism (Hoffmann et al., 2009; Lauritzen et al., 1993). However, cholesterol content also

mediates cytoskeletal organization and the modulation of VRAC by cholesterol has been shown to be accompanied by alterations in the organization or membrane attachment of F-actin, linking the observed cholesterol effects to the already discussed role of F-actin in VRAC gating (Byfield et al., 2004, 2006; Klausen et al., 2006).

APOPTOTIC STIMULI. In agreement with the putative role of VRAC in the induction of apoptosis through apoptotic volume decrease (AVD; see section 1.2.4), a chloride current that resembled $I_{Cl,vol}$ in outward rectification, dependence on intracellular ATP and pharmacological profile, has been shown to be activated under isovolumic conditions by several pro-apoptotic stimuli, including staurosporine (Coca-Prados et al., 1995; Okada et al., 2006; Porcelli et al., 2003, 2004; Shimizu et al., 2004), the death receptor ligand TNFα (Nietsch et al., 2000; Schumann et al., 1993; Shimizu et al., 2004), doxorubicin (d'Anglemont de Tassigny et al., 2004) and reactive oxygen species (see below).

REACTIVE OXYGEN SPECIES (ROS). ROS have been found to be produced in response to cell swelling in some but not all cell types (Hoffmann et al., 2009). Several studies suggested a regulatory role of NADPH oxidase-generated ROS in VRAC activation (Akita and Okada, 2011, 2014; Akita et al., 2011; Harrigan et al., 2008; Liu et al., 2009). Extracellular application of H_2O_2 activated $I_{Cl,vol}$ in HTC, HeLa and mesangial cells under isotonic conditions (Jiao et al., 2006; Shimizu et al., 2004; Varela et al., 2004, 2007). Furthermore, there is evidence for a role of NADPH oxidase-generated ROS in apoptotic signaling and subsequent activation of VRAC leading to AVD (Jiao et al., 2006; Okada et al., 2006; Shimizu et al., 2004). As mentioned before, NADPH oxidase-generated ROS were also shown to be involved in integrin stretch-mediated $I_{Cl,vol}$ induction (Browe and Baumgarten, 2004).

1.2.4. Physiological and pathophysiological roles

As the molecular identity of VRAC remained unknown and pharmacological agents targeting the channel are notoriously unspecific, approaches to elucidate its physiological relevance were greatly hindered. VRACs role in cellular volume regulation is well established (Hoffmann et al., 2009; Nilius et al., 1997; Okada, 1997), but it is not known what phenotype cells or even organisms lacking the channel might exhibit. Several other processes have been suggested to involve VRAC and the most prominent of these will be summarized in this section. However, it should be kept in mind that all these hypotheses rely heavily on imperfect pharmacological tools (see section 1.2.2) and will have to pass meticulous tests as soon as the channel is identified. Furthermore, the identification of the protein(s) comprising VRAC will probably lead to the apprehension of further unexpected physiological and pathophysiological roles.

While VRAC probably does not contribute greatly to the resting membrane potential in most cell types because of its low basal activity, small increases in Cl^-

conductance can already cause drastic membrane potential alterations, thereby affecting the excitability of cells and driving forces for membrane transport systems (Nilius et al., 1997). For example, $I_{Cl,vol}$ was shown to modulate action potentials in cultured cardiac cells and may thus contribute to arrhythmia under pathological conditions that affect serum osmolarity (Vandenberg et al., 1994; Zhang et al., 1993). VRAC activation also depolarized chromaffin cells, leading to the opening of voltage-dependent Ca^{2+} channels and subsequent Ca^{2+}-triggered exocytosis (Moser et al., 1995). However, the physiological role of this mechanism is still unclear.

Another interesting hypothesis linking VRAC to membrane excitability concerns the mechanism of insulin secretion by pancreatic islet β-cells upon the elevation of blood glucose levels. The generally accepted process is as follows: Uptake and metabolism of glucose by β-cells causes a rise in the intracellular ATP/ADP ratio, which inhibits K_{ATP} channels, resulting in a membrane depolarization, opening of Ca_V channels, and a subsequent rise in $[Ca^{2+}]_i$, triggering the exocytic release of insulin (Ashcroft and Rorsman, 1989). However, glucose-induced electrical activity has been shown to partially depend on $[Cl^-]_i$ (Best, 2005), and was found to some extent in β-cells lacking functional K_{ATP} channels (Rosário et al., 2008; Szollosi et al., 2007), suggesting the additional contribution of an anion conductance. Pharmacological and biophysical evidence suggested that this conductance is provided by VRAC, which is presumably activated by glucose or its metabolic derivatives in pancreatic β-cells (Best et al., 2010). However, the studies cited by Best and colleagues allegedly reporting glucose-evoked $I_{Cl,vol}$ in β-cells show a $Br^- > Cl^- > I^-$ selectivity (Best et al., 1996; Kinard and Satin, 1995), not compatible with VRAC but rather with the cystic fibrosis transmembrane conductance regulator (CFTR). CFTR is a cAMP/PKA-dependent Cl^- channel gated by intracellular ATP (Aleksandrov et al., 2007), which is expressed in pancreatic islets (Boom et al., 2007), and is thus a good candidate for the anion channel contributing to glucose-induced electrical activity in β-cells. Furthermore, cystic fibrosis patients often develop a special form of diabetes mellitus called cystic fibrosis-related diabetes (Hodson, 1992). Indeed, a recent study found that specific inhibition, knockdown or mutation of CFTR abolished or reduced glucose-elicited currents, Ca^{2+} oscillations and insulin secretion in mouse β-cells (Guo et al., 2014). Future studies have to clarify if VRAC really contributes to insulin secretion as well.

As mentioned earlier, high neuronal activity can cause the accumulation of intracellular Na^+, Cl^- and water, resulting in neuronal swelling (Akita and Okada, 2014; Iwasa et al., 1980). Activity-dependent release of K^+ from neurons further leads to swelling of astrocytes, which maintain low extracellular K^+ through KCl uptake (MacVicar et al., 2002). Thus, regulatory mechanisms for cell volume are of special importance in

the central nervous system. Pharmacological inhibition of $I_{Cl,vol}$ revealed a central role of VRAC in the RVD of neurons, astrocytes and microglia (Akita and Okada, 2014). Mature neurons, whose low intracellular Cl^- concentration does not support Cl^- extrusion as a driver of RVD are thought to rely on the efflux of cellular organic osmolytes such as taurine through VRAC or another volume-sensitive pathway (Akita and Okada, 2014).

In brain injury and ischemia, VRAC is thought to wreak havoc by releasing excitatory amino acids from astrocytes, causing widespread excitotoxic neuronal death (Akita and Okada, 2014). Astrocytes swell strongly and rapidly upon ischemia and traumatic brain injury through mostly unknown mechanisms, resulting in the prolonged activation of $I_{Cl,vol}$ (Kimelberg, 2005; Mongin, 2007). Since VRAC may be permeable to glutamate and aspartate which are present in the cytosol of astrocytes at millimolar concentrations (Danbolt, 2001), these excitatory neurotransmitters could be released upon swelling and evoke continued depolarization in surrounding neurons, resulting in a massive Ca^{2+} influx that causes rapid neuronal death (Liu et al., 2009; Mongin, 2007). Indeed, inhibitors of VRAC such as tamoxifen and DCPIB greatly reduced infarct size and extracellular glutamate concentrations in animal models of ischemic stroke, hinting at possible therapeutic approaches (Feustel et al., 2004; Kimelberg, 2005; Seki et al., 1999; Zhang et al., 2008).

The role of VRAC in the nervous system under physiological conditions, e.g. without severe cell swelling, is less clear. There is accumulating evidence that the channel plays an important role in the intercellular signaling between astrocytes and neurons, also termed gliotransmission. One well-described example where this mechanism is of importance and in which VRAC is possibly involved is osmosensation in magnocellular neurosecretory cells (MNCs) of the supraoptic nucleus (SON) and paraventricular nucleus (PVN) of the hypothalamus. These cells regulate the systemic electrolyte-water balance by secreting the antidiuretic hormones vasopressin and oxytocin in response to systemic osmotic perturbations (Bourque and Oliet, 1997; Hussy et al., 1997). MNCs integrate signals from Na^+- and osmosensitive neurons in the subfornical organ (SFO) and the organum vasculosum lamina terminalis (OVLT), which are in direct contact with the plasma (Bourque and Oliet, 1997). However, MNCs are also intrinsically osmosensitive. Hypertonic shrinking of MNCs themselves activates TRPV1 channels, which leads to increased firing and subsequent hormone secretion (Prager-Khoutorsky et al., 2014; Sharif Naeini et al., 2006). The excitability of MNCs is in turn dampened by surrounding astrocytes. In response to hypotonic swelling these cells release taurine which activates inhibitory glycine receptors on MNCs and thus suppresses hormone secretion (Hussy et al., 1997). The swelling-induced taurine efflux from SON astrocytes was blocked by several rather unspecific inhibitors of $I_{Cl,vol}$ such as

DIDS, NPPB and niflumic acid (Brès et al., 2000; Deleuze et al., 1998), but was completely insensitive to tamoxifen (Brès et al., 2000), which was shown to block $I_{Cl,vol}$ in astrocytes (Abdullaev et al., 2006; Liu et al., 2009, also see section 1.2.2).

While it remains to be clarified whether VRAC is indeed the efflux pathway for taurine from SON astrocytes, this example illustrates an attractive hypothesis for the role of the channel in gliotransmission that might not be limited to taurine as substrate and swelling as the activating stimulus. Because VRAC may also conduct other potent neurotransmitters such as glutamate, a broader role of the channel in neuron-astrocyte communication is feasible. Interestingly, as of yet unidentified plasma membrane channels have been proposed as conduits for the release of several signaling molecules from astrocytes in addition to the extensively studied vesicular pathway (Verkhratsky et al., 2016). One conceptual problem is that hypotonic stimuli sufficient for the activation of VRAC may not occur in healthy neuronal tissue and therefore, gliotransmitter release through it might be of limited physiological relevance. However, autocrine activation of VRAC, for example by P2Y-mediated purinergic signaling (see section 1.2.3) has been demonstrated in astrocytes (Mongin and Kimelberg, 2005) and may be sufficient to establish an appreciable neurotransmitter conductance also under isotonic conditions.

As discussed in section 1.2.1.1, several studies reported that ATP may also permeate VRAC. The channel may therefore contribute to non-vesicular ATP release, which serves as an important signal in processes such as inflammation (Idzko et al., 2014), phagocytosis of apoptotic cells (Elliott et al., 2009), neurotransmission and neuromodulation (Burnstock, 2008), or regulation of blood vessel tone (Lohman et al., 2012). While pannexins and connexin hemichannels are widely accepted as major pathways for non-vesicular ATP release (Idzko et al., 2014; Lohman and Isakson, 2014) and maxi-anion channel(s) have been discussed as another conduit for nucleotide and neurotransmitter release (Sabirov et al., 2016), the overlapping pharmacological profiles of these channels with VRAC have made it difficult to assess the specific physiological roles of each of them.

Since two daughter cells of similar size as the parent cell are produced during cell division, proliferation generally requires an increase in cell volume (Hoffmann et al., 2009; Lang et al., 2007). Cell proliferation was found to be stimulated by swelling and inhibited by shrinkage (Burg, 2002; Dubois and Rouzaire-Dubois, 2004; Lang et al., 2000; Rouzaire-Dubois et al., 2005). Progression through cell cycle phases correlated with orchestrated cell volume changes in different cell types (Habela and Sontheimer, 2007; Michea et al., 2000; Pendergrass et al., 1991). Considering the important role of VRAC in cell volume regulation, it is therefore not surprising that blockers of $I_{Cl,vol}$ also inhibited cell proliferation at similar concentrations (Chen et al., 2007; Klausen et al.,

2007; Pappas and Ritchie, 1998; Rouzaire-Dubois et al., 2000; Shen et al., 2000; Voets et al., 1995; Wondergem et al., 2001). $I_{Cl,vol}$ amplitudes differed throughout the cell cycle (Doroshenko et al., 2001; Klausen et al., 2007; Shen et al., 2000; Varela et al., 2004) and switching from proliferation to differentiation led to downregulation of VRAC currents in myoblasts, which may explain the different $I_{Cl,vol}$ current densities observed in cultured and freshly isolated cells (Manolopoulos et al., 1997b; Voets et al., 1997b). In line with a stimulatory effect of VRAC activation in cell proliferation, VRAC inhibition also curbed angiogenesis in different model systems (Manolopoulos et al., 2000; Nilius and Droogmans, 2001; Ziegelhoeffer et al., 2003).

Cell motility has been shown to at least partially depend on localized cell volume changes (Schwab et al., 2012). Since cell migration is important for tumor metastasis, specific interference with this process may be beneficial for the containment of malignant carcinoma. Indeed, several inhibitors of $I_{Cl,vol}$ also suppressed migration and tissue invasion of glioma and nasopharyngeal carcinoma cells (Mao et al., 2007; Ransom et al., 2001; Soroceanu et al., 1999). Fibroblasts expressing the H-*ras* oncogene exhibited increased migratory activity that was accompanied by $I_{Cl,vol}$ upregulation, inhibition of which in turn decreased migration (Schneider et al., 2008).

One hallmark of apoptosis is an initial isosmotic shrinkage of the cell, a process termed apoptotic volume decrease (AVD) that is thought to be one of the earliest triggers for the induction of the apoptotic cascade through as of yet unknown mechanisms (Maeno et al., 2000; Poulsen et al., 2010; Shimizu et al., 2008). Since AVD, like RVD, is the result of cellular KCl and organic osmolyte loss, VRAC is thought to play a major role in this process (Bortner and Cidlowski, 1998; Lang et al., 2007; Okada and Maeno, 2001). Indeed, cell shrinkage and induction of apoptosis could be inhibited by typical $I_{Cl,vol}$ blockers in several cell types (d'Anglemont de Tassigny et al., 2004, 2008; Ise et al., 2005; Okada et al., 2006; Poulsen et al., 2010). Conversely, $I_{Cl,vol}$ and AVD were induced under isovolumic conditions by pro-apoptotic stimuli activating intrinsic mitochondrion-mediated and extrinsic death receptor-mediated apoptotic pathways (see section 1.2.2, Okada et al., 2006; Shimizu et al., 2004). VRAC's involvement in apoptosis seems paradoxical when considering a possible role in cancer: On one hand, VRAC activation is pro-apoptotic and cancer cells should downregulate the channel to evade cell death; on the other hand it stimulates proliferation and migration and thus should be upregulated. However, while proliferation and migration can be stimulated by a specific, short-term or localized activation of VRAC, induction of apoptosis requires a long-term increase in $I_{Cl,vol}$ (Pedersen et al., 2013). Thus, cancer cells may decrease overall VRAC expression to protect themselves from apoptosis, while still permitting $I_{Cl,vol}$ activation in a time- or space-limited fashion to promote cell cycle progression and cell migration.

Indeed, $I_{Cl,vol}$ was decreased in several cancer cell types (Ise et al., 2005; Lee et al., 2007; Lehen'kyi et al., 2011; Min et al., 2011; Poulsen et al., 2010).

The drug resistance developed by some cancer cells, specifically to the major anti-cancer drug cisplatin, has also been linked to VRAC (Poulsen et al., 2010). Like with other pro-apoptotic drugs, apoptosis induction by cisplatin has been shown to depend on VRAC and AVD (Lee et al., 2007; Poulsen et al., 2010). Cisplatin slowly induced cell shrinkage and currents resembling $I_{Cl,vol}$ (Cai et al., 2015; Ise et al., 2005; Min et al., 2011), and inhibition of VRAC rendered cells resistant to cisplatin treatment (Poulsen et al., 2010). Interestingly, $I_{Cl,vol}$ and cisplatin sensitivity could be restored simultaneously in the tumor cell line KCP-4 by treatment with histone deacetylase inhibitors, suggesting an epigenetic downregulation of VRAC in these cells (Lee et al., 2007). It has to be noted that apoptosis is not the major mechanism by which cisplatin kills cancer cells (Borst et al., 2001). It is, however, induced at very high cisplatin concentrations not reached in clinical settings through cytosolic off-target effects (Berndtsson et al., 2007; Fayad et al., 2009). Therefore, the use of very high cisplatin concentrations in some of the studies cited above warrants some caution.

1.2.5. Attempts at the molecular identification of VRAC

Several factors have severely hampered conventional approaches to identify the molecular entities underlying $I_{Cl,vol}$. Most importantly, VRAC is ubiquitously expressed in all vertebrate cells, including *Xenopus* oocytes, which have been a principle tool to clone and study ion channels in the past (Dascal, 1987). Thus, no expression system with a $I_{Cl,vol}$-free background was available; a problem that was further exacerbated by other confounding background currents such as Ca^{2+}-activated Cl^- currents which are similarly found in many cell types including oocytes (Nilius et al., 1997). Furthermore, it turned out that endogenous anion currents are rather sensitive to the overexpression of unrelated proteins (Buyse et al., 1997; Tzounopoulos et al., 1995). High-affinity blockers or ligands have been used in the past to biochemically purify ion channel proteins (Noda et al., 1984). However, no blocker with a high enough specificity and affinity is known for VRAC (see section 1.2.2). The promiscuity of VRAC regarding pharmacological alterations is paralleled by the many factors claimed to be involved in its activation (see section 1.2.3), which might limit $I_{Cl,vol}$ current amplitudes to endogenous levels. Conversely, depletion of factors involved in the activation of VRAC may reduce $I_{Cl,vol}$ without affecting the channel itself. Another possible issue was the heterogeneity in certain characteristics of $I_{Cl,vol}$ (e.g. inactivation, organic osmolyte permeability) that hinted at the involvement of different tissue-specific proteins or even a heteromeric channel with functionally redundant subunits. Despite these obstacles, many efforts have produced a number of molecular

candidates, all of which turned out to be wrong. The most prominent of these previous candidates will be briefly discussed in this section.

The Band 3 anion exchanger protein (AE1) was suggested to mediate volume activated taurine fluxes in skate erythrocytes based on pharmacological evidence (Goldstein and Brill, 1991; Goldstein et al., 1990). Expression of trout AE1, but not of the mouse orthologue, in *Xenopus* oocytes led to Cl^- currents and taurine transport, not compatible with a role of the mammalian transporter as VRAC (Fiévet et al., 1995). AE1 was finally discarded as a candidate after it was found that cells completely lacking anion exchange activity still displayed $I_{Cl,vol}$ (Sánchez-Olea et al., 1995).

Overexpression of the ABC membrane transporter family protein P-glycoprotein encoded by the *MDR1* gene in mammalian cells led to volume-sensitive Cl^- currents that were absent in control cells (Gill et al., 1992; Valverde et al., 1992). However, P-glycoprotein expression did not correlate with $I_{Cl,vol}$ in several cell types (De Greef et al., 1995a, 1995b; Tominaga et al., 1995), and expression in *Xenopus* oocytes did not lead to enhanced swelling-activated chloride currents (Morin et al., 1995).

Expression cloning identified pI_{Cln}, a small ubiquitously expressed protein, that induces a current termed I_{Cln} in *Xenopus* oocytes (Paulmichl et al., 1992). I_{Cln} resembled $I_{Cl,vol}$ in outward rectification, $I^- > Cl^-$ selectivity, inactivation and block by extracellular nucleotides. Mutations in pI_{Cln} abolished the nucleotide sensitivity and drastically altered I_{Cln} gating. It was therefore proposed that pI_{Cln} forms plasma membrane channels that also mediate $I_{Cl,vol}$ (Paulmichl et al., 1992, 1993). Yet, the highly acidic pI_{Cln} lacks sufficiently long hydrophobic regions to span a lipid bilayer and was subsequently found to localize to the cytosol (Buyse et al., 1997; Krapivinsky et al., 1994). Furthermore, the current elicited by pI_{Cln} expression differed from $I_{Cl,vol}$ in several respects, including its insensitivity to swelling and presence in defolliculated *Xenopus* oocytes (Voets et al., 1996b). Strikingly, a current identical to I_{Cln} was found in oocytes expressing ClC-6, a protein unrelated to pI_{Cln}, and even in a small fraction of uninjected control oocytes (Buyse et al., 1997). This rather suggested that I_{Cln} is mediated by an anion channel endogenous to *Xenopus* oocytes that can be activated by overexpression of different exogenous proteins. Later, pI_{Cln} was shown to be a chaperone that regulates the assembly of spliceosomal small nuclear ribonucleoproteins, ending its short tenure as a molecular candidate for VRAC (Chari et al., 2008; Pu et al., 1999).

ClC-2, a member of the CLC family of chloride channels and transporters, forms a plasma membrane channel, is ubiquitously expressed and sensitive to cell volume changes (Gründer et al., 1992; Thiemann et al., 1992). It was briefly discussed as a molecular candidate for VRAC, but never seriously considered given the drastically different biophysical characteristics of ClC-2-mediated currents and $I_{Cl,vol}$ (see section

1.2.1; Nilius et al., 1997). Another member of the CLC family, ClC-3, was also proposed to embody VRAC. ClC-3 is rather broadly expressed and gave rise to a time- and voltage-independent anion conductance when expressed in *Xenopus* oocytes or in CHO cells (Kawasaki et al., 1994, 1995). The current exhibited $I^- > Cl^-$ selectivity and was blocked by DIDS, cytosolic Ca^{2+}, and PKC activation. However, these findings were quickly met with skepticism as others were unable to record currents induced by ClC-3 in *Xenopus* oocytes and mammalian cells (Borsani et al., 1995; Friedrich et al., 1999; Jentsch et al., 1995; Steinmeyer et al., 1995; Weylandt et al., 2001). In another study, stable expression of ClC-3 in fibroblasts led to a current resembling $I_{Cl,vol}$ in several characteristics such as outward rectification, $I^- > Cl^-$ selectivity, pharmacological profile and modulation by cell volume (Duan et al., 1997b). Furthermore, Duan et al. could demonstrate that mutations in ClC-3 alter gating behavior and halide selectivity of the elicited current, posing strong evidence for ClC-3 forming the observed anion channel. On the other hand, the current was already pronounced under isotonic conditions, only modestly altered by cell swelling, and was potently inhibited by PKC activation, properties not observed for $I_{Cl,vol}$ (Miwa et al., 1997; Nilius et al., 1994a, 1997; Szücs et al., 1996c). The ClC-3 hypothesis was eventually rejected when several groups reported unchanged $I_{Cl,vol}$ in many different cell types from ClC-3 knockout mice and ClC-3 was found to localize to intracellular organelles (Arreola et al., 2002; Gong et al., 2004; Stobrawa et al., 2001). Today it is largely accepted that ClC-3 is not a plasma membrane channel but an intracellular Cl^-/H^+-exchanger (Guzman et al., 2013; Jentsch, 2008, 2015). The true nature of the current induced by ClC-3 remains puzzling. As for pI_{Cln}, an increase of endogenous anion currents by ClC-3 overexpression has been proposed as a possible explanation (Jentsch et al., 2002).

Bestrophins are a family of Ca^{2+}-activated Cl^- channels that has been identified in relation to vitelliform macular dystrophy (VMD or Best disease), a condition leading to progressive loss of central vision (Qu et al., 2003; Sun et al., 2002; Tsunenari et al., 2003). Currents mediated by bestrophins were shown to be sensitive to osmolarity changes and it was proposed that they contribute to cell volume regulation in retinal pigmented epithelium cells (Fischmeister and Hartzell, 2005). Intriguingly, the *Drosophila* orthologues of bestrophin also mediate Ca^{2+}-activated Cl^- currents in *Drosophila* S2 cells (Chien et al., 2006). Currents mediated by dBest1 are activated by cell swelling and are crucial for cellular volume regulation (Chien and Hartzell, 2007; Stotz and Clapham, 2012). Thus, bestrophins probably form the channel mediating a current functionally similar to $I_{Cl,vol}$ in insect cells. However, $I_{Cl,vol}$ was unaffected in cells from bestrophin 1/2 double knockout mice (Chien and Hartzell, 2008) and mammalian bestrophins differ from VRAC in biophysical properties (see section 1.2.1), tissue distribution and

pharmacological sensitivity (Hartzell et al., 2008). Thus, while bestrophins may contribute to cell volume regulation under certain conditions, for example in human retinal pigmented epithelium cells (Kunzelmann, 2015; Milenkovic et al., 2015), they are not the classical vertebrate VRAC.

Members of the TMEM16/anoctamin family were also discussed as VRAC candidates. The extent of $I_{Cl,vol}$ activation and RVD have been shown to be modulated by the expression of several different anoctamins, including TMEM16F (Almaça et al., 2009). Furthermore, $I_{Cl,vol}$ was reduced in colonic epithelium and in salivary acinar cells from TMEM16A knockout mice (Almaça et al., 2009). Thus far, the only anoctamins convincingly shown to form Ca^{2+}-activated Cl^- channels are TMEM16A and TMEM16B. However, currents mediated by these differ drastically from $I_{Cl,vol}$ in biophysical properties like rectification, unitary conductance, inactivation and Ca^{2+}-dependence (Hoffmann et al., 2015; section 1.2.1; Pedemonte and Galietta, 2014). Also, the VRAC inhibitors DCPIB and NS3728 did not affect Ca^{2+}-activated Cl^- currents (Harrigan et al., 2008; Hélix et al., 2003), and TMEM16A inhibitors $T16_{inh}$-A01 and $CaCC_{inh}$-A01 did not block $I_{Cl,vol}$ (De La Fuente et al., 2008; Namkung et al., 2011). Earlier findings suggesting a role of TMEM16F in $I_{Cl,vol}$ activation and RVD were contradicted by other studies which reported no such effect (Juul et al., 2014; Shimizu et al., 2013). Finally, TMEM16F has been shown to be an ATP-independent phospholipid scramblase (Suzuki et al., 2010; Yang et al., 2012) and the nonselective currents found in cells overexpressing this protein have been attributed to a leak pathway formed during phospholipid translocation (Yu et al., 2015).

1.3. The LRRC8 protein family

Since leucine-rich repeat-containing 8 (LRRC8) proteins will be shown to be essential components of VRAC in the results section of this thesis, the pre-existing literature on them will be summarized here. The LRRC8 family comprises 5 paralogues in vertebrates, LRRC8A, LRRC8B, LRRC8C, LRRC8D and LRRC8E. All LRRC8 proteins are thought to contain 4 transmembrane (TM) domains in the N-terminal half and a leucine-rich repeat domain (LRRD) with up to 17 leucine-rich repeats (LRRs) in the C-terminal half (Kubota et al., 2004; Smits and Kajava, 2004).

The eponymous LRRs are polypeptide motifs of 20 to 29 amino acids defined by the consensus sequence **LxxLxLxx(N/C)xL** with **x** = any amino acid; and **L** = leucine, valine, isoleucine or phenylalanine (Kobe and Kajava, 2001). A multitude of proteins with diverse functions and subcellular locations are known to contain tandem arrays of LRRs, so-called LRRDs (Kobe and Deisenhofer, 1994), which are thought to act as motifs mediating protein-protein recognition and binding (Kobe and Kajava, 2001). Crystal

structures of LRR-containing proteins demonstrated the three-dimensional assembly of LRRDs, in which each LRR corresponds to a structural unit. Every unit consists of a β strand and an α helix connected by loops (Kobe and Deisenhofer, 1993). Multiple units arrange in a way that all strands and helices are parallel to a common axis, forming a horseshoe-shaped curved domain (thus called α/β horseshoe fold; Enkhbayar et al., 2004) in which the parallel β sheets line the inner circumference and the helices flank the outer circumference of the horseshoe (Kobe and Kajava, 2001). The concave face and the adjacent loops of this structure form the major surfaces on LRRDs involved in protein-protein interactions (Kobe and Deisenhofer, 1993, 1995; Papageorgiou et al., 1997). An extracellular localization of the LRRD-containing C-terminus of the plasma membrane-localized LRRC8s has been proposed (Sawada et al., 2003). This topology would be compatible with LRRC8s mediating intercellular protein-protein interactions. Indeed, most other LRRD-containing receptors, including Toll-like receptors and several hormone receptors have extracellular LRRDs (Dolan et al., 2007; Gay et al., 2014).

After they had been first described in 2003 (Sawada et al., 2003), further research on LRRC8 proteins was limited and their biology remained poorly understood. A recent bioinformatics study revisited the LRRC8 family, coming to several surprising but well-supported conclusions (Abascal and Zardoya, 2012). Sequence comparison showed that the N-terminal TM domain of LRRC8 proteins was likely derived from pannexins, a class of channel forming plasma membrane proteins structurally related to the gap junction forming connexins. Indeed, pannexins and LRRC8s share well-conserved sequences and structural motifs in this domain. By analyzing online databases, Abascal and Zardoya could also show that the loops connecting the TM domains in LRRC8s contain several posttranslational modifications, including glycosylation, phosphorylation, ubiquitination and acetylation, the distribution of which was only compatible with a pannexin-like topology (Figure 6A).

These findings were further corroborated by results from several TM topology prediction algorithms and cell surface proteome database entries of peptides found in the TM1–2 and TM3–4 loops of LRRC8A and LRRC8D. Furthermore, four cysteines that form stabilizing disulfide bridges in the extracellular loops of gap-junction proteins (innexins/pannexins and connexins) were also found to be conserved in LRRC8s (Abascal and Zardoya, 2012). The strong support for the pannexin-like topology of LRRC8s and the high degree of conservation of the TM domains between pannexins and LRRC8s led Abascal and Zardoya to propose that LRRC8s might, like pannexins and connexins, form hexameric channel complexes. Indeed, the volume of the LRRCDs of LRRC8 proteins would be compatible with such an assembly, as demonstrated by a simple structural model (Figure 6B). Furthermore, the recently identified Ca^{2+} channel

CALHM1 (calcium homeostasis modulator 1) which bears structural and functional similarities to connexins and pannexins, has also been found to form hexameric complexes (Ma et al., 2012; Siebert et al., 2013).

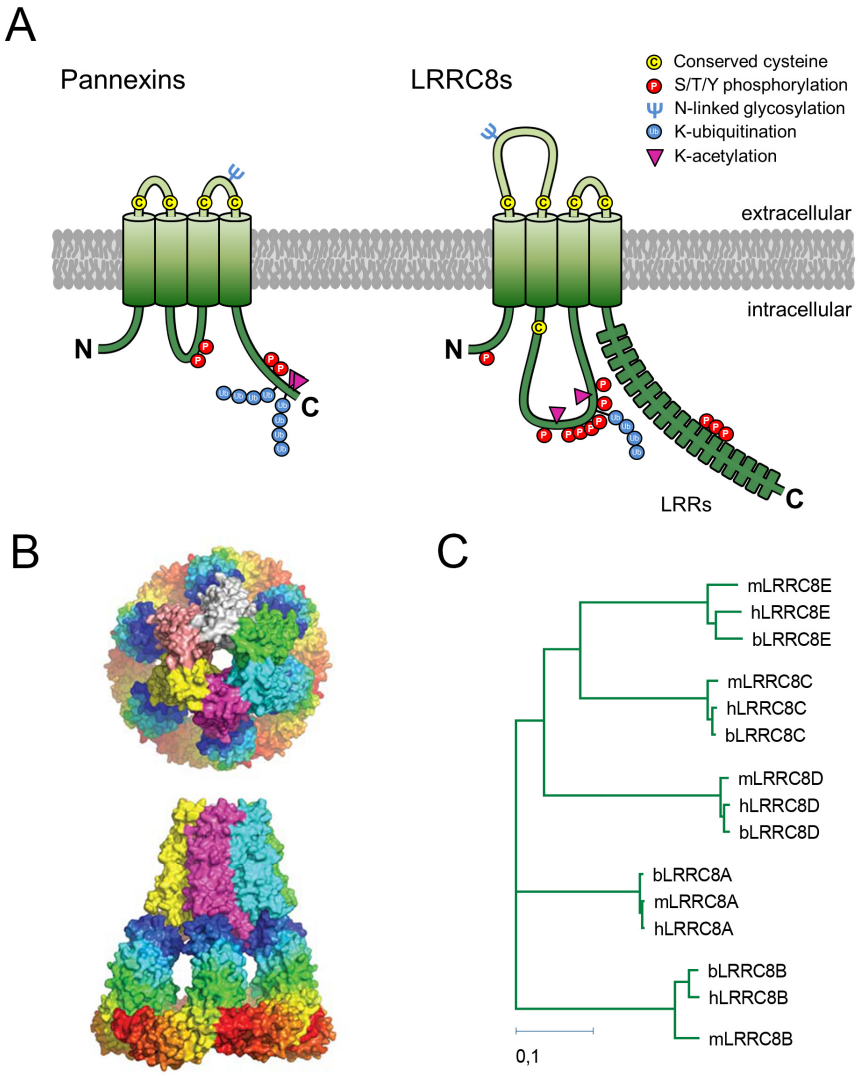

Figure 6 | Homology between pannexins and LRRC8s
(A) Schematic of the proposed transmembrane topology and posttranslational modifications of pannexins and LRRC8 proteins. **(B)** 3D model of a LRRC8 hexamer as a channel based on connexin and LRR crystal structures. Extracellular (top) and membrane view (bottom). **(C)** Maximum likelihood phylogeny of LRRC8 proteins from *H. sapiens*, *M. musculus* and *B. taurus*. The distance metric is uncorrected pairwise distance. Modified from Abascal and Zardoya, 2012.

Evolutionary analysis revealed that LRRC8s arose at the origin of chordates, likely by combination of an ancestor shared with pannexins, and an unknown LRR-containing protein (Abascal and Zardoya, 2012). Protein families identified as close relatives to the LRRC8 LRRDs included SHOC2, LAP, RSU1 and LRRIQ4. Since the LRRC8 paralogues *LRRC8B*, *LRRC8C* and *LRRC8D* cluster together in the human genome (1p22.2; Flicek et al., 2011), it was hypothesized that they emerged by tandem

duplication events (Abascal and Zardoya, 2012). *LRRC8A* (9q34.11) and *LRRC8E* (19p13.12) likely arose later by the duplication of *LRRC8B* and *LRRC8C*, respectively. The five LRRC8 paralogues share a high sequence similarity when compared to pannexins, suggesting a higher selective pressure (Figure 6C). Human LRRC8s are, on average, 45.92% identical, while human pannexins are only 34.29% identical (Abascal and Zardoya, 2012). The highest sequence identity is found between LRRC8C and LRRC8E (63.39%), while LRRC8B and LRRC8D are the least identical proteins of the family (37.08%). When comparing each paralogue to orthologues of other species, a high conservation of LRRC8A, LRRC8C and LRRC8D is found, suggesting a higher functional relevance (Figure 6C). On the other hand, LRRC8B and LRRC8E, which are the paralogues least conserved amongst species, are even lost in actinopterygians and birds (Abascal and Zardoya, 2012).

Only few studies reported on the physiological role of LRRC8 proteins. LRRC8A was the first member of the family to be described in 2003, when a heterozygous mutation in *LRRC8A* was found in a human patient suffering from congenital agammaglobulinemia, minor facial anomalies and a lack of B cells in peripheral blood (Sawada et al., 2003). The mutation was caused by a chromosome translocation that led to a truncated version of LRRC8A lacking part of the LRRD. It has been speculated that the apparent haploinsufficiency may be due to integration of truncated LRRC8A into multimeric protein complexes where it exerts a dominant-negative effect (Abascal and Zardoya, 2012). Another study suggested a role of *LRRC8C* in adipocyte differentiation (Tominaga et al., 2004), and the gene was subsequently named fad158 (for factor for adipocyte differentiation). The subsequently generated *Lrrc8c*$^{-/-}$ mouse exhibited a mild phenotype including reduced body weight gain and attenuated development of insulin resistance under a high-fat diet (Hayashi et al., 2011). LRRC8D and E have not been studied thus far and their physiological role remains to be elucidated.

Several large-scale gene expression studies found altered expression of LRRC8s under different pathological conditions. Serotonin transporter (*Htt*) knockout mice, a laboratory model for depression disorders, displayed reduced *Lrrc8a* expression in the brain, while *Lrrc8a* expression was increased in brains of mice treated with the HTT inhibitor fluoxetine (Ichikawa et al., 2008). However, it has to be noted that fluoxetine also potently inhibits $I_{Cl,vol}$ (see section 1.2.2). In another study, *LRRC8A* expression was found to be increased in different cellular models for vascular atrophy (Kenagy et al., 2011). Microarray analysis of transcripts isolated from colorectal cancer specimens revealed an increased expression of *LRRC8A* and *LRRC8E* (Piepoli et al., 2012). Furthermore, *LRRC8B* was downregulated in brain tissue obtained from patients who died from spontaneous intracerebral hemorrhage (Rosell et al., 2011).

2. AIM OF THE WORK

While many important functions have been assigned to the biophysically well-described VRAC based on experiments using unspecific pharmacological manipulations, the confirmation and further elucidation of these roles has been precluded by the lack of a known molecular entity comprising the channel.

The initial aim of this work was to electrophysiologically verify hits from a genome-wide siRNA screen to finally identify VRAC. After LRRC8A emerged as a promising candidate, the aim shifted towards proving that this protein is forming the VRAC pore. However, it quickly emerged that VRAC is not formed by LRRC8A alone and that the other LRRC8 family proteins are also involved. My task was to elucidate the role of LRRC8 proteins in mediating $I_{Cl,vol}$, while others performed crucial experiments to determine how LRRC8s traffic within the cell, what their transmembrane topology is and where they are expressed. Furthermore, several cell lines were generated in which *LRRC8* genes were disrupted, and these were then probed for $I_{Cl,vol}$ or served as clean background for overexpression and functional characterization of LRRC8s.

After our identification of LRRC8 heteromers as essential component of VRAC was published, I concentrated on the analysis of the structure-function relationship of LRRC8 channels, taking a special interest in the characteristic voltage-dependent inactivation gating. My goal was to identify the molecular determinants of $I_{Cl,vol}$ inactivation via a chimeric approach to gain insights into the molecular mechanism underlying this process. Other pressing questions I was striving to answer were if the VRAC pore is indeed formed by LRRC8 complexes, and if so, which parts of the proteins contribute to it and which specific properties they confer.

3. RESULTS

3.1. Identification of LRRC8 proteins as essential VRAC components

3.1.1. A genome-wide screen identifies LRRC8A as likely constituent of VRAC

To identify the protein(s) forming VRAC, a genome-wide RNAi screen was employed (performed by Felizia Voss and Tobias Stauber, see preface). Methodology and results are presented in detail elsewhere (Voss, 2015; Voss et al., 2014). Briefly, HEK293 cells stably expressing an I^--sensitive yellow fluorescent protein YFP(H148Q/I152L) were used in an imaging approach. Cells were subjected to hypotonic saline containing 50 mM NaI in a fluorometric imaging plate reader. Because VRAC conducts I^-, swelling-induced influx of I^- through VRAC and subsequent I^--dependent quenching of YFP fluorescence could be used as readout (Figure 7A).

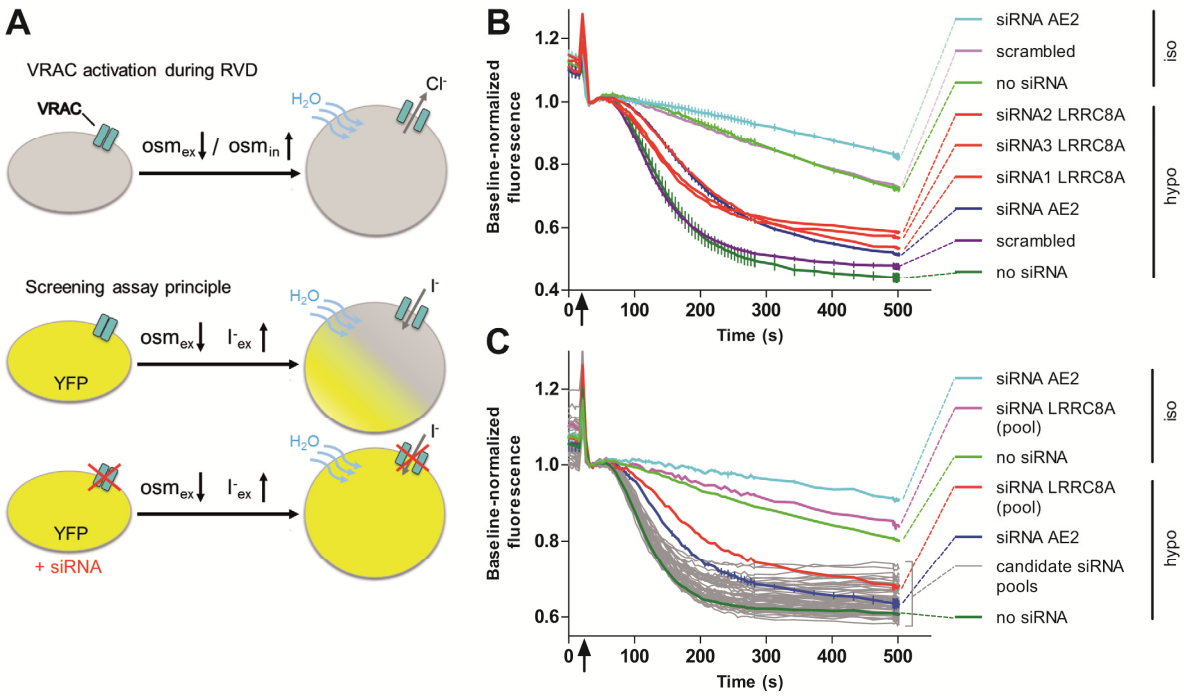

Figure 7 | Genome-wide RNAi screen identifies LRRC8A as candidate for VRAC
(A) Schematic of the screening principle. Top: VRAC is activated by swelling, which can be induced by a drop in extracellular osmolarity (osm_{ex}) or a rise in intracellular osmolarity (osm_{in}). Cl^- leaves the cell through VRAC, following its electrochemical gradient. Bottom: By simultaneously lowering osm_{ex} and raising the extracellular I^- concentration (I^-_{ex}), VRAC is activated and I^- forced into the cell, where it quenches the YFP fluorescence. Upon disruption of VRAC, the YFP fluorescence is quenched to a lesser extent. **(B)** Normalized and averaged example traces. siRNA against the Cl^-/HCO_3^--exchanger AE2 was used as positive control. **(C)** Fluorescence traces from the secondary screen using independent smartpool siRNAs. The LRRC8A trace is shown in red, other candidates in grey. Control traces from wells treated with control siRNAs against AE2 (n=3) and no siRNA (n=2) were averaged. Arrow indicates addition of iodide-containing hypotonic or isotonic saline. Error bars, SEM.

A prescreen found no effects of siRNAs targeting several previous VRAC candidates, including anoctamins, ClC-3, bestrophins and several anion transporters (Voss et al., 2014). One exception was the Cl^-/HCO_3^- exchanger AE2 which mediated a swelling-independent I^- flux and was therefore well suited as a positive control. In the first round of the genome-wide screen, three independent siRNAs per gene were transfected (Figure 7B).

Hits were defined by the maximal slope of fluorescence quenching and refined by properties of the encoded protein, such as a wide expression pattern and at least one predicted transmembrane domain. Independent smartpool siRNAs were used to evaluate 87 genes that satisfied all hit criteria. Of those, only LRRC8A knockdown resulted in a robust slowing of swelling-induced YFP quenching (Figure 7C).

3.1.2. siRNA knockdown and overexpression of LRRC8A reduce $I_{Cl,vol}$

To confirm LRRC8A as a candidate for VRAC, the effect of siRNA-mediated knockdown of *LRRC8A* on $I_{Cl,vol}$ was tested. In HEK293 cells, $I_{Cl,vol}$ could be evoked in cells patched in the whole-cell configuration by extracellular perfusion with hypotonic solution. Currents activated with the characteristic time course and exhibited prominent voltage-dependent inactivation at potentials above 80 mV (Figure 8A,B). These typical currents were strongly suppressed in cells treated with siRNA targeting *LRRC8A*, suggesting that the LRRC8A protein is either part of VRAC or an essential factor in the signal transduction cascade leading to its activation (Figure 8).

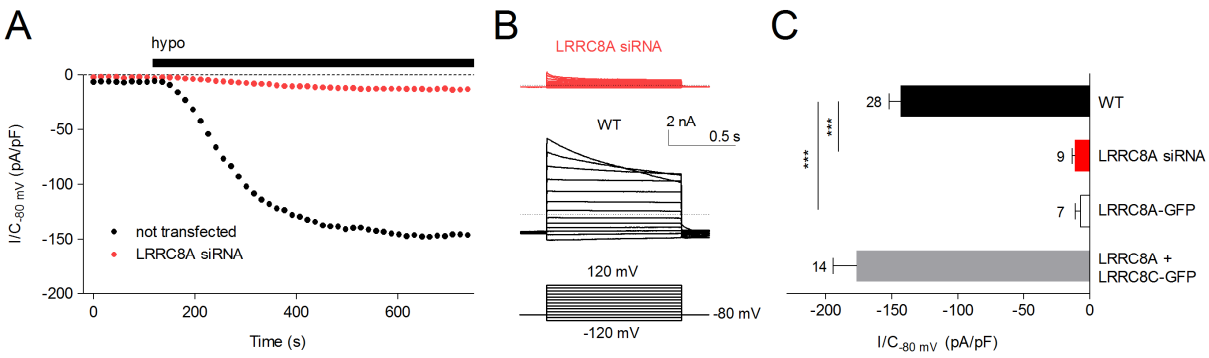

Figure 8 | siRNA knockdown of LRRC8A drastically reduces $I_{Cl,vol}$
(A) Example time course of $I_{Cl,vol}$ activation in WT and siRNA-treated HEK293 cells. Hypotonic saline (hypo) was washed in as indicated. Current densities (I/C) were taken at −80 mV. **(B)** Representative current traces of fully activated $I_{Cl,vol}$ in response to the voltage clamp protocol shown below. Dashed lines indicate zero current. **(C)** $I_{Cl,vol}$ current densities (at −80 mV) in WT HEK293 cells or cells treated with LRRC8A siRNA, or transfected with indicated LRRC8 cDNAs. Error bars, SEM; number of experiments is indicated; *** P < 0.001 (one-way ANOVA, Tukey's test).

In most cases, overexpression of an ion channel protein leads to an increase in current. However, this was not true for LRRC8A. While overexpressed LRRC8A-GFP could be detected at the plasma membrane, it suppressed $I_{Cl,vol}$ to a similar extent as siRNA knockdown (Figure 8C). We hypothesized that this unexpected effect might be due to LRRC8A being part of a heteromer containing other LRRC8 proteins and that overexpression of LRRC8A adversely affects the assembly of functional channels by altering their subunit stoichiometry. Indeed, co-expression of LRRC8A with LRRC8C did not result in suppression, but neither in a significant increase of $I_{Cl,vol}$ (Figure 8C).

3.1.3. Localization and trafficking of LRRC8 proteins

The subcellular localization of LRRC8 proteins was studied by Felizia Voss and Tobias Stauber using confocal microscopy (see preface).

GFP-tagged LRRC8A reached the plasma membrane when overexpressed in HeLa (Figure 9A), HCT116 and HEK293 cells (data not shown). Native LRRC8A could also be detected at the plasma membrane (Figure 9B,C). Therefore, LRRC8A could be part of a plasma membrane channel such as VRAC. In a patient with agammaglobulinemia, a mutation in *LRRC8A* has been identified that leads to a premature stop codon, truncating the C-terminus of the protein (see section 1.3). We observed that the truncated protein is retained in the ER upon overexpression (Figure 9D).

Overexpressed LRRC8B–E did not reach the plasma membrane on their own (Figure 9E–H) but only when co-expressed with LRRC8A (Figure 9I–L). This hints at an interaction between LRRC8A and LRRC8B–E, which is required for correct trafficking to the plasma membrane. Such a physical interaction could indeed be confirmed between LRRC8A and LRRC8B–E in co-immunoprecipitation experiments with overexpressed as well as native proteins (Voss et al., 2014). We thus concluded that LRRC8 proteins form heteromers, in which LRRC8A plays a central role.

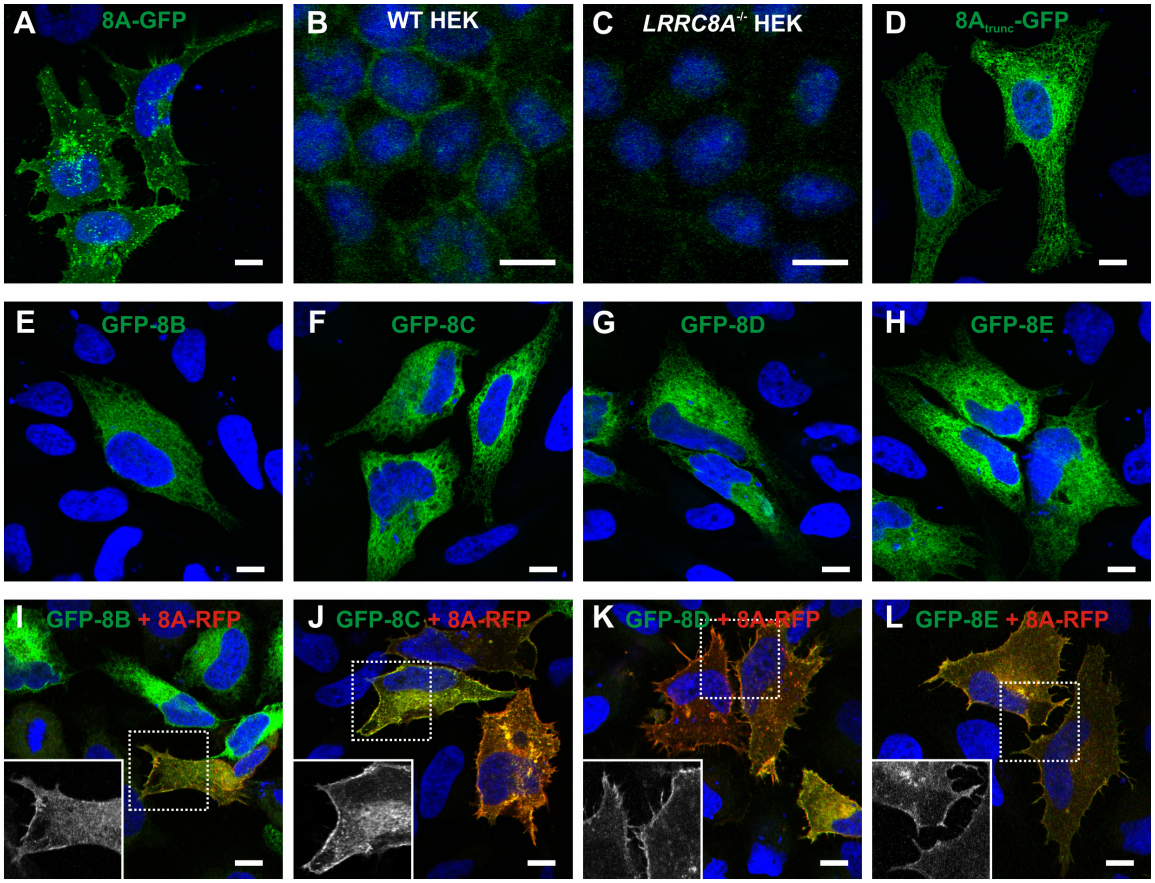

Figure 9 | Subcellular localization of LRRC8 proteins
(A) LRRC8A-GFP (8A-GFP), when overexpressed in HeLa cells, localizes to the plasma membrane. **(B)** Endogenous LRRC8A is detected at the plasma membrane of permeabilized native HEK293 cells by immunostaining using an antibody against LRRC8A. **(C)** The specificity of the LRRC8A antibody was confirmed by the absence of signal in *LRRC8A*$^{-/-}$ HEK293 cells generated using CRISPR/Cas (see section 5.2.1.2). **(D)** Truncated LRRC8A fused at R719 to GFP did not reach the plasma membrane. **(E–H)** GFP-tagged LRRC8B–E (GFP-8B–E) localize to the ER when overexpressed alone. **(I–L)** Upon co-expression with LRRC8A-RFP (8A-RFP), LRRC8B–E reach the plasma membrane.

3.1.4. LRRC8A and at least one other LRRC8 isoform are required for $I_{Cl,vol}$

One major problem for the further characterization of the role of LRRC8 proteins in VRAC function was that overexpression did not result in $I_{Cl,vol}$ current densities above wild type (WT) levels. Hence, functional studies would be confounded by endogenous currents. To overcome this issue, we opted to generate multiple cell lines in which *LRRC8* genes and combinations thereof were disrupted. To this end, we used commercially available zinc finger nucleases and the CRISPR/Cas technique (Cong et al., 2013). As target, we chose the stably diploid human colorectal carcinoma cell line HCT116 and HEK293 cells. First, we sought to confirm our results from siRNA knockdown experiments on the role of LRRC8A. Several different *LRRC8A*$^{-/-}$ HEK293 and HCT116 clones were generated using different targeting and knockout strategies

(Table 4). All *LRRC8A*$^{-/-}$ cell lines were confirmed by sequencing of genomic DNA (Table 5) and Western blot (Figure 10). Generation and validation of knockout cell lines was done in collaboration with Felizia Voss and Tobias Stauber (see preface).

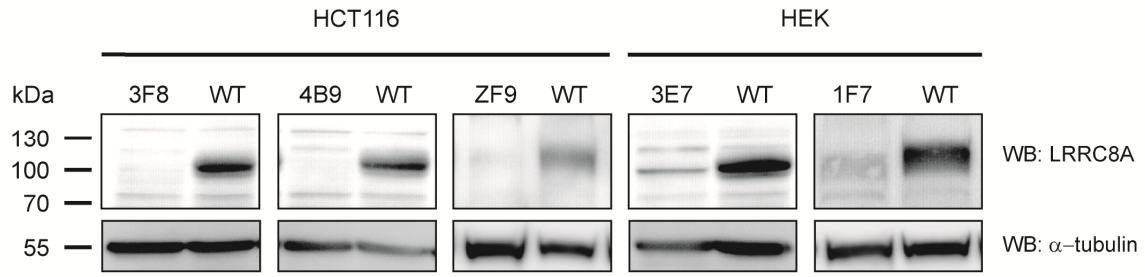

Figure 10 | Western blots confirm LRRC8A disruption in mutant cell lines
The first number in the knockout clone name indicates construct number. ZF9 is the clone generated using a zinc finger nuclease. α-tubulin, loading control.

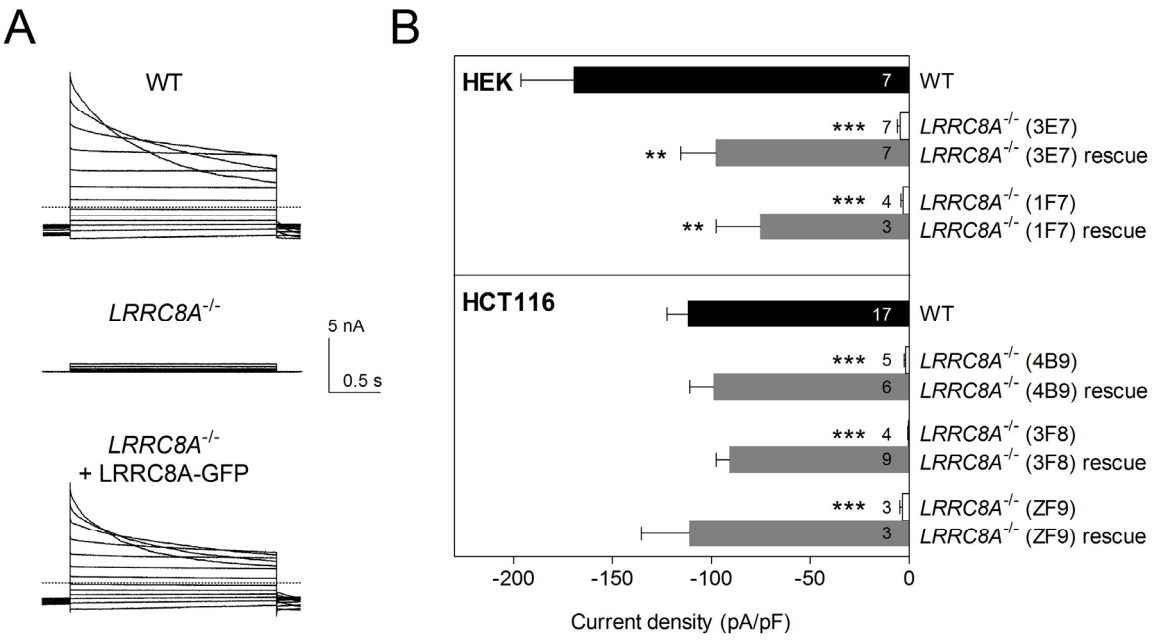

Figure 11 | $I_{Cl,vol}$ is abolished upon *LRRC8A* disruption and can be rescued
(A) Representative $I_{Cl,vol}$ traces from HEK293 WT and *LRRC8A*$^{-/-}$ cells (clone 3E7) in response to the voltage clamp protocol shown in Figure 8B, but with 2-s-pulses. **(B)** Current densities of maximally activated $I_{Cl,vol}$ (at −80 mV) of WT HEK293, WT HCT116 and different *LRRC8A*$^{-/-}$ cell lines, rescued by transfection of LRRC8A-GFP cDNA. Mean currents ± SEM, number of measurements is indicated. **, $p<0.01$ and ***, $p<0.001$ compared to the respective WTs (one-way ANOVA, Tukey's test). For description of cell lines see Table 5.

$I_{Cl,vol}$ was completely abolished in all the differently targeted *LRRC8A*$^{-/-}$ cell lines (Figure 11). It is therefore very unlikely that off-target effects lead to the loss of the current. Furthermore, overexpression of LRRC8A restored $I_{Cl,vol}$ partially in *LRRC8A*$^{-/-}$ HEK293 cells and completely in *LRRC8A*$^{-/-}$ HCT116 cells (Figure 11). The partial rescue in HEK293 cells may be due to the suppression of $I_{Cl,vol}$ upon overexpression of LRRC8A, a phenomenon not observed in HCT116 cells. In conclusion, our data clearly demonstrate that LRRC8A is essential for $I_{Cl,vol}$.

LRRC8B–E were shown to interact physically with LRRC8A (data not shown, see Voss, 2015; Voss et al., 2014), which facilitates their correct trafficking to the plasma membrane. Furthermore, co-expression of LRRC8A with LRRC8C prevented suppression of $I_{Cl,vol}$ in HEK293 cells. These observations indicate that LRRC8A and LRRC8B–E form heteromeric complexes. However, apart from LRRC8A, no other LRRC8 protein appeared as a major hit in our genome-wide siRNA screen, hinting at a functional redundancy. To further investigate the role of LRRC8B–E, we analyzed cell lines in which these genes were disrupted alone or in combination. Again, all cell lines were confirmed by DNA sequencing (Table 5) and subsequently by Western blot (Voss, 2015).

Compatible with apparent functional redundancy of LRRC8B–E, no single knockout cell line apart from *LRRC8A*$^{-/-}$ showed abolished $I_{Cl,vol}$ (Figure 12A,B). Only *LRRC8E*$^{-/-}$ cells exhibited significantly reduced $I_{Cl,vol}$, which was even lower in *LRRC8(C/E)*$^{-/-}$ double knockout, *LRRC8(C/D/E)*$^{-/-}$ triple knockout, and similar in size in *LRRC8(D/E)*$^{-/-}$ double knockout cells, indicating that LRRC8C and LRRC8E are the major LRRC8 proteins apart from LRRC8A involved in $I_{Cl,vol}$ in HCT116 cells (Figure 12A,B). Strikingly, $I_{Cl,vol}$ was completely abolished in *LRRC8(B/C/D/E)*$^{-/-}$ quadruple knockout cells (Figure 12A,B). We thus conclude that concurrent expression of LRRC8A and at least one other LRRC8 protein is required for $I_{Cl,vol}$.

Furthermore, we noticed a pattern of differential voltage-dependent inactivation in our knockout cells. Since the current decay is not appropriately fitted using single, double or even triple exponential functions, we opted to use the ratio of current after 2 s and peak current (I_{2s}/I_{max}) to quantitatively assess voltage dependence of current inactivation. While $I_{Cl,vol}$ from cells in which *LRRC8C* was disrupted inactivated much faster and at less depolarized potentials than WT cells, currents from cells in which LRRC8D and LRRC8E were lacking inactivated slower and at more positive voltages (Figure 12A,C). These slowly inactivating currents resembled $I_{Cl,vol}$ in WT HEK293 cells, which generally inactivated slower than $I_{Cl,vol}$ in WT HCT116 cells (Figure 12C and Figure 11A). As voltage-dependent current inactivation on similar timescales is generally mediated by

proteins either forming an ion channel pore or closely associated with it, these findings hint that LRRC8 proteins might be part of the VRAC channel complex.

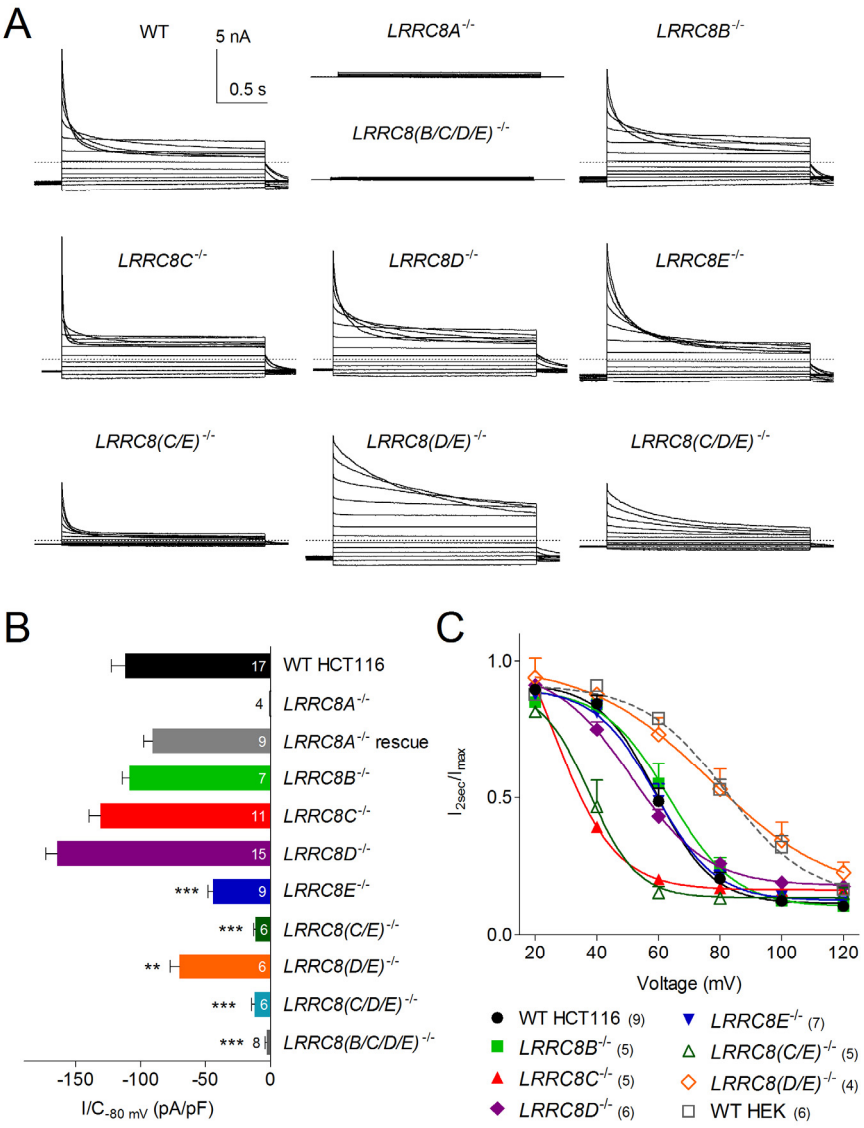

Figure 12 | Characterization of $I_{Cl,vol}$ in *LRRC8* knockout cells
(A) Representative $I_{Cl,vol}$ traces from WT and mutant HCT116 cells in response to the voltage clamp protocol shown in Figure 8B, but with 2-s-pulses. **(B)** Current densities of maximally activated $I_{Cl,vol}$ (at −80 mV) of WT and mutant HCT116 cells. **(C)** $I_{Cl,vol}$ inactivation assessed by the ratio of current at the end and in the beginning of a 2-s-pulse to the indicated voltages. Data are mean ± SEM, number of measurements is indicated. **, p<0.01 and ***, p<0.001 compared to WT HCT116 (one-way ANOVA, Tukey's test). For description of knockout cell lines see Table 5.

Next, we sought to confirm our results from knockout cell lines by reconstitution of currents upon overexpression of combinations of LRRC8 proteins. To this end, we used a quintuple knockout HCT116 cell line, in which all LRRC8 genes had been disrupted (*LRRC8(A/B/C/D/E)*$^{-/-}$, henceforth called *LRRC8*$^{-/-}$). $I_{Cl,vol}$ could not be elicited in

LRRC8$^{-/-}$ cells when untreated or when transfected with LRRC8A alone (Figure 13A,B), corroborating our results from *LRRC8(B/C/D/E)*$^{-/-}$ quadruple knockout cells (Figure 12A,B). Co-expression of LRRC8A with LRRC8C and LRRC8E yielded robust volume-activated currents that were not different in amplitude from WT HCT116 $I_{Cl,vol}$ (Figure 13A,B). Current amplitudes mediated by LRRC8A and LRRC8D were a bit lower, which is probably owed to a poor expressibility of the LRRC8D-GFP construct that we observed. Similarly, overexpressed LRRC8B-GFP could hardly be detected. Thus, we could not observe any $I_{Cl,vol}$ with the LRRC8A/B combination, even though a low but detectable $I_{Cl,vol}$ was measured in the *LRRC8(C/D/E)*$^{-/-}$ triple knockout cell line, suggesting that LRRC8A and LRRC8B can also form functional VRACs (Figure 12A,B). Very low currents in *LRRC8(C/E)*$^{-/-}$ double knockout HCT116 cells further suggest that LRRC8B and LRRC8D might be poorly expressed not only upon overexpression, but also in native HCT116 cells. The inactivation phenotypes of rescued currents in *LRRC8*$^{-/-}$ quintuple knockout cells agreed well with our findings from single, double, and triple knockout cell lines. Co-expression of LRRC8A with LRRC8C yielded currents that inactivated more slowly and at more positive voltages than WT currents (Figure 13A,C). This fits to the slowly inactivating currents observed in *LRRC8(D/E)*$^{-/-}$ double knockout cells (Figure 12A,C).

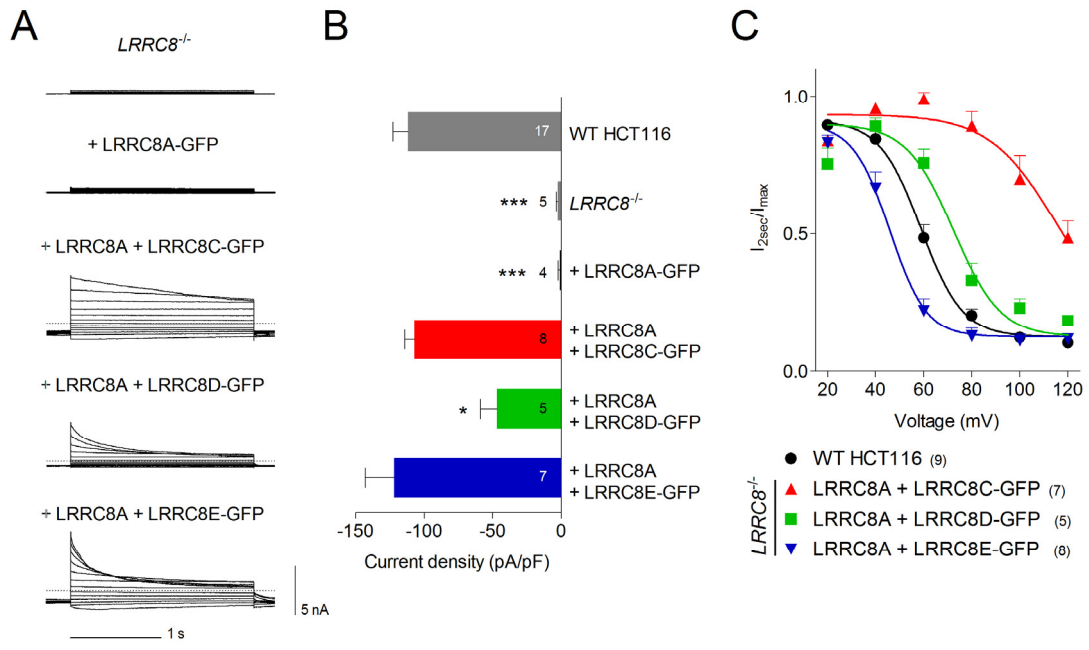

Figure 13 | Characterization of $I_{Cl,vol}$ reconstituted in *LRRC8*$^{-/-}$ cells
(A) Representative $I_{Cl,vol}$ traces from *LRRC8*$^{-/-}$ cells transfected with the indicated LRRC8 combinations in response to the voltage clamp protocol shown in Figure 8B, but with 2-s-pulses. **(B)** Current densities of maximally activated $I_{Cl,vol}$ (at −80 mV). **(C)** $I_{Cl,vol}$ inactivation assessed by the ratio of current at the end and in the beginning of a 2-s-pulse to the indicated voltages. Data are mean ± SEM, number of measurements is indicated. *, p<0.05 and ***, p<0.001 compared to WT HCT116 (one-way ANOVA, Tukey's test).

On the other hand, co-expression of LRRC8A with LRRC8D or LRRC8E led to currents that inactivated similarly as or faster than WT currents, respectively (Figure 13A,C), matching the fast current inactivation observed in *LRRC8C*$^{-/-}$ cells. In summary, LRRC8C has a 'decelerating' effect on $I_{Cl,vol}$ inactivation, while LRRC8D and LRRC8E act as 'accelerating' subunits. Since inactivation in 'fast' VRACs, e.g. those formed in *LRRC8C*$^{-/-}$ cells or in *LRRC8*$^{-/-}$ cells co-transfected with LRRC8A/E, reached saturation in tens of milliseconds, an involvement of LRRC8 proteins through signaling pathways like phosphorylation can be almost excluded, as these processes are generally slower. It rather suggests that LRRC8 heteromers are integral to the VRAC channel complex.

The inactivation of $I_{Cl,vol}$ had earlier been shown to differ drastically among different cell lines and native tissues (Nilius et al., 1997). For example, vascular smooth muscle cells (Wang et al., 2004), neurons (Leaney et al., 1997) and blood cells like the human promyelocytic leukemia cell line HL-60 (Hernández-Carballo et al., 2010) exhibit almost non-inactivating $I_{Cl,vol}$, while HEK293 cells (Hernández-Carballo et al., 2010; Nilius et al., 2001) and HCT116 cells (Figure 12) displayed pronounced $I_{Cl,vol}$ inactivation. As we have shown, inactivation is determined by the expression of LRRC8 isoforms in HCT116 cells (Figure 12 and Figure 13). To test whether LRRC8 expression might explain the observed variability in inactivation between cell types, we performed quantitative real-time PCR (qRT-PCR) in HEK293, HL-60 and HCT116 cells to assess the relative mRNA expression levels of the LRRC8 family. In agreement with their slowly inactivating $I_{Cl,vol}$, HL-60 cells expressed only low amounts of the 'accelerating' subunit LRRC8E (Figure 14). On the other hand, HCT116 cells expressed little of the 'decelerating' LRRC8C when compared to HEK293 cells, where $I_{Cl,vol}$ inactivated more slowly. Furthermore, EST databases suggested a similar correlation between LRRC8C/LRRC8E expression and the observed $I_{Cl,vol}$ inactivation kinetics in other cell types such as neurons and vascular smooth muscle cells

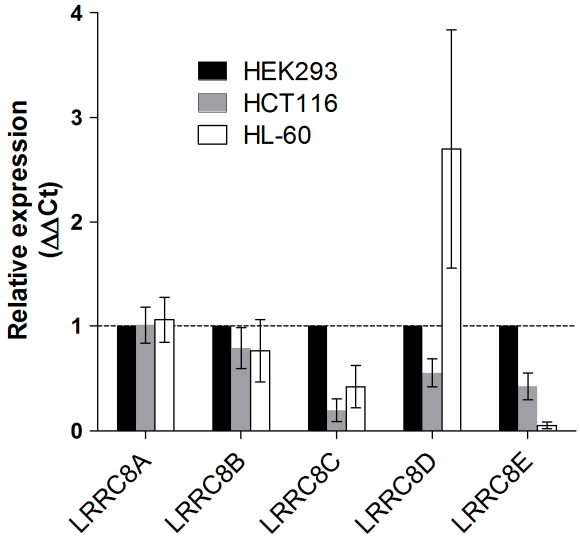

Figure 14 | Relative LRRC8 mRNA expression in different cell types

LRRC8A–E mRNA expression determined by quantitative RT-PCR. Values were normalized to the respective value of HEK293 cells. Values represent the means from 4 experiments. Error bars indicate SEM. qRT-PCR experiments were performed by Felizia Voss (see preface).

As discussed earlier, one major attribute used to discern VRAC currents from other anion currents is their typical anion permeability sequence ($SCN^- > I^- > NO_3^- > Br^- > Cl^- > F^- >$ gluconate > aspartate), corresponding to an Eisenmann type I sequence (Nilius et al., 1997). Therefore, we opted to determine anion selectivities to ascertain that the swelling-induced currents recorded from knockout HCT116 cells and, more importantly, upon overexpression of different LRRC8 combinations in *LRRC8*$^{-/-}$ cells, were indeed identical to $I_{Cl,vol}$. To this end, we elicited currents in the whole-cell patch clamp configuration by subjecting cells to hypotonic saline. After maximal activation, we recorded reversal potentials for NaCl-containing saline using 2-s-ramp protocols from −100 to 100 mV. Subsequently, we perfused cells with hypotonic salines in which NaCl was substituted for by NaI, $NaNO_3$ or Na-D-gluconate and measured reversal potentials. From the relative shift in reversal potentials, the relative permeability (P_X/P_{Cl}) for the substituting anions could be calculated (also see section 5.2.5).

$I_{Cl,vol}$ in WT HCT116 cells displayed the typical anion permeability sequence, which was unchanged in currents mediated by LRRC8A co-expressed with LRRC8C, LRRC8D or LRRC8E in *LRRC8*$^{-/-}$ HCT116 cells (Figure 15A,B). We also tested all other HCT116 *LRRC8* knockout cell lines that mediated appreciable $I_{Cl,vol}$ (Figure 12). While the measurement of reversal potentials was difficult in *LRRC8(C/E)*$^{-/-}$ and *LRRC8(C/D/E)*$^{-/-}$ cells, because they mediated very low currents that may be confounded by background and leak currents, all of the cell lines retained the typical $I^- > NO_3^- > Cl^- >>$ gluconate selectivity (Figure 15C). Thus, the swelling-activated and LRRC8-dependent currents recorded are indeed identical to what is normally referred to as $I_{Cl,vol}$. Whereas the LRRC8 subunit composition determines voltage-dependent inactivation of VRAC, we found no evidence for different permeabilities for halides and the larger organic compound gluconate between different LRRC8 combinations.

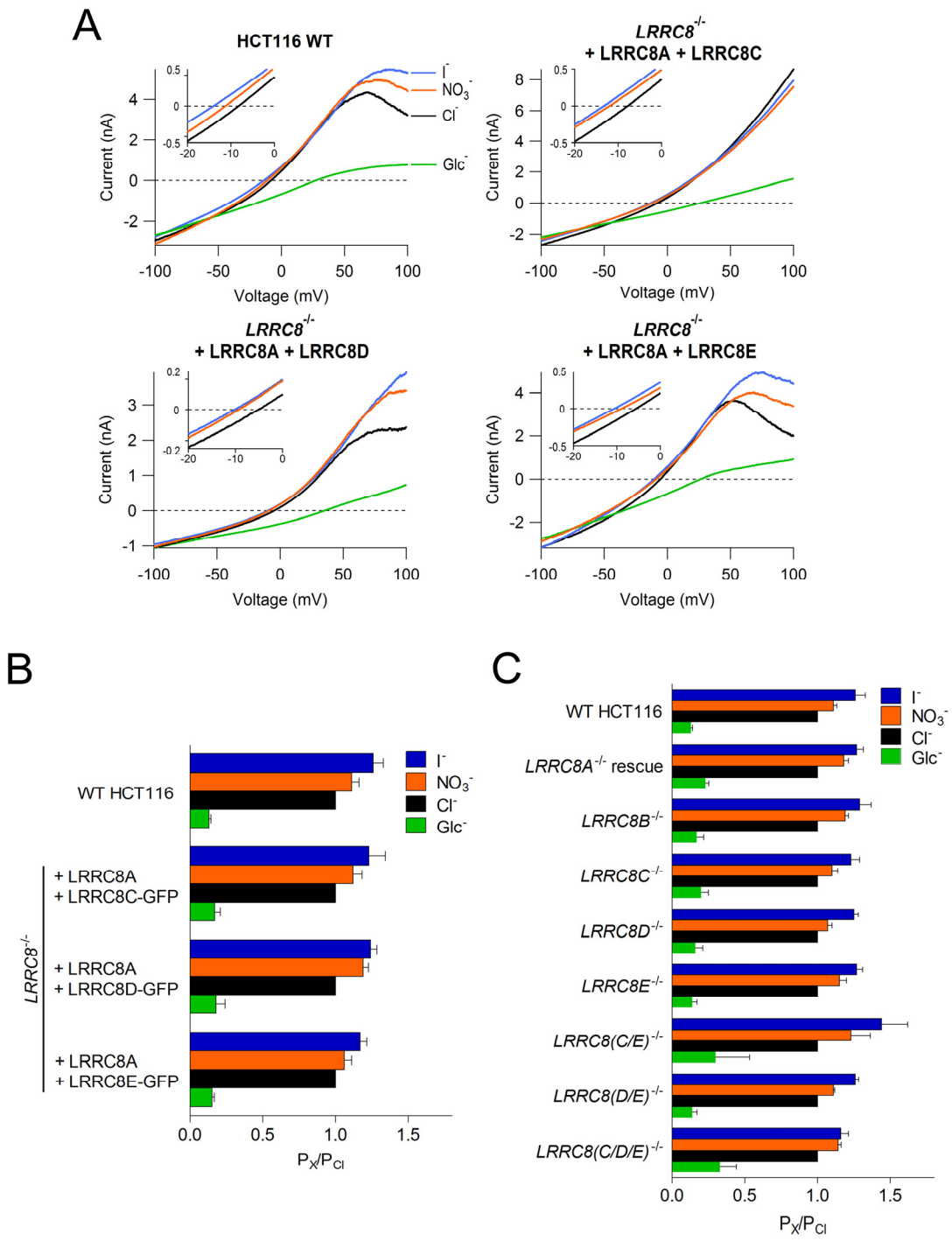

Figure 15 | Anion selectivity of $I_{Cl,vol}$ mediated by different LRRC8 combinations
(A) Example current-voltage relationships obtained at the time of maximal current activation of endogenous and reconstituted $I_{Cl,vol}$ with normal and anion substituted hypotonic extracellular solutions. Insets show a magnification of reversal potentials for Cl^-, I^- and NO_3^-. The reversal potential is shifted to slightly more negative voltages when extracellular Cl^- is replaced by I^- and NO_3^- and to drastically more positive voltages upon replacement by D-gluconate (Glc^-). **(B, C)** Relative anion permeabilities (P_X/P_{Cl}) as determined from shifts in reversal potential of $I_{Cl,vol}$ upon anion substitution **(B)** in *LRRC8*$^{-/-}$ cells transfected with the combinations indicated and **(C)** in *LRRC8* knockout HCT116 cell lines. Mean ± SEM, number of cells ≥ 4.

3.2. Molecular determinants of differential VRAC inactivation

As shown in Section 3.1.4, when co-expressing LRRC8A and LRRC8C or LRRC8E in *LRRC8*$^{-/-}$ HCT116 cells, the differences in inactivation kinetics of $I_{Cl,vol}$ are striking (Figure 13). The highly depolarized voltages at which these differences can be observed are only rarely reached under physiological conditions. Thus they are unlikely to be of high physiological relevance. However, since the voltage-dependent inactivation can be considered a channel-intrinsic characteristic of VRAC, identification of the molecular determinants of these differences could provide a starting point for the further exploration of the structure-function relationship of this newly identified ion channel.

3.2.1. Kinetic differences between $I_{Cl,vol}$ mediated by LRRC8A/C and LRRC8A/E

First, the differences between inactivation kinetics of $I_{Cl,vol}$ mediated by LRRC8A/E and LRRC8A/C heteromers were analyzed in more depth. Whereas LRRC8A/C yielded currents that did not inactivate at potentials more negative than ~60 mV, LRRC8A/E-mediated currents showed pronounced inactivation already at 40 mV (Figure 16A,B). We used the ratio of current after 2 s and peak current (I_{2s}/I_{max}) to assess the voltage-dependence of inactivation. This yielded a ~40 mV difference in the potential of half-maximal inactivation (V_{50}) between LRRC8A/C- and LRRC8A/E-mediated currents (Figure 16B). Whereas the inactivation of $I_{Cl,vol}$ in WT cells could not be fitted by single or double exponentials, likely because they contain a complex mixture of different VRACs, inactivation of heteromers containing just two isoforms could be adequately approximated by exponential functions (Figure 16A). The resulting time constants of inactivation ($\tau_{inactivation}$) were voltage-dependent and generally much smaller for LRRC8A/E- than LRRC8A/C heteromers (Figure 16C). $\tau_{inactivation}$ of LRRC8A/E reached steady state at voltages more positive than ~80 mV, whereas LRRC8A/C currents did not reach similar inactivation time constants even at 120 mV.

The observed differences could be either purely kinetic, implying that LRRC8C-containing heteromers inactivate to the same extent, but much slower than those containing LRRC8E, so that steady state cannot be reached within 2 s pulses; or LRRC8C could confer a higher residual current even when inactivated to steady state. To clarify this issue, we applied very long pulses to depolarized potentials to cells co-expressing LRRC8A and LRRC8C (Figure 16D). Just as LRRC8E-mediated currents, the resulting currents inactivated to around 15% of peak current at steady state (Figure 16D,E).

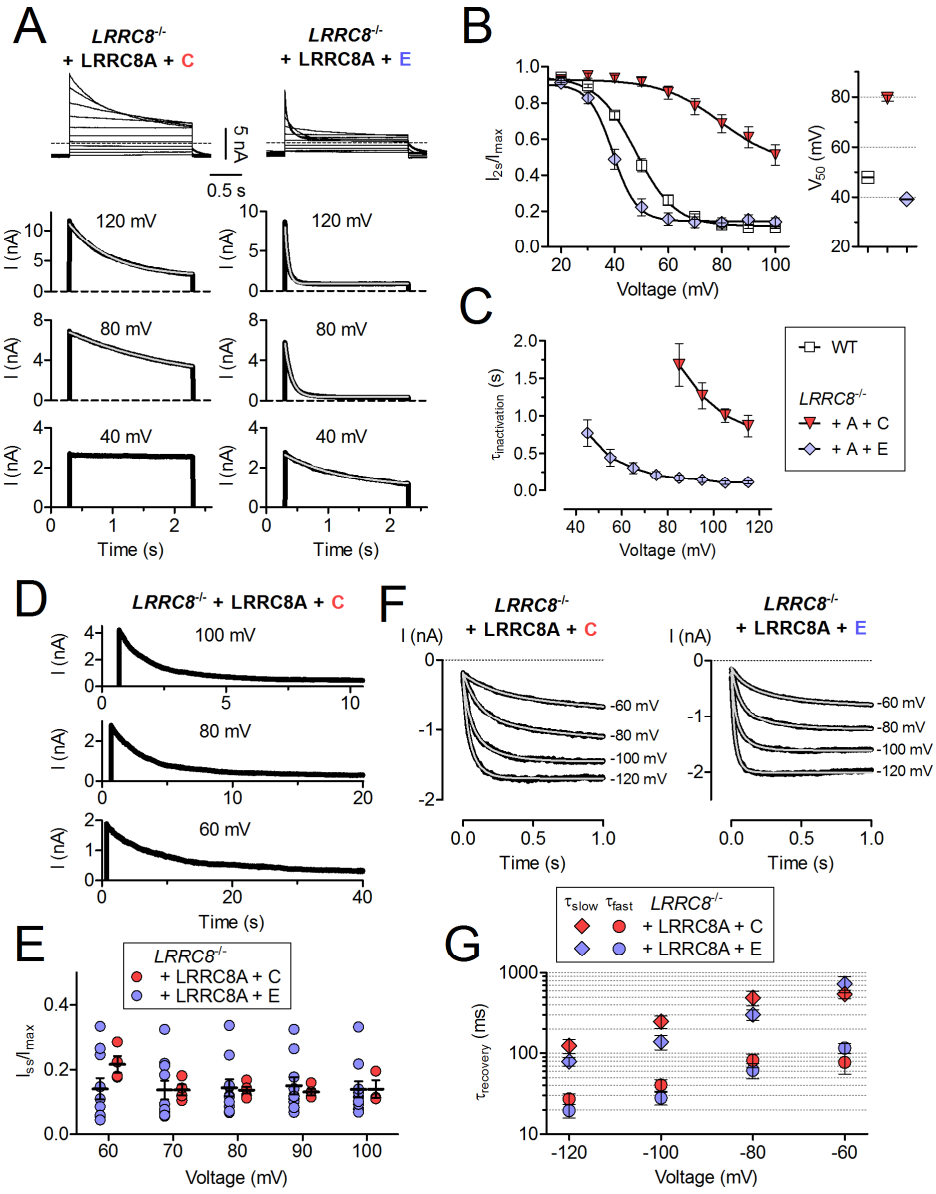

Figure 16 | Kinetic differences between LRRC8C- and E-mediated $I_{Cl,vol}$ inactivation

(A) Representative swelling-activated current traces of *LRRC8*$^{-/-}$ HCT116 cells transfected with LRRC8A and the indicated isoform in response to 2 s voltage steps between −100 mV and 100 mV in 20 mV increments (top) or to the voltages given (bottom). Cells were held at −80 mV for 500 ms before and after voltage steps to allow for complete recovery from inactivation. In the bottom panels, only the outward component of the current is shown. Light lines are from monoexponential fits to the current decay. **(B)** Left: $I_{Cl,vol}$ inactivation assessed by ratio of current at end (I_{2s}) and beginning (I_{max}) of 2-s-pulse. Solid lines are Boltzmann fits. Right: V_{50} values from Boltzmann fits. **(C)** Inactivation time constants ($\tau_{inactivation}$) obtained from monoexponential fits to $I_{Cl,vol}$ current traces in response to 2-s-pulses to given voltages. WT currents could not be adequately fitted by monoexponentials and are thus absent. **(D)** Representative $I_{Cl,vol}$ traces. Cells were held at indicated voltages until steady state inactivation was reached. **(E)** Relative steady state $I_{Cl,vol}$ (I_{ss}/I_{max}) as determined from long depolarizing pulses. **(F)** Representative currents recovering from inactivation. Currents were inactivated to near steady state with 4-s- (LRRC8C) or 1-s-pulses (LRRC8E) to 100 mV (not shown) and recovered during 1-s-pulses to −120, −100, −80 and −60 mV. Light lines are double-exponential fits to the currents. **(G)** Recovery time constants from double exponential fits to currents as shown in F. All experiments have been repeated in 5–10 cells. Error bars, SEM.

We next asked whether also hyperpolarization-facilitated recovery from inactivation differs between LRRC8A/C- and LRRC8A/E-mediated currents. After inactivating channels to near steady state with 1-s- (LRRC8A/E) or 4-s-pulses (LRRC8A/C) to 100 mV, 1-s-pulses to voltages from −120 to −60 mV in 20 mV increments were applied. These pulses elicited rapidly increasing inward currents (Figure 16F) which reflect the reopening of inactivated VRACs and can be fitted by double exponentials (Voets et al., 1997a). Such fits (Figure 16F) yielded voltage-dependent time constants that were only slightly different between LRRC8A/C and LRRC8A/E (Figure 16G). Hence, whereas inactivation is drastically faster in LRRC8A/E than in LRRC8A/C channels, both heteromers recover from inactivation on a similar timescale.

3.2.2. $I_{Cl,vol}$ inactivation in LRRC8 triple knockout cells

Before exploring the molecular basis of VRAC inactivation, we asked if the kinetic differences observed upon heterologous overexpression of different LRRC8 combinations in *LRRC8*$^{-/-}$ cells are comparable at near-physiological expression levels to exclude overexpression artifacts. To this end, we used CRISPR/Cas-generated HCT116 cells in which LRRC8B, -D and -E (*LRRC8(B/D/E)*$^{-/-}$) or LRRC8B, -C and -D (*LRRC8(B/C/D)*$^{-/-}$) were disrupted in parallel. These cells only express LRRC8A/C and LRRC8A/E heteromers, respectively. Gene disruption was confirmed by DNA sequencing (Table 5) and Western blot (Figure 17).

Both cell lines still gave robust swelling-activated currents (Figure 18), but current densities were approximately 50% lower in *LRRC8(B/D/E)*$^{-/-}$ than in WT, probably due to the observed higher expression of LRRC8E in HCT116 cells (Voss et al., 2014). At first glance, inactivation in the triple knockouts was strikingly similar to that observed in overexpression experiments, with *LRRC8(B/C/D)*$^{-/-}$ cells showing much faster inactivation than WT, while currents from *LRRC8(B/D/E)*$^{-/-}$ cells inactivated slower (Figure 18A), demonstrating the applicability of our results also to endogenous VRACs. However, quantification showed a slight left-shift of the voltage-dependence I_{2s}/I_{max} and $\tau_{inactivation}$ of currents from both cell lines when compared to their overexpression counterparts (Figure 18B,C, and Figure 16B,C). This suggests that overexpression in LRRC8$^{-/-}$ cells generally leads to marginally slower current inactivation. We hypothesize that LRRC8A also affects inactivation kinetics and that the LRRC8A:LRRC8X stoichiometry upon overexpression is different from that at endogenous expression levels, causing a slightly different inactivation behavior.

Figure 17 | Expression of LRRC8 proteins in triple knockout cells ▶

Western blot analysis of several LRRC8 knockout cell lines using the specific antibodies listed in Table 10. Tubulin was used as loading control.

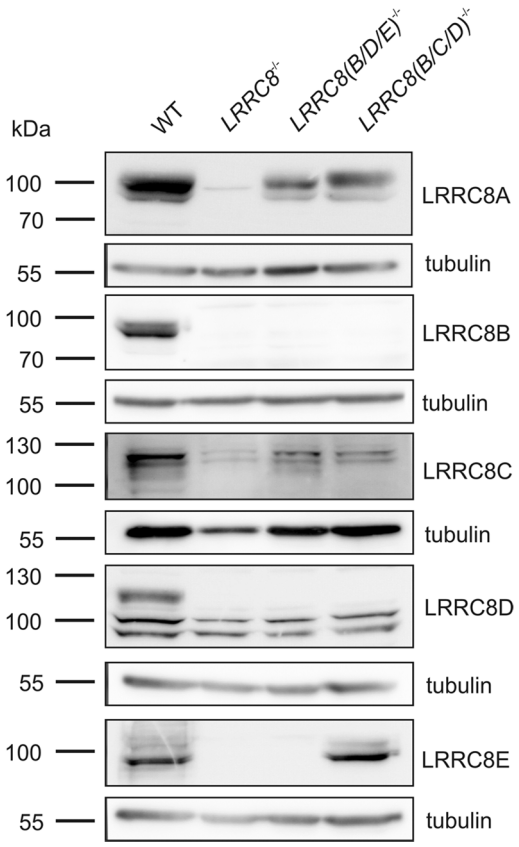

Figure 18 | $I_{Cl,vol}$ inactivation in LRRC8 triple knockout cells ▼

(A) Representative swelling-activated current traces (as in Figure 16A) of HCT116 cells with the indicated *LRRC8* genotypes. Light lines are from monoexponential fits to the current decay, when possible. **(B)** Left: $I_{Cl,vol}$ inactivation assessed by ratio of current at end (I_{2s}) and beginning (I_{max}) of 2-s-pulse. Solid lines are Boltzmann fits. Right: V_{50} values from Boltzmann fits. **(C)** Inactivation time constants ($\tau_{inactivation}$) obtained from monoexponential fits to $I_{Cl,vol}$ current traces in response to 2-s-pulses to given voltages. WT currents could not be adequately fitted by monoexponentials and are thus absent.

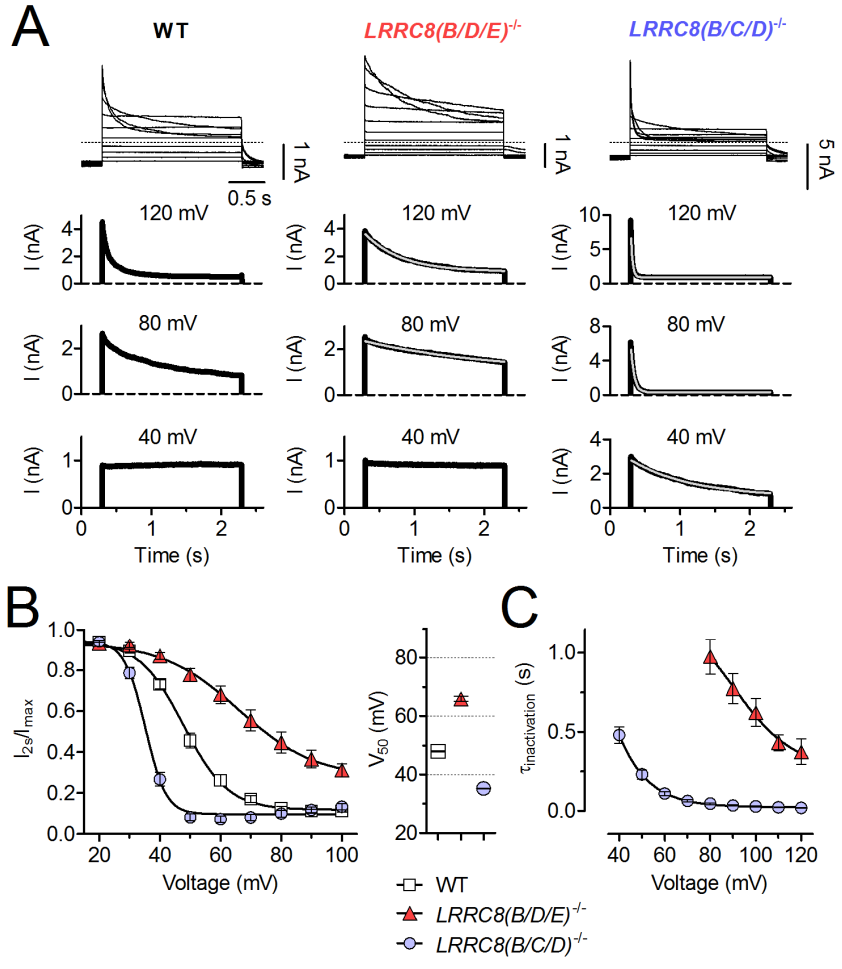

3.2.3. Molecular determinants of differential $I_{Cl,vol}$ inactivation kinetics

To identify the regions determining the observed differences between LRRC8C- and LRRC8E-mediated currents, we constructed chimeric proteins based on LRRC8C and LRRC8E (Figure 19A). The chimeras were co-expressed with LRRC8A in *LRRC8*$^{-/-}$ HCT116 cells. Chimeras containing the N-terminus and the first TM segment of LRRC8E in LRRC8C-background (chimera 1, LRRC8E$^{1–42}$/LRRC8C$^{43–830}$, Figure 19A) or the N-terminus, first TM segment and first extracellular loop (ECL1) of LRRC8C (chimera 2, LRRC8C$^{1–125}$/LRRC8E$^{117–796}$, Figure 19A) in LRRC8E background mediated slowly-inactivating currents that were indiscernible from LRRC8A/C currents (Figure 19B–D). These results argue for a major role of the LRRC8C ECL1 in slow inactivation, since the ECL1 was the only segment in both chimeras that was constantly LRRC8C-derived.

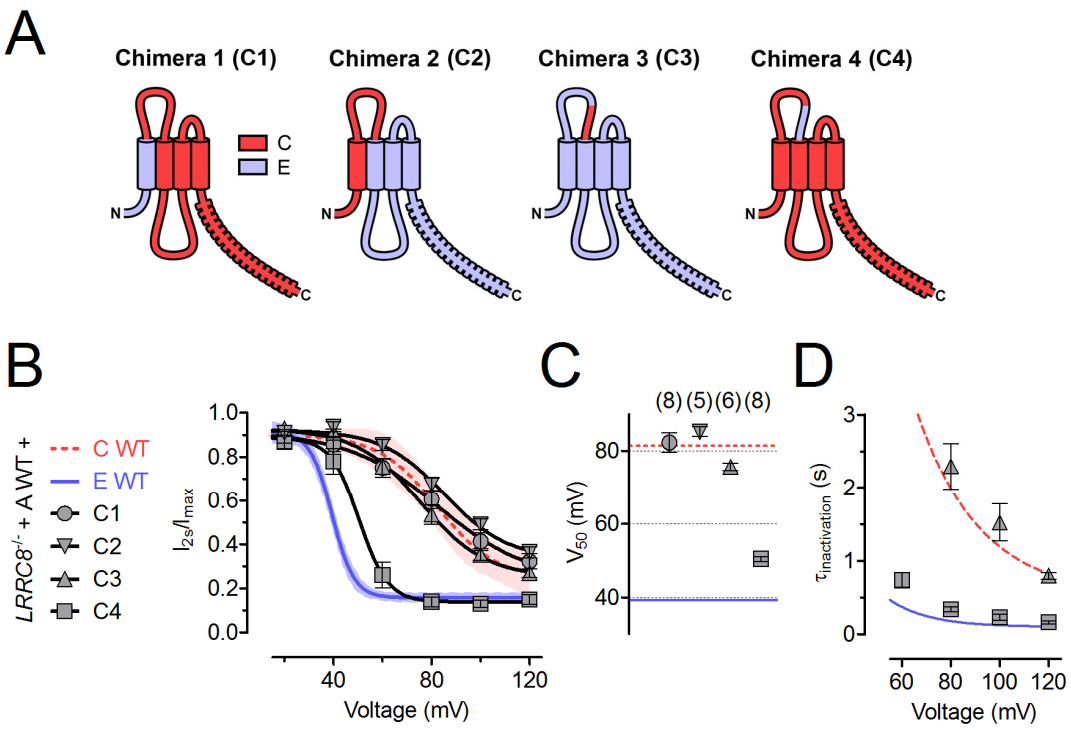

Figure 19 | Part of the ECL1 determines differences in inactivation between LRRC8C and E
(A) Scheme of LRRC8C/E chimeric constructs. Light blue: LRRC8E, red: LRRC8C. **(B)** Inactivation of $I_{Cl,vol}$ mediated by the indicated LRRC8 combinations, assessed by the ratio of current at end/beginning of 2-s-pulse. Solid lines are Boltzmann fits. **(C)** V_{50} values from Boltzmann fits shown in B. Number of cells in brackets. **(D)** Inactivation time constants ($\tau_{inactivation}$) obtained from monoexponential fits to $I_{Cl,vol}$ current traces in response to 2-s-pulses to given voltages. All experiments have been repeated in 5–8 cells. Error bars, SEM.

To corroborate this finding and to further narrow down the region determining inactivation kinetics, we generated a chimera in which part of ECL1 of LRRC8E was substituted for by the homologous LRRC8C segment (chimera 3, $LRRC8E^{1–84,117–796}$/$LRRC8C^{94–125}$, Figure 19A). This chimera also mediated LRRC8C-like inactivation (Figure 19B–D), carving out the importance of LRRC8C residues 94–125 for slow inactivation. Remarkably, the converse chimera, in which these residues in LRRC8C were replaced by the corresponding LRRC8E residues (chimera 4, $LRRC8C^{1–93,126–803}$/$LRRC8E^{85–116}$, Figure 19A) mediated fast inactivation, very similar to that observed in LRRC8E-mediated currents (Figure 19B–D), revealing that LRRC8E residues 85–116 largely account for fast inactivation kinetics.

Sequence comparison between LRRC8C and LRRC8E showed a high level of conservation of this region (Figure 20A). To identify single residues responsible for the differences in inactivation, we introduced point mutations into LRRC8C that changed the respective residues to those found in LRRC8E (Figure 20B–D). While the LRRC8C-to-LRRC8E mutations LRRC8C(T101N) (Figure 20B–D) as well as LRRC8C(M96V), LRRC8C(M114L), and LRRC8C(R118T) (data not shown) resulted in inactivation indistinguishable from LRRC8A/C, the LRRC8C(D102N) mutant exhibited faster inactivation and a substantial left-shift of V_{50} (Figure 20B–D). Although LRRC8C(T101N) had no effect by itself, it further accelerated inactivation in the LRRC8C-to-LRRC8E double-mutant LRRC8C(T101N,D102N), leading to almost LRRC8E-like inactivation (Figure 20B–D), similar to that of chimera 4 (Figure 19). The critical role of LRRC8C Asp102 was further corroborated by the converse LRRC8E-to-LRRC8C mutation LRRC8E(N93D), which exhibited slow inactivation indistinguishable from that mediated by LRRC8C (Figure 20E–G) when co-expressed with LRRC8A. Lack of an effect of the LRRC8E-to-LRRC8C mutation LRRC8E(N92T) alone or within the double-mutant LRRC8E(N92T,N93D) suggested a negligible role of this LRRC8E residue (Figure 20E–G).

For clarity, the position that had the larger influence on inactivation (LRRC8C 102, and LRRC8E 93) will from now on be referred to as position 0 (p0, Figure 20A).

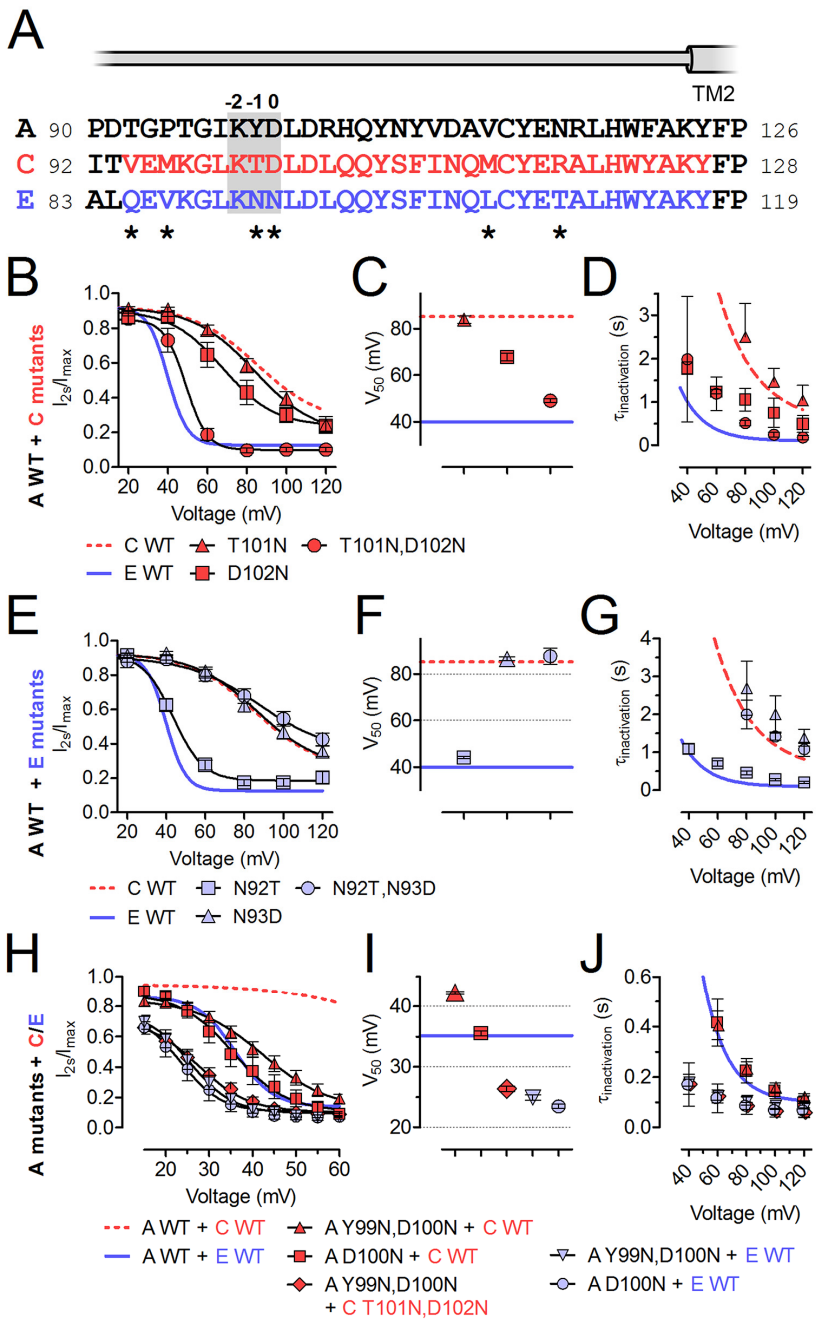

Figure 20 | Two non-conserved residues in the C-terminal part of ECL1 affect $I_{Cl,vol}$ inactivation

(A) Protein sequence alignment of the second half of ECL1 of LRRC8A/C/E. The segment swapped in chimeras 3 and 4 is highlighted in red and blue, respectively. The beginning of predicted TM2 is indicated. According to the UniProt database (UniProt Consortium, 2015), TM1 in LRRC8A ends at L45 while TM2 begins at Y124. LRRC8A residue D102 and the homologous residues in LRRC8C/E are designated as position 0. Residues differing between LRRC8C and -E are indicated by asterisks. **(B–J)** Effects of LRRC8 point mutations on inactivation. **(B–D)** Inactivation of $I_{Cl,vol}$ mediated by LRRC8C mutants or **(E–G)** LRRC8E mutants co-expressed with WT LRRC8A and **(H–J)** LRRC8A mutants co-expressed with WT or mutant LRRC8C/E in *LRRC8*$^{-/-}$ HCT116 cells. **(B,E,H)** $I_{Cl,vol}$ inactivation assessed by ratio of current at end/beginning of 2-s-pulse. Solid lines are Boltzmann fits. **(C,F,I)** V_{50} values from Boltzmann fits shown in B, E and H. **(D,G,J)** Inactivation time constants ($\tau_{inactivation}$) obtained from monoexponential fits to $I_{Cl,vol}$ current traces in response to 2-s-pulses. All experiments have been repeated in 4–12 cells. Error bars, SEM.

3.2.4. LRRC8A also contributes to $I_{Cl,vol}$ inactivation kinetics

Since our results from triple knockout cell lines suggested a role of LRRC8A in inactivation, we compared its sequence in this region to the other isoforms. LRRC8A is similar to LRRC8C in that it contains an Asp at p0 (Asp100, Figure 20A). Since an Asp in this position seemed to produce slow inactivation, we hypothesized that LRRC8A might have a decelerating effect on VRAC inactivation and LRRC8A-to-LRRC8E mutations should therefore accelerate inactivation independent of the co-expressed isoform. Because only the double mutant LRRC8C(T101N,D102N) led to LRRC8E-like fast inactivation (Figure 20B–D), we generated the LRRC8A-to-LRRC8E double mutant LRRC8A(Y99N,D100N) and co-expressed it with LRRC8E in *LRRC8*$^{-/-}$ HCT116 cells. Indeed, LRRC8A(Y99N,D100N)/E inactivated even faster than LRRC8A/E, with inactivation apparent already at ~20 mV (Figure 20H–J) and a slight shift of V_{50} to less positive voltages (Figure 20I). Likewise, currents mediated by LRRC8A(Y99N,D100N)/C inactivated much faster and at less positive potentials than LRRC8A/C (Figure 20H–J). In accord with LRRC8A/C(T101N,D102N) showing LRRC8A/E-like fast inactivation (Figure 20B–D), LRRC8A(Y99N,D100N)/ C(T101N,D102N) inactivated like LRRC8A(Y99N,D100N)/E channels (Figure 20H–J). LRRC8A(D100N) and LRRC8A(Y99N,D100N) displayed almost equal inactivation in heteromers with either LRRC8C or -E (Figure 20H–J), revealing the dominant role of the p0 residue.

3.2.5. Concurrent mutation of key residues in LRRC8s drastically alters $I_{Cl,vol}$

Next, we set out to further elucidate the molecular mechanism of VRAC inactivation by simultaneously mutating the p0 residue in both LRRC8E and LRRC8A to amino acids that are not present at this position in any LRRC8 isoform. We then co-expressed both mutants in *LRRC8*$^{-/-}$ HCT116 cells. Substitution by Ala drastically accelerated inactivation between 30 and 70 mV, an effect that was even more pronounced when positively charged Lys or Arg were inserted (Figure 21A–C) Substitution for negatively charged Glu resulted in slow inactivation comparable to that observed with LRRC8A/C or LRRC8A/E(N93D) (Figure 21A–C, and Figure 20E–G). All p0 mutant combinations still yielded robust $I_{Cl,vol}$ (Figure 21D). Qualitatively similar, but generally less pronounced effects were obtained when mutants of LRRC8A or LRRC8E were co-expressed with the corresponding wild type partners, or when equivalent mutations in LRRC8A and LRRC8C were co-expressed (data not shown). We conclude that residues at p0 are central determinants of $I_{Cl,vol}$ inactivation. Positive and, to a lesser extent, uncharged amino acids in this position led to inactivation that rapidly reached steady state even at mildly positive membrane potentials. In contrast, negative charges caused inactivation to set in only at strongly depolarized potentials, as observed with the

LRRC8A/C combination. Similar inactivation properties in Lys and Arg, or Ala and Asn mutants, respectively, indicate that side chain volume is less important.

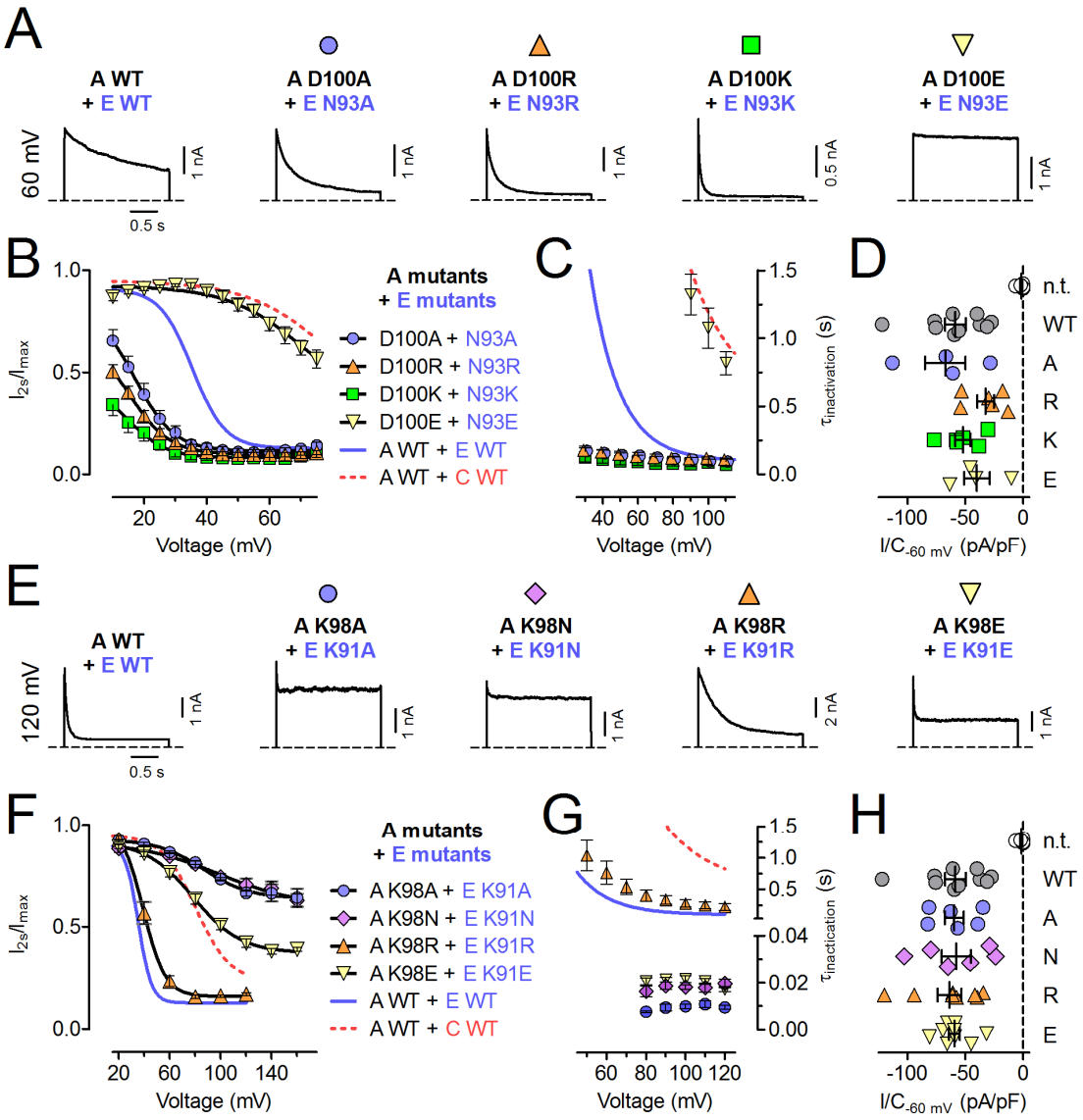

Figure 21 | Charged side chains of residues at p0 and p−2 drastically affect $I_{Cl,vol}$ inactivation

(A–D) Effects of p0 and **(E–H)** p−2 mutations on $I_{Cl,vol}$ inactivation. **(A,E)** Example $I_{Cl,vol}$ currents at indicated voltages mediated by the indicated LRRC8A/LRRC8E mutants co-expressed in *LRRC8*$^{-/-}$ HCT116 cells. **(B,F)** $I_{Cl,vol}$ inactivation assessed by ratio of current at end/beginning of 2-s-pulse. Solid lines are Boltzmann fits. **(C,G)** Inactivation time constants ($\tau_{inactivation}$) obtained from monoexponential fits to $I_{Cl,vol}$ current traces in response to 2-s-pulses. **(D,H)** Current densities of maximally activated $I_{Cl,vol}$ (at −60 mV) mediated by the indicated p0 (D) or p−2 (H) mutant combinations. All p0 and p−2 mutants tested gave rise to robust swelling-activated currents of similar magnitude as observed in WT. All experiments have been repeated in 6–12 cells. Error bars, SEM. n.t., not transfected.

Given the dramatic effects of charged amino acids at p0, we next investigated the role of the conserved Lys at p−2 (Figure 20A). Charge reversal or neutralization of this residue in LRRC8A and LRRC8E strongly altered inactivation when both mutants were co-expressed in *LRRC8*$^{-/-}$ cells, while a charge-conserving mutation to Arg exerted only a minor decelerating effect (Figure 21E–H). In Ala and Asn substitutions, inactivation appeared to be almost absent save for a very fast component that was detected only at the most strongly depolarized potentials (Figure 21E–H). Very fast inactivation was also observed when negatively charged Glu was introduced (Figure 21E–H). The inactivation of currents from p−2 mutants displayed a very shallow voltage-dependence and appeared to saturate at larger remaining currents than observed with WT combinations (>40% of current left vs. ~15% for WT, Figure 21F). Co-expression of LRRC8A wild type or p−2 mutants with LRRC8C WT or p−2 mutants gave results undistinguishable from those obtained with the equivalent LRRC8A/E combinations (data not shown). All p−2 mutant combinations showed robust $I_{Cl,vol}$ amplitudes not different from WT (Figure 21G).

We next asked whether p−2 mutations alter the characteristic $I^- > Cl^-$ selectivity of VRACs. Cells in which $I_{Cl,vol}$ was maximally activated were superfused with solutions in which Cl^- was substituted by I^-, and the resulting shifts in reversal potential (ΔE_{rev}) were used to calculate relative permeabilities. Whereas the mutant combinations LRRC8A(K98A)/E(K91A) and LRRC8A(K98N)/E(K91N) did not alter ΔE_{rev} compared to the WT combination, ΔE_{rev} was significantly smaller for the charge reversal mutants LRRC8A(K98E)/E(K91E), reducing the relative permeability (P_I/P_{Cl}) from 1.25 to 1.12 (Figure 22A–C). None of these mutations significantly changed the NO_3^-, gluconate, or Na^+ permeability of VRACs (Figure 22B). When only one of the two co-expressed LRRC8 subunits contained the p−2 Lys-to-Glu mutation, ΔE_{rev} was only significantly altered in LRRC8A/E(K91E), but not in LRRC8A(K98E)/E, suggesting a larger contribution of LRRC8E to the selectivity of the pore (Figure 22D).

Introduction of p−2 Lys-to-Glu mutations also altered ΔE_{rev} in the LRRC8A/C combination (Figure 22D). As reported by ourselves as well as others (Qiu et al., 2014; Voss et al., 2014), ΔE_{rev} upon iodide substitution was not significantly different between LRRC8A/C and LRRC8A/E heteromers (Figure 22D). We also investigated if p0 mutations affect $I_{Cl,vol}$ selectivity, but did not find significant changes in P_I/P_{Cl} or P_{NMDG}/P_{Na} (Figure 22E).

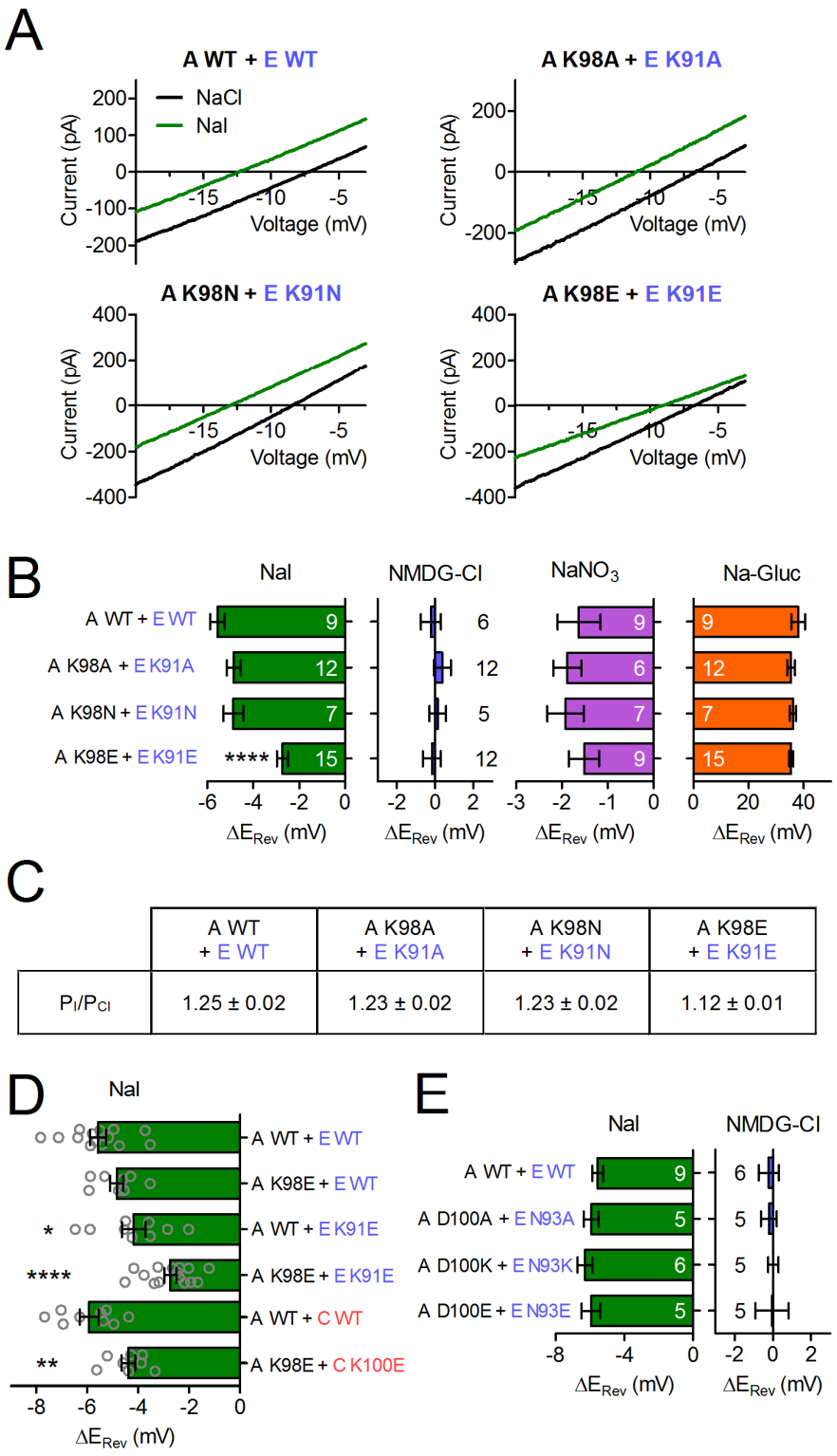

Figure 22 | Charge reversal of the conserved Lys in p−2 affects $I_{Cl,vol}$ anion selectivity
(A) Example $I_{Cl,vol}$ current traces in response to voltage ramps. **(B,D,E)** Relative shifts in reversal potential (ΔE_{rev}) upon substitution of NaCl with the indicated substances. The number of cells is indicated (B,E) or single experiments are plotted (D). Error bars, SEM. *, P < 0.05; **, P < 0.01; ****, P < 0.0001 (one-way ANOVA, Bonferroni's test). **(C)** Relative iodide permeability as calculated from ΔE_{rev}.

4. DISCUSSION

4.1. LRRC8A as an essential component of VRAC

Our findings unambiguously demonstrate that LRRC8A is an essential component of VRAC. Using a genome-wide siRNA screen with a cell line expressing a halide-sensitive YFP variant, we found that knockdown of *LRRC8A* resulted in a strong reduction of swelling-activated I^- influx. This result was confirmed in a secondary screen with independent siRNAs, where the effect was even more pronounced. Furthermore, siRNA-mediated knockdown of *LRRC8A* drastically reduced $I_{Cl,vol}$ in whole-cell patch clamp recordings, and disruption of the gene using the CRISPR/Cas and zinc finger technologies abolished the current completely. The specificities of siRNAs and gene targeting approaches were ascertained by the use of different target sequences within the *LRRC8A* gene.

In most cases, overexpression of an ion channel leads to a pronounced increase in the currents it mediates, even if the channels are already expressed endogenously. Surprisingly, overexpression of LRRC8A in HEK293 cells did not increase $I_{Cl,vol}$, but rather suppressed it to a similar extent as the siRNA-mediated knockdown. We attributed this result to a requirement for hetero-oligomerization of LRRC8A with other LRRC8 proteins to form functional channels, a hypothesis we followed up on in some detail (discussed in section 4.2). However, expression of LRRC8A in *LRRC8A*$^{-/-}$ cells did rescue $I_{Cl,vol}$, demonstrating that VRAC requires the LRRC8A protein.

We found that LRRC8A localizes to the plasma membrane upon overexpression using fluorescently labeled constructs and in native cells using specific antibodies, in agreement with a role as a plasma membrane channel. However, LRRC8A containing a mutation found in a patient with agammaglobulinemia causing a truncation of the C-terminus (Kubota et al., 2004), did not reach the plasma membrane. The reported weak homology of LRRC8 proteins to pannexins and connexins, both of which form plasma membrane channels, is in accordance with the channel hypothesis (Abascal and Zardoya, 2012). However, while the bioinformatical analysis done by Abascal and Zardoya provided strong evidence for a pannexin-like transmembrane topology of LRRC8 proteins, experimental support was lacking. On the contrary, comparison to other LRRD-containing proteins rather suggested an extracellular localization of the LRRC8A LRRD, which would not be compatible with a similar structure as pannexins (Abascal and Zardoya, 2012; Sawada et al., 2003). Therefore, we set out to ascertain the pannexin-like topology in deglycosylation experiments and accessibility studies using mutated or HA-tagged LRRC8A proteins (not shown in this thesis, see Voss et al., 2014). Indeed, we found that the orientation of LRRC8A is similar to that of pannexins: The first and

third loops connecting the putative TM domains are on the extracellular side, while the LRRD-containing C-terminus is located intracellularly. It is therefore tempting to speculate that LRRC8A might, like connexins and possibly pannexins, assemble to hexamers and form an ion-conducting pore.

In addition to the electrophysiological evidence presented in this thesis, we also investigated if LRRC8A is required for two other processes in which VRAC was thought to play a major role: Regulatory volume decrease (RVD) and swelling-activated efflux of the important cellular osmolyte taurine (not shown in this thesis, see Voss et al., 2014). Radioactive ^{3}[H]-Taurine efflux from preloaded WT and *LRRC8A*$^{-/-}$ HEK293 cells subjected to isotonic or hypotonic saline was measured over time. Whereas taurine release was substantially stimulated by hypotonicity in WT cells, no such stimulation was found in *LRRC8A*$^{-/-}$ cells (Voss et al., 2014). Hence, LRRC8A is probably essential for both proposed pathways, the anion channel VRAC and the organic osmolyte channel VSOAC. Because Cl^- and organic osmolytes both drive RVD, we also investigated the ability of LRRC8A-deficient cells to regulate their volume. When cells were subjected to hypotonic saline and cell volume was monitored by calcein fluorescence, a pronounced volume decrease was measured for WT, but not for LRRC8A$^{-/-}$ cells. This is an expected result, as pharmacological inhibition of VRAC causes similar effects (Hoffmann et al., 2009).

On the same day our findings were first published, Ardem Patapoutian and coworkers (Scripps Research Institute, La Jolla, USA) reported on a remarkably similar siRNA screen that also identified LRRC8A as a component of VRAC (Qiu et al., 2014). As in our own screen, HEK293 cells stably expressing an I^--sensitive YFP variant were generated, and the fluorescence quenching of YFP was used as readout for swelling-induced I^- influx through VRAC. However, different siRNA libraries and analysis procedures were employed. In a prescreen similar to ours, Qiu et al. tested siRNAs against the previous VRAC candidates pI_{Cln}, ClC-2, ClC-3, and bestrophin 1, which did not affect YFP quenching, further adding to the many studies refuting their role in $I_{Cl,vol}$. Both, primary and secondary screens yielded *LRRC8A* as the major hit. Knockdown of *LRRC8A* using several different siRNAs reduced the swelling-induced quenching responses to the same extent as the VRAC inhibitor DCPIB. Whole-cell patch clamp experiments revealed that *LRRC8A* knockdown also abolished $I_{Cl,vol}$ in different cell lines.

Furthermore, Qiu et al. found that siRNA-mediated knockdown of *LRRC8A* expression drastically impaired RVD and swelling-induced taurine efflux, closely resembling our own findings.

Since VRAC is ubiquitously expressed, an essential component of the channel should exhibit a broad expression pattern. Whereas we relied on EST databases and

previous reports (Kubota et al., 2004) that indeed suggested a widespread expression of *LRRC8A*, Qiu et al. addressed the issue experimentally by probing different tissues for *LRRC8A* mRNA, confirming the other studies. Experiments aimed to clarify the subcellular localization and membrane topology of LRRC8A were very similar in approach to the ones we conducted. The results again verified that LRRC8A is a plasma membrane protein and has a pannexin-like structure with LRRDs in the cytoplasm, matching its implied role as a channel.

Importantly, Qiu et al. also confirmed our finding that overexpression of LRRC8A does not increase $I_{Cl,vol}$ but rather suppresses it. On the other hand, LRRC8A expression in stable *LRRC8A* knockdown cells restored currents which exhibited all characteristics of $I_{Cl,vol}$, excluding off-target effects. Currents were not rescued by the truncated LRRC8A mutant found in an agammaglobulinemia patient, which fits to our observation that the truncated protein does not reach the plasma membrane but is retained in the endoplasmic reticulum.

To investigate if LRRC8A is part of the VRAC channel itself, Qiu et al. individually mutated all residues within the putative transmembrane segments (TM) to cysteines, expressed these mutants in stable *LRRC8A* knockdown cells and probed if modification by the membrane-impermeable thiol-reactive reagent 2-sulfonatoethyl methane-thiosulfonate (MTSES) affected VRAC function. Out of 62 mutants assessed in the YFP reporter assay, only T44C located at the extracellular end of TM1 led to reduced VRAC activity upon MTSES application. In patch clamp experiments, inward but not outward currents mediated by the T44C mutant were significantly reduced upon MTSES application. While these findings hinted that LRRC8A indeed contributes to the VRAC pore, only an alteration of a channel-intrinsic property such as ion selectivity can be considered more definitive proof. Therefore, Qiu et al. investigated if mutations to T44 alter the characteristic $I^- > Cl^-$ selectivity of VRAC. The relative permeability of I^- (P_I/P_{Cl}) was calculated from reversal potential changes upon replacement of NaCl with NaI. Surprisingly, the structurally conservative mutant T44C displayed an increased P_I/P_{Cl} (1.59 ± 0.02 compared to 1.29 ± 0.03 in WT), while mutation to a positively charged arginine (T44R) decreased P_I/P_{Cl} (1.15 ± 0.03) and a mutant carrying a negatively charged glutamate (T44E) displayed unaltered selectivity. However, the very low currents observed with the T44 mutants increase the risk of a contamination by background currents, which may be an alternative explanation for the rather miniscule changes in P_I/P_{Cl}. Whereas an alteration of ion selectivity caused by a mutation within a protein is generally considered as good evidence for that protein forming the channel pore, a few examples illustrate that caution should be exercised with this interpretation. For instance, the potassium channel β subunit KCNE1 (MinK) can alter the ion selectivity

of the channels it associates with while not forming a pore by itself (Kaczmarek and Blumenthal, 1997).

It is assuring that two completely independent studies arrived at the same conclusions (Qiu et al., 2014; Voss et al., 2014). This convergence certainly strengthens the arguments of both studies and establishes LRRC8A as a protein essential for VRAC function beyond reasonable doubt. However, the notion that LRRC8A contributes to the VRAC pore is not sufficiently backed by the evidence discussed so far. The dependence of VRAC function on LRRC8A expression could equally well be explained by other roles of LRRC8A, e.g. as indispensable β subunit, stabilizing factor or essential part of the signaling cascade leading to VRAC activation.

4.2. VRAC is formed by LRRC8 heteromers

The observation that LRRC8A overexpression suppresses $I_{Cl,vol}$ in HEK293 cells led us to hypothesize that LRRC8A may be part of a multimeric complex which also requires other proteins to function correctly. The obvious candidates for such a hypothesis were the closely related LRRC8 homologs LRRC8B to LRRC8E. Indeed, the suppression effect was not detected when co-expressing LRRC8A and LRRC8C. While fluorescently labeled LRRC8B through LRRC8E on their own did not leave the endoplasmic reticulum upon overexpression, co-expressed LRRC8A efficiently carried them to the plasma membrane. This suggested that the other LRRC8 proteins are also involved in VRAC function, but the fact that these proteins are expressed endogenously by most cell types required an unusual approach to study their functional role. We therefore generated knockout HCT116 cells in which the corresponding genes were disrupted singly or in combinations. While all single LRRC8s except for LRRC8A were dispensable for $I_{Cl,vol}$, currents were reduced in *LRRC8E*$^{-/-}$ and *LRRC8(D/E)*$^{-/-}$ cells, almost abolished in *LRRC8(C/E)*$^{-/-}$ and *LRRC8(C/D/E)*$^{-/-}$ cells; and no current could be evoked in *LRRC8(B/C/D/E)*$^{-/-}$ cells. We also noticed differences in the speed of inactivation between different knockout cell lines. LRRC8C knockout led to a faster inactivation while disruption of LRRC8D, LRRC8E or both yielded currents that inactivated slower than WT. Furthermore, we found that not only $I_{Cl,vol}$ but also swelling-activated taurine efflux depends on LRRC8B–E, as it was fully abolished in *LRRC8(B/C/D/E)*$^{-/-}$ cells. Three conclusions could be drawn from these findings: First, VRAC and VSOAC require LRRC8A and at least one other LRRC8 protein, hinting that they are very likely both formed by LRRC8 heteromers. Second, LRRC8A, LRRC8E, and LRRC8C are the main contributors to the endogenous VRAC in HCT116 cells. And third, the combination of LRRC8 homologues apparently determines the inactivation kinetics of $I_{Cl,vol}$.

These conclusions were further backed by results from overexpression studies in *LRRC8*$^{-/-}$ cells, in which all *LRRC8* genes were disrupted. Rescue of $I_{Cl,vol}$ could not be achieved by expression of LRRC8A alone, but required co-expression of LRRC8A with at least one other LRRC8 protein. However, it has to be noted that while we did not manage to overexpress LRRC8B, modest $I_{Cl,vol}$ could be evoked in *LRRC8(C/D/E)*$^{-/-}$ cells, suggesting that LRRC8B also contributes to endogenous VRACs. Inactivation kinetics depended on the expressed LRRC8 isoform, resembling results from the knockout cell lines: LRRC8A/C mediated slowly inactivating $I_{Cl,vol}$, while LRRC8A/D and LRRC8A/E caused rapid inactivation which saturated within tens of milliseconds. As similarly fast current inactivation in other ion channels is generally mediated by either the pore-forming α-subunits themselves, as observed in Na_V and K_V channels (Catterall, 2012; Hoshi et al., 1990), or closely associated accessory proteins such as K_V β-subunits (Rettig et al., 1994), but cannot be explained by a signal transduction cascade, we concluded that LRRC8 proteins must be an integral part of the VRAC channel.

If LRRC8 proteins indeed form heteromers, as strongly suggested by our functional studies and the observation that LRRC8A facilitates trafficking of LRRC8B–E to the plasma membrane, LRRC8 proteins should physically interact. We could indeed show such an interaction in co-immunoprecipitation experiments (not shown in this thesis, see Voss, 2015; Voss et al., 2014). LRRC8A co-precipitated LRRC8A through LRRC8E and, conversely, LRRC8A through LRRC8E co-precipitated LRRC8A, demonstrating that LRRC8A can interact with all other LRRC8 proteins.

4.3. Molecular mechanisms of VRAC inactivation and permeation

Voltage-dependent inactivation, defined as spontaneous decay of currents after the establishment of a certain transmembrane voltage, is a hallmark of many ion channels. It is most often due to a closure of the channel pore. Whereas fast inactivation is crucial for certain cation channels involved in action potential generation, its biological role is less clear for ion channels like VRACs whose functions are normally not related to fast voltage changes. Voltage-dependent inactivation has been studied in great detail over several decades for various voltage-dependent K^+ and Na^+ channels. Fast N-type inactivation of K_v channels involves a cytoplasmic N-terminal blocking particle that binds to the intracellular opening of the pore (Hoshi et al., 1990, 1991), whereas the mechanism of the slower C-type inactivation is less clear but may involve a constriction of the channel pore (Cuello et al., 2010). In contrast, nothing was known about the structural basis of the inactivation of VRACs, the molecular composition of which remained unknown. We now identified amino acids in the highly conserved extracellular stretch preceding the second transmembrane domain of LRRC8 proteins as key

determinants of inactivation (see section 3.2). Mutations in one of these residues also changed the ion selectivity of VRACs, suggesting that this stretch forms part of the extracellular opening of the ion-conducting pore which might constrict with channel inactivation.

As discussed before, differences in voltage-dependent inactivation of native $I_{Cl,vol}$ (Nilius et al., 1997) can be attributed to tissue-specific expression patterns of LRRC8 isoforms. Analysis of cultured cells expressing the obligatory LRRC8A together with particular other LRRC8 isoforms showed that differences in inactivation were largest between channels containing LRRC8C or -E, which induced the slowest and fastest inactivation of $I_{Cl,vol}$, respectively (see section 3.1.4). Co-expression of different LRRC8C/E chimeras with LRRC8A now identified the C-terminal half of the first extracellular loop (ECL1) as a major determinant of VRAC inactivation. In this stretch we identified the negatively charged Asp102 of LRRC8C, which is replaced by uncharged Asn at this position (p0) in LRRC8E, as a key determinant of channel inactivation. Mutations at p−1 modulated the effect of the p0 mutation on inactivation in LRRC8C, but not in the other subunits tested. The charge, rather than size, of the residue at p0 strongly influenced the rate and voltage-dependence of $I_{Cl,vol}$ inactivation. Likewise the charge at p−2 (Lys in all LRRC8 isoforms but LRRC8B) markedly affected voltage-dependence and kinetics of inactivation, but surprisingly also VRAC's ion selectivity.

The strong influence of charges at positions p−2 and p0 on voltage-dependent inactivation raises the question whether these residues directly act as voltage-sensors. A positive charge at p0 accelerated channel inactivation and shifted its voltage-dependence to the left, whereas negative charges at p−2 shifted the voltage-dependence to the right, but also accelerated inactivation. The similar effect of positive charges at position p−2 and p0 on the voltage-dependence evokes the hypothesis that a putative, and possibly pore-forming, re-entrant loop in the stretch delimited by the glycosylation site and the predicted extracellular end of the second transmembrane span (N83 and Y126, respectively, in LRRC8A) dips into the electric field of the outer mouth of the channel and causes inactivation by an electrostatically induced movement in response to depolarization. However, the observation that neutralization of the positive charge at p−2 leads to a more pronounced right shift of the voltage-dependence of inactivation than charge reversal is difficult to reconcile with this hypothesis, as is the similar effect of opposite charges at p0 and p−2 on inactivation kinetics.

Inactivation of $I_{Cl,vol}$ was not complete, but saturated, depending on the particular channel composition, at maximum values of 80–95% that were asymptotically reached at long times and strong depolarization. Even less complete inactivation was observed with p−2 mutants. Previous single-channel recordings of native $I_{Cl,vol}$ currents suggested that

voltage-dependent inactivation involves the stepwise closure of single VRAC channels that display a single-channel conductance of 50–80 pS at positive potentials (Jackson and Strange, 1995a; Okada et al., 1994; Voets et al., 1997a). Therefore, the current remaining after maximal inactivation may represent the spontaneous flickering of such channels with a low average open probability. However, the observation that LRRC8A/C and LRRC8A/E channels display similar steady state inactivation while showing markedly different time constants for entering, but not for leaving inactivated states, argues against the possibility that steady state inactivation represents an equilibrium of direct transitions between an open and an inactivated state. Instead, inactivation may lead to a partial closure of the pore that would result in a reduced single channel conductance. While such a behavior has not been observed in any of the studies reporting single VRAC currents, the expected small steady state currents (~10%) may have been below the detection limit. High-resolution single channel recordings, especially of p−2 mutants which exhibit much higher steady state currents could help to clarify this issue. However, we failed to record swelling-induced single channel activity in pre-swollen HCT116 cells.

It is instructive to compare our results to those obtained for pannexins and connexins. LRRC8 proteins display weak, but significant sequence homology to pannexin channels (Abascal and Zardoya, 2012), which in turn display structural similarity, but no sequence homology, to gap-junction forming connexins. The highest degree of homology between pannexins and LRRC8 proteins is found in TM1 and TM2 (Abascal and Zardoya, 2012), which in connexins line the pore as revealed by high-resolution structures (Maeda et al., 2009). The homology between pannexins and LRRC8 channels extends about 10 residues beyond the predicted end of TM1 into ECL1. By contrast, there is no significant homology between both channel classes in the C-terminal part of ECL1 (Abascal and Zardoya, 2012) and pannexin hemichannel currents lack conspicuous inactivation (Barbe et al., 2006). Structure-function studies indicated that besides TM1, ECL1 is important for the permeation of both pannexins (Qiu et al., 2012; Wang and Dahl, 2010) and connexins (Kronengold et al., 2003; Trexler et al., 2000). For instance, a change from anion- to cation-preferring hemichannels was observed when ECL1 of connexin32 was replaced by that from connexin46 (Kronengold et al., 2003). Moreover, the crystal structure of connexin26 showed that ECL1 contributes to the formation of the outer pore funnel that contacts the hemichannel from the other cell (Maeda et al., 2009).

In contrast to the very low currents mediated by T44 mutants described by Qiu et al. (2014), the Lys to Glu mutations at p−2 described in this thesis did not reduce current densities and decreased rather than increased the $I^- > Cl^-$ permeability of VRACs. As

expected for a pore-lining residue, the change in selectivity was larger when both co-expressed subunits carried the mutation.

In summary, our results reveal that the portion of the first extracellular loop that directly precedes TM2, and which is highly conserved over a length of 30 amino acids in all mammalian LRRC8 isoforms, plays a pivotal role in the voltage-dependent inactivation of VRACs. Unexpectedly, mutations in this region also change VRAC's ion selectivity and hence suggest that it is in contact with the permeation pathway. I speculate that VRAC inactivation involves a constriction of the pore close to its extracellular opening.

4.4. Selected new findings since the molecular identification of VRAC

The identification of LRRC8 proteins as essential components of VRAC by us and others (Qiu et al., 2014; Voss et al., 2014) has enabled several seminal advances in the understanding of the physiological role and the functional properties of these exciting new channels. The most relevant studies to date will be summarized and discussed in this section.

4.4.1 The *Lrrc8a* knockout mouse

The phenotype of a *Lrrc8a* knockout mouse was published shortly after the role of LRRC8A as an essential component of VRAC was first reported (Kumar et al., 2014). *Lrrc8a*$^{-/-}$ mice showed increased pre- and postnatal lethality, with few animals surviving past an age of 4 weeks and none past 16 weeks. The appearance of newborn *Lrrc8a*$^{-/-}$ animals was described as normal, but after only one week, severe growth retardation and other abnormalities including curly hair, hind limb weakness, progressive hydronephrosis, and sterility were noted. Histological examination exposed various pathologies in skin, muscles, kidney, and ovaries (Kumar et al., 2014). Only homozygous knockout animals exhibited these defects, whereas heterozygous animals were described as normal. The severe phenotype of *Lrrc8a*$^{-/-}$ mice suggests a major physiological role of VRAC in many different tissues. It will be interesting to see how these pathologies relate to volume regulation and the many other physiological processes linked to VRAC.

Kumar et al. further focused on lymphocyte development and function in *Lrrc8a*$^{-/-}$ mice. They found severe impairments of thymic development, thymocyte proliferation and T cell function, while the function of peripheral B cells, which was reportedly perturbed by a truncated version of LRRC8A heterozygously expressed in a patient with agammaglobulinemia (Sawada et al., 2003), appeared to be largely unaffected (Kumar et al., 2014).

Thus, considering that *Lrrc8a*$^{+/-}$ and *Lrrc8a*$^{-/-}$ mice showed no B cell phenotype (Kumar et al., 2014), and that the LRRC8A truncation implied in agammaglobulinemia did not exert a dominant-negative effect on $I_{Cl,vol}$ (Qiu et al., 2014), it may be necessary to reconsider if the LRRC8 truncation was really causative for the observed pathology (Sawada et al., 2003).

Using antibodies against the C-terminus and the loop connecting TM2 and TM3 of LRRC8A, as well as a C-terminally FLAG-tagged LRRC8A construct and anti-FLAG antibodies, Kumar et al. could detect LRRC8A in FACS experiments using non-permeabilized cells. These findings suggested a transmembrane topology where N-terminus, TM2–TM3 loop and LRRD-containing C-terminus of LRRC8A are located on the extracellular side. However, such topology would be in conflict with the topology proposed by Abascal and Zardoya (2012), which was later confirmed independently in both reports identifying LRRC8A as a VRAC component via different albeit similar experimental approaches (Qiu et al., 2014; Voss et al., 2014), as well as another recent study, employing well-controlled FACS experiments (Lee et al., 2014). Given that the majority of experimental evidence suggests a pannexin-like topology, and that the study by Kumar et al. lacks appropriate negative controls (e.g. antibodies against the TM1–TM2 or TM3–TM4 loops) the extracellular localization of the LRRC8A LRRDs can probably be discarded as an experimental artifact (Abascal and Zardoya, 2012; Lee et al., 2014; Qiu et al., 2014; Voss et al., 2014).

Assuming the receptor-like topology, Kumar et al. hypothesized that LRRC8A can be activated by an extracellular ligand. They found evidence that thymic epithelial cells may express such a ligand that promoted thymocyte differentiation and survival in vitro. ‘Activation’ of LRRC8A with a monoclonal anti-LRRC8A antibody and subsequent crosslinking led to AKT phosphorylation. The authors also found that LRRC8A associates with LCK (lymphocyte-specific protein tyrosine kinase), a member of the Src family, which activates AKT through the LCK-ZAP-70-GAB2-PI3K pathway (Kumar et al., 2014). Interestingly, involvement of LCK signaling in VRAC activation has been reported in the past (Lepple-Wienhues et al., 1998). Thus, while it seems unlikely that LRRC8A is a receptor that binds ligands through outward-facing LRRDs, it may be worthwhile to investigate how these signaling pathways relate to the activation of VRAC.

4.4.2 Excitatory amino acid release from astrocytes requires LRRC8A

After learning that VRAC depends on LRRC8 expression, the research group of Alexander A. Mongin (Albany Medical College, Albany, USA) rapidly investigated the proposed role of the channel in the release of excitatory amino acids (see section 1.2.4) from primary rat astrocytes (Hyzinski-García et al., 2014). Quantitative RT-PCR revealed that these cells express *LRRC8A*, *LRRC8B*, *LRRC8C*, and *LRRC8D* at a ratio of

approximately 1:2:2:2, while *LRRC8E* was only poorly expressed. This finding is compatible with the very slow inactivation of $I_{Cl,vol}$ in astrocytes (see Table 1). As expected from many studies relying on pharmacological inhibition of VRAC, siRNA-mediated knockdown of LRRC8A led to dramatically reduced release of aspartate, glutamate and taurine in response to hypotonic stimuli (Hyzinski-García et al., 2014). ATP-stimulated release of aspartate and taurine in non-swollen astrocytes was also abolished, adding to the evidence for a role of VRAC in physiological gliotransmission.

4.4.3 LRRC8D is essential for cellular blasticidin S uptake

A specialized role for LRRC8D in drug transport was first suggested in a report appearing shortly after publication of the identification of LRRC8 proteins as essential VRAC constituents (Lee et al., 2014). In a preceding study, the same authors found *LRRC8A* and *LRRC8D* as hits in a genetic screen for endogenous NF-κB inhibitors, which used cells carrying a transcriptional reporter that drives the expression of a gene conferring resistance to the antibiotic blasticidin S (BlaS; Lee et al., 2013). While cells containing gene-trap insertions in *LRRC8A* and *LRRC8D* were indeed resistant to BlaS, no defects in NF-κB regulation were found. Noting that other genetic screens in which tunicamycin and 3-bromopyruvate were used as selecting agents actually identified transporters for these substances, the authors hypothesized that LRRC8A and LRRC8D may likewise be involved in the cellular uptake of the large, polar BlaS molecule. To test this hypothesis, they measured cellular BlaS levels in a LC/MS-based assay and found drastically reduced BlaS contents in LRRC8D-deficient KBM7 cells when compared to WT cells. Thus, LRRC8D deficiency indeed leads to defective BlaS uptake. LRRC8A and to a lesser extent also LRRC8D were detected at the plasma membrane, as is required for an uptake pathway.

A role of LRRC8 proteins in solute transport would be in accord with the proposed similarity of LRRC8s to channel-forming pannexins (Abascal and Zardoya, 2012), which have been shown to conduct larger substrates such as ATP (Bao et al., 2004; Chekeni et al., 2010; Penuela et al., 2013). To investigate if LRRC8s indeed have the same transmembrane topology as pannexins, Lee et al. conducted a series of well controlled experiments, revealing that both LRRC8A and LRRC8D have a cytosolic C-terminus like pannexins. These findings are entirely consistent with the topology found by Qiu et al. (2014) and us (Voss et al., 2014). Finally, Lee et al. could show that LRRC8A, LRRC8B, LRRC8C and LRRC8D stably interact in biochemical assays, again confirming our findings.

4.4.4 Specialized VRACs mediate organic osmolyte and drug transport

In a more recent study, we revisited the role of VRAC in drug resistance, apoptosis, and organic osmolyte transport in a collaborative effort together with the groups of Sven Rottenberg (Bern) and Piet Borst (Amsterdam, Planells-Cases et al., 2015). Although I was involved in this work, it was highly collaborative and therefore my contributions do not stand alone. I therefore decided not to include them in the results section of this thesis. However, since this study substantially expands our understanding of how LRRC8 proteins determine VRAC function and because they uncovered a new and unexpected role of VRAC in drug transport, I want to summarize and discuss them in some detail here.

A genome-wide gene-trap mutagenesis screen was used to identify mediators of carboplatin and cisplatin resistance in haploid KBM7 cells. Cells that resisted carboplatin treatment accumulated insertions disrupting *LRRC8A* and, more prominently, *LRRC8D*. *LRRC8D*-deficent cells generated for the study investigating LRRC8D-dependent blasticidin S uptake (Lee et al., 2014) were more resistant to clinically relevant concentrations of cisplatin and carboplatin, but not to the larger oxaliplatin.

We next asked whether Pt-drug resistance correlates with $I_{Cl,vol}$ and cell volume regulation. KBM7 and KBM7-derived HAP1 cells in which *LRRC8D* was disrupted displayed unchanged $I_{Cl,vol}$ current densities and gating behavior when compared to WT cells, while no VRAC currents could be elicited in *LRRC8A*$^-$ HAP1 cells. These results resemble our findings in HCT116 cells which required LRRC8A for $I_{Cl,vol}$, while LRRC8D was dispensable (Figure 12, Voss et al., 2014). RVD, like $I_{Cl,vol}$, depended on LRRC8 heteromers in HEK293 cells because it was similarly abolished in *LRRC8A*$^{-/-}$ and *LRRC8(B/C/D/E)*$^{-/-}$ clones. Surprisingly, RVD was also mildly impaired in *LRRC8D*$^{-/-}$ cells, suggesting that LRRC8D-containing VRACs, while being dispensable for $I_{Cl,vol}$, contribute to cell volume regulation.

Because VRAC is thought to be involved in the induction of apoptosis through AVD (section 1.2.4; Maeno et al., 2000; Shimizu et al., 2004), and high concentrations of platinum anti-cancer drugs induce apoptosis, it is tempting to speculate that the Pt-drug resistance of *LRRC8* knockout cells is at least partially due to an impairment of their ability to undergo programmed cell death. To test this hypothesis, we monitored caspase activity as a marker for apoptosis in cells treated with high amounts of cisplatin and staurosporine. Indeed, caspase induction by cisplatin was significantly reduced in *LRRC8A*$^{-/-}$, *LRRC8D*$^{-/-}$ and *LRRC8*$^{-/-}$ cells. Staurosporine-induced caspase activity was strongly reduced in *LRRC8A*$^{-/-}$ and *LRRC8*$^{-/-}$ cells but largely unaffected in *LRRC8D*$^{-/-}$ cells, thus resembling $I_{Cl,vol}$ in its LRRC8-dependence. It is thought that activation of VRAC by pro-apoptotic stimuli leads to AVD, which is an obligate early step in the

initiation of apoptosis (see section 1.2.3). If this is indeed the case, it should be possible to observe VRAC activity after exposing cells to such stimuli. While others were able to record a current resembling $I_{Cl,vol}$ a few minutes after acutely applying staurosporine or Fas-ligand to cells patched in the whole-cell configuration (Shimizu et al., 2004), we could not observe such a rapid activation in HeLa, HEK293 or HCT116 cells within 30 minutes after application (unpublished observation). However, when monitoring $I_{Cl,vol}$ through the YFP-quenching assay used in the genome-wide screen, we recorded a slow but robust activation in cells treated with cisplatin and staurosporine, an effect that was absent in *LRRC8A*$^{-/-}$ cells. Thus, as suggested before, VRAC is indeed activated by pro-apoptotic stimuli, and because cells lacking essential VRAC constituents were protected from drug-induced apoptosis, the resulting AVD is probably an important step facilitating programmed cell death. While several other studies already suggested that this is the case (see sections 1.2.3 and 1.2.4), our work provides the first solid evidence not based on unspecific pharmacological manipulations.

When applying the pro-apoptotic stimuli under hypotonic conditions, we were surprised to find that caspase induction by cisplatin, but not by the larger staurosporine, was drastically increased when compared to isotonic conditions. The effect depended on VRAC since it was completely abolished in *LRRC8A*$^{-/-}$ and *LRRC8*$^{-/-}$ cells, and reduced in *LRRC8D*$^{-/-}$ cells. This hinted that cisplatin may enter cells through VRACs opened by cell swelling. Indeed, it is assumed that only about 50% of cisplatin enters cells by passive diffusion, while the other 50% depend on an as of yet unknown protein component, the absence of which may be a major hallmark of cellular cisplatin resistance (Gately and Howell, 1993).

To test more rigorously if VRAC is indeed a pathway for Pt-drug uptake, we measured cellular Pt contents under various conditions. Isotonic cisplatin uptake was reduced in *LRRC8A*$^{-/-}$ and *LRRC8D*$^{-/-}$ HEK293 cells, but only after long uptake periods of >4 hours, while Pt contents were unchanged in *LRRC8C*$^{-/-}$ cells. Likewise, isotonic uptake of carboplatin was diminished in *LRRC8D*$^{-}$ KBM7 cells. Because LRRC8D is dispensable for $I_{Cl,vol}$, but apparently important in Pt-drug uptake, we hypothesized that LRRC8D-containing VRACs may have an increased permeability for larger transport substrates such as cisplatin. To study the role of different LRRC8 heteromers in isolation, we analyzed *LRRC8(B/D/E)*$^{-/-}$ and *LRRC8(B/C/E)*$^{-/-}$ cells, which only express LRRC8A/C and LRRC8A/D heteromers, respectively. While VRACs containing LRRC8A/D mediated normal cisplatin uptake, in cells only expressing LRRC8A/C it was reduced to the same extent as in *LRRC8A*$^{-/-}$ cells. Differences in hypotonic cisplatin uptake were even more pronounced. Hypotonic uptake was completely abolished in *LRRC8A*$^{-/-}$ cells, but was only reduced by ~50% in *LRRC8D*$^{-/-}$ cells and unaffected in

LRRC8C$^{-/-}$ cells. Results from triple knockout cells resembled those under isotonic conditions: While LRRC8A/D heteromers supported robust hypotonicity-induced cisplatin uptake, only low uptake was observed in cells expressing LRRC8A/C. We also measured $I_{Cl,vol}$ in those cell lines and found similar current densities in WT, *LRRC8D*$^{-/-}$ and *LRRC8(B/D/E)*$^{-/-}$ cells (expressing LRRC8A/C), but significantly lower currents in *LRRC8(B/C/E)*$^{-/-}$ cells (expressing LRRC8A/D). Thus, LRRC8D-containing VRACs have a much higher cisplatin/Cl^- transport ratio than VRACs containing LRRC8C or the mixtures found endogenously.

If VRAC is indeed responsible for the uptake of chemotherapeutic drugs, tumors may select against it during the acquisition of resistance to those drugs. We analyzed data from ovarian cancer patients treated with Pt-drugs for a correlation of survival with expression of *LRRC8A* or *LRRC8D*. While reduced *LRRC8A* expression had no effect on survival, patients with a lower expression of *LRRC8D* displayed significantly reduced survival. We hypothesize that while both LRRC8A and LRRC8D are important for Pt-drug uptake, *LRRC8A* downregulation may be selected against because functional VRAC is crucial for tumor cell proliferation due to its essential role in volume regulation. On the other hand, *LRRC8D* is dispensable for this task and can thus be downregulated without harm. We concluded that LRRC8D is also partially responsible for tumor Pt-drug resistance in patients. However, further studies are required to experimentally confirm these findings, as they are solely based on data from expression databases.

A high-throughput pharmacology screen conducted in our lab had revealed a modest blocking effect of cisplatin on VRAC transport when initially dissolved in DMSO. However, DMSO-free cisplatin did not exert a measureable effect. Cisplatin reacts with DMSO to form adducts such as $Pt(NH_3)_2(Cl)(DMSO)$ (Fischer et al., 2008), which may explain the requirement of DMSO for VRAC inhibition. When directly measuring effects of cisplatin-DMSO on $I_{Cl,vol}$, we found that the block develops very slowly with time. Since VRAC currents are not stable but change with time, the onrate of the block could not be measured reliably. We therefore resorted to a 30-min pre-incubation of cells with cisplatin-DMSO and found $I_{Cl,vol}$ to be blocked in a dose-dependent manner. High concentrations of cisplatin (200 µM, with 0.3% DMSO) reduced currents by 50–70%, and affected currents equally at voltages between −100 and 100 mV. The blocking effect depended on the presence of LRRC8D, demonstrating that differently composed VRACs can be specifically targeted by pharmacological means. It is tempting to speculate that cisplatin-DMSO adducts may occlude LRRC8D-containing channels by entering the pore but not passing due to the increased molecular size, whereas cisplatin cannot enter the pore of channels not containing LRRC8D and therefore does not block them. However,

due to the slow onset of the inhibition and our inability to elicit single channel activity in our cells, we could not find any evidence for a pore block mechanism.

As we had previously shown, swelling-induced release of taurine depends on LRRC8 heteromers. Given the importance of LRRC8D in drug transport, the role of different LRRC8 isoforms in taurine transport was also investigated in more detail. While *LRRC8D*$^{-/-}$ cells exhibited unaltered $I_{Cl,vol}$ when compared to WT cells, swelling-induced taurine efflux was strongly reduced. This result is compatible with the finding that *LRRC8D*$^{-/-}$ cells also show impaired volume regulation. RVD is not carried solely by the extrusion of KCl, but also of uncharged organic osmolytes like taurine that do not contribute to measureable $I_{Cl,vol}$. Experiments in triple knockout cell lines revealed that the LRRC8A/D combination supports substantial taurine fluxes, while fluxes in LRRC8A/C- and LRRC8A/E-expressing cells were only marginally greater than in *LRRC8A*$^{-/-}$ controls. Furthermore, LRRC8-dependent taurine fluxes were not only induced by swelling, but also by long-term incubation with cisplatin.

In summary, our study found that VRAC conducts the anticancer drugs cisplatin and carboplatin as well as the important cellular osmolyte taurine in a largely LRRC8D-dependent manner. In addition to its role in the uptake of pro-apoptotic drugs, we also found VRACs to be directly activated by pro-apoptotic stimuli, which increased VRAC-dependent drug uptake even more and independently led to facilitation of apoptosis, possibly through AVD. This dual role of VRACs in Pt-drug action is illustrated in Figure 23.

While we did not investigate apoptosis in detail and induction of apoptosis is assumed by some to be only a secondary effect of clinically irrelevant high Pt-drug concentrations, VRAC-deficient cells also exhibited strongly decreased caspase induction by staurosporine, a drug commonly used to induce apoptosis that is not taken up via VRACs. Therefore, our results add to the existing evidence that VRAC is an important part of the apoptosis induction machinery, possibly mediating apoptotic volume decrease. Further research is required to elucidate the impact of VRAC disruption on apoptosis induction and the underlying molecular mechanisms.

The special role of LRRC8D in taurine and drug transport makes this VRAC subunit especially interesting for further research. Specific disruption of LRRC8D could be used to estimate the differential contributions of halides and organic osmolytes to cell volume regulation. As LRRC8D expression correlated with survival of Pt-drug treated cancer patients, it may be used as a marker to predict drug responsiveness of tumors and to improve chemotherapy success rates. LRRC8D-containing VRACs could also be interesting targets for potential activators that may specifically increase Pt-drug uptake.

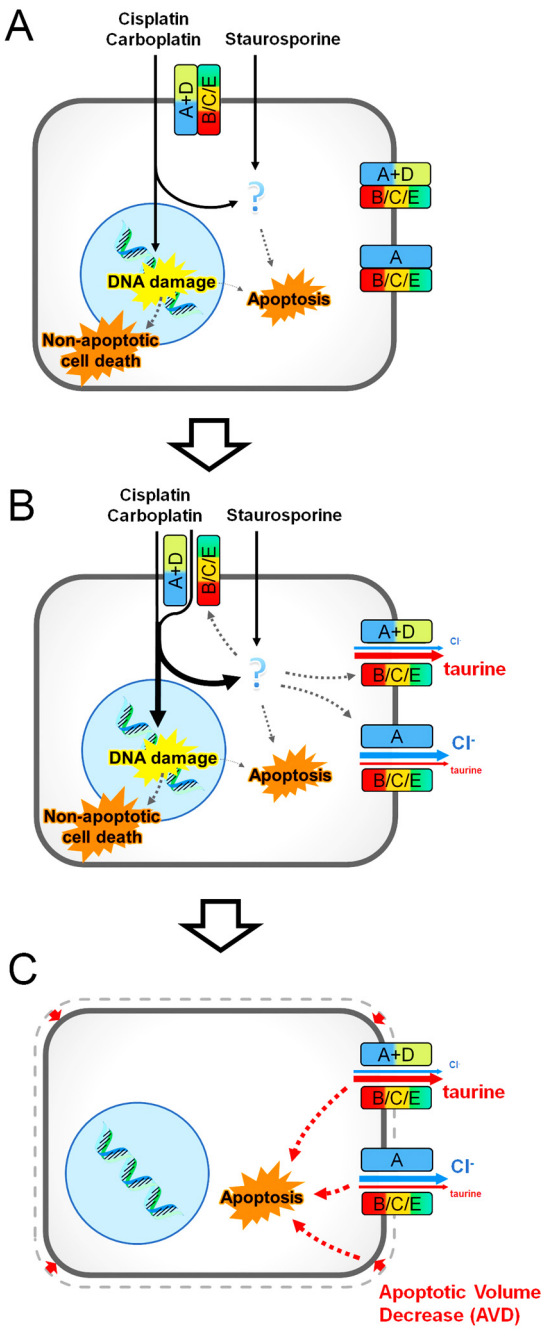

Figure 23 | Dual role of VRACs in drug uptake and apoptosis

(A) Anticancer drugs cisplatin and carboplatin and the pro-apoptotic staurosporine enter cells through passive diffusion. Pt-based drugs induce non-apoptotic cell death, and to a lesser extent, apoptosis through DNA damage, while both Pt-based drugs and staurosporine can induce apoptosis through an additional, poorly characterized pathway (indicated by "?"). **(B)** Pro-apoptotic stimuli also activate VRACs, which mainly transport osmolytes but also provide a further pathway for uptake of Pt-based drugs, but not for the larger staurosporine. Incorporation of the LRRC8D subunit greatly increases the permeability of VRACs for taurine and Pt-drugs. Therefore, disruption of the essential VRAC subunit LRRC8A, but also of LRRC8D reduces transport of Pt-drugs and taurine. **(C)** Cl^- and organic osmolyte efflux through drug-activated VRACs trigger AVD, which facilitates the progression of apoptosis. Thus, apoptosis induction by both, the VRAC-permeable cisplatin and the impermeable staurosporine is supressed upon disruption of the essential VRAC subunit LRRC8A. A, B, C and D indicate the different LRRC8 subunits.

Finally, the finding that the substrate specificity of VRACs depends on their LRRC8 subunit composition is strong evidence that LRRC8 proteins indeed form the VRAC pore. Given that LRRC8A may coassemble with LRRC8B–LRRC8E in hexamers or even higher-order multimers (see sections 4.4.5 and 4.5), there may be a great diversity of different VRACs with distinct permeation properties, even within one cell. Furthermore, the stoichiometry of LRRC8 subunits within one channel complex may also determine its selectivity. We may thus expect many different VRACs even when the complexity of expressed LRRC8 isoforms is reduced in triple knockout cells, possibly explaining why we could observe both taurine fluxes and $I_{Cl,vol}$ in *LRRC8(B/C/E)*$^{-/-}$ cells (only expressing LRRC8A/D). This hypothesis is very attractive because it offers a simple solution for the

problem of how one channel can so strongly select anions over cations, but also conduct much larger uncharged substrates. It may also explain the apparent differences between anion selective 'VRACs' and organic osmolyte conducting 'VSOACs' (see section 1.2.1.1). Much additional research is required to clarify how the heteromeric assembly of LRRC8 proteins affects the selectivity of VRACs and to identify the molecular determinants for the distinct permeability profiles conferred by different LRRC8s.

4.4.5 Functional reconstitution of purified LRRC8 complexes

In a study from the Patapoutian lab published in early 2016, it was demonstrated that purified LRRC8 complexes mediate anion currents activated by osmolarity changes when reconstituted into lipid bilayers (Syeda et al., 2016).

Affinity purification of a C-terminally FLAG-tagged LRRC8A stably expressed in HeLa cells yielded complexes that ran at approximately 800 kDa on native gels. Reactivity with a specific anti-LRRC8A antibody and mass spectrometry analysis of the purified ~800 kDa band confirmed that it contained LRRC8A. Peptides derived from all other LRRC8 family members were detected in high abundance, hinting that these isoforms are efficiently co-purified. The mass spectrometry results gave no indication for the presence of non-LRRC8 proteins in the complex. Whereas the 800 kDa band would suggest an octamer of LRRC8s, native gels commonly overestimate the size of membrane protein complexes. Therefore, the authors were noncommittal regarding the actual oligomeric state of LRRC8 complexes, which may contain six to eight LRRC8 proteins.

Upon reconstitution of LRRC8 complexes in a droplet lipid bilayer system, channel activity was only observed upon stimulation with hypotonicity. A broad spectrum of single channel conductances between 10 pS and 50 pS at −100 mV was reproducibly recorded from these preparations. Currents did not require ATP on either side, were blocked by DCPIB and reduced in amplitude when Cl^- was substituted for with gluconate. While the selectivity and pharmacology match typical $I_{Cl,vol}$, the lack of ATP-dependence and voltage-dependent inactivation do not. Another conundrum is the large variety of unitary conductances which had not been reported for canonical VRACs (see section 1.2.1.3).

The authors then explored the contribution of different LRRC8 isoforms to the observed conductances by purifying LRRC8 complexes from triple knockout cell lines expressing only LRRC8A together with one other isoform, LRRC8C, LRRC8D or LRRC8E. Remarkably, the observed unitary conductances were much more limited with these simplified heteromers, with each combination covering a certain part of the spectrum observed in preparations from WT cells (LRRC8A/C: 35–47 pS, LRRC8A/D: 14–19 pS, and LRRC8A/E: 23–33 pS at −100 mV) Thus, the single channel conductance of VRACs depends on their subunit composition, a finding that is compatible with our

results for taurine and cisplatin (Planells-Cases et al., 2015). The authors were not able to record whole-cell $I_{Cl,vol}$ in *LRRC8(B/C/D/E)*$^{-/-}$ cells, which is in accord with our results (Voss et al., 2014). However, a distinct channel activity was mediated by homo-multimeric LRRC8A complexes purified from these cells. The current was only seen at inside-negative potentials and exhibited a much lower unitary conductance (8–16 pS) than those observed with heteromeric VRACs. It was however sensitive to the somewhat specific VRAC inhibitor DCPIB. Hence, LRRC8A homomers may be able to mediate anion currents under certain experimental conditions. It is currently unclear whether this is physiologically relevant or an experimental artifact associated with bilayer recordings.

To verify that the LRRC8 subunit composition determines VRAC unitary conductance also in cells, the authors then recorded single channels in on-cell patches from pre-swollen HeLa cells. Despite the technical limitations of this method, the results from bilayer recordings were qualitatively confirmed in *LRRC8(B/D/E)*$^{-/-}$ and *LRRC8(B/C/E)*$^{-/-}$ cells, which exhibited greater and smaller single channel conductances, respectively.

The macroscopic rectification of $I_{Cl,vol}$ was previously described to be a result of the rectification of the unitary conductance of VRAC (see section 1.2.1.3). In bilayer experiments, Syeda et al. found no difference in the ratios of single channel conductances at 100 mV and −100 mV between VRACs composed of LRRC8A/C, LRRC8A/D and LRRC8A/E. Consequently, while LRRC8 heteromers formed single channels with different conductances, all of them exhibited similar intrinsic rectification with a rectification ratio (100 mV / −100 mV) of ~1.8. However, the ratio of single channel open probabilities (P_o) at 100 mV and −100 mV was significantly greater with LRRC8A/D heteromers than with the LRRC8A/C and LRRC8A/E combinations, which should result in a more pronounced outward rectification of macroscopic currents. Indeed, macroscopic currents from *LRRC8(B/C/E)*$^{-/-}$ cells rectified more strongly than those from *LRRC8(B/D/E)*$^{-/-}$ or *LRRC8(B/C/D)*$^{-/-}$ cells. We also observed a similar rectification behavior in HEK293 knockout cells (unpublished observation). It has to be noted, however, that apparently the gating behavior of VRACs in bilayers differed from that in cells, as illustrated by the conspicuous lack of inactivation at 100 mV.

To further demonstrate that LRRC8C–E contribute to the VRAC pore, the authors then measured I^- versus Cl^- permeability ratios (P_I/P_{Cl}) in *LRRC8(B/C/D/E)*$^{-/-}$ cells transfected with WT LRRC8C, LRRC8D or LRRC8E, or T44C mutants thereof, as the Patapoutian lab had previously reported that this mutation alters the characteristic P_I/P_{Cl} of $I_{Cl,vol}$ when present in LRRC8A (Qiu et al., 2014). Surprisingly, all LRRC8 combinations led to slightly but significantly different P_I/P_{Cl} ratios. Furthermore, the T44C mutation generally increased P_I/P_{Cl} to a similar extent, regardless of the LRRC8 isoform harboring

it. These results are in conflict with our own data, as we did not find altered P_I/P_{Cl} ratios in several different knockout cell lines or in rescue experiments (Figure 15). We also could not reproduce the results for the T44C mutation, which in our hands led to a drastic reduction of $I_{Cl,vol}$, but did not alter P_I/P_{Cl}, even when present in both, LRRC8A and the co-expressed subunit (unpublished observation).

Finally, Syeda et al. examined different hypotheses for the activation mechanism of VRAC in their lipid bilayer system. Volume increase and membrane stretch were simulated by asymmetrically increasing the volume of *cis* or *trans* droplets through injection of solution during the recording. This activated mechanosensitive MscS channels used as a positive control, but failed to activate VRACs. Next, ionic strength was symmetrically reduced while keeping the osmolarity constant by using solutions in which KCl was substituted for mannitol. This induced robust DCPIB-sensitive currents with LRRC8A purifications from all available triple knockout cell lines. It was concluded that differently composed VRACs can be activated by reduced ionic strength in a minimal lipid bilayer system; confirming earlier studies which proposed that VRAC is activated by ionic strength alterations instead of directly sensing volume changes (see section 1.2.3).

In summary, this impressive study demonstrated that LRRC8 complexes, probably hexamers, are sufficient to form the VRAC pore via several converging lines of evidence. LRRC8A was able to form channels with some limited functionality, but for full VRAC activity, at least one of the other isoforms LRRC8C–LRRC8E was required. It was further shown that LRRC8C–LRRC8E also contribute to the VRAC pore and shape its single channel conductance, voltage-dependent gating and the extent of its $I^- > Cl^-$ selectivity. Finally, LRRC8 channels were directly gated by ionic strength in bilayers. The most obvious interpretation of these results is that VRAC is solely formed by LRRC8 proteins, which also contain a sensor for changes in ionic strength that opens the channel. However, the requirement for an obligatory non-LRRC8 component, while unlikely, cannot fully be excluded. Mass spectrometry did not detect any significant signal for non-LRRC8 proteins in the 800 kDa complex, but this might just reflect low abundance. Because the bilayer system selects for functional complexes, very low amounts of an essential β subunit or ionic strength sensor could be sufficient to measure currents.

All in all, Syeda et al. could unambiguously show that low ionic strength leads to activation of VRAC in a minimalistic functional assay, confirming previous studies (Sabirov et al., 2000; Voets et al., 1999). However, it remains unclear how the many other proposed mechanisms of activation and modulation are integrated by VRACs. While several questions remain, the study provides ample evidence that LRRC8 proteins indeed form the VRAC pore, whose biophysical properties depend on the subunit composition.

4.5. Outlook

The identification of LRRC8 heteromers as constituents of VRAC has opened an entirely new avenue of research devoted to the physiological role of this long elusive channel and its structure-function relationship.

An essential role in cell volume regulation and several other functions in physiology and pathophysiology have been previously proposed for VRAC as the result of a great number of studies, but all these relied heavily on unspecific inhibitors (see section 1.2.4). Now that we know that LRRC8 proteins form the channel, disruption of *LRRC8* genes can be utilized to specifically eliminate VRACs in cells or organisms and to study the consequences in detail.

The constitutive *Lrrc8a*$^{-/-}$ mouse was published shortly after the initial identification of LRRC8 proteins as VRAC components (Kumar et al., 2014). The severe defects found in many different tissues from these animals confirmed the great importance of the channel (see section 4.4.1). However, because only few *Lrrc8a*$^{-/-}$ mice survive long enough to study their complex phenotype in depth, the constitutive knockout may not be optimal to elucidate the physiological roles of VRAC. Tissue specific *LRRC8A* knockouts that can be generated with the Cre/LoxP system are probably better suited to do so. Apart from LRRC8A, whose disruption renders VRAC nonfunctional, the generation of knockouts of other *Lrrc8* genes in mice may help to resolve the question if any of these serve specific roles, as suggested by the dependence of VRAC permeation properties on the co-expressed LRRC8 isoforms described by ourselves and others (Planells-Cases et al., 2015; Syeda et al., 2016). In this regard, the LRRC8D subunits appears most promising as it was found to dramatically increase VRAC's permeability for drugs and organic osmolytes (Planells-Cases et al., 2015). For the elucidation of possible tissue-specific roles of the different LRRC8 proteins, it is also necessary to precisely clarify where they are expressed — and where not.

In addition to its physiological role, the identification of VRAC now permits the study of its structure-function relationship. LRRC8 proteins are only distantly related to pannexins and connexins and therefore represent an entirely new ion channel family. Topics like gating by ionic strength or cell swelling, pore architecture and overall structure are of special interest as they may uncover new biological concepts.

The many wrong candidates that have been proposed to form VRAC raised the bar for new approaches to finally identify this elusive channel. However, the evidence for LRRC8 heteromers forming the VRAC pore is by now overwhelming: The subunit composition of VRACs determined their permeability for Pt-drugs and the important osmolyte taurine (Planells-Cases et al., 2015), as well as their biophysical properties such as unitary conductance, rectification (Syeda et al., 2016) and voltage-dependent

inactivation (this work, Ullrich et al., 2016; Voss et al., 2014). Mutation of several key residues in LRRC8 proteins also altered their characteristic $I^- > Cl^-$ selectivity (this work, Qiu et al., 2014; Syeda et al., 2016; Ullrich et al., 2016). Furthermore, reconstituted LRRC8 proteins were sufficient to induce $I_{Cl,vol}$-like currents, hinting that LRRC8 heteromers are sufficient to form fully functional VRACs.

However, several observations still point to the requirement for another protein. If LRRC8 complexes are indeed sufficient to form functional VRACs, it is puzzling why whole-cell $I_{Cl,vol}$ is not increased by their overexpression. Similarly, no VRAC activity could thus far be induced by expressing LRRC8 proteins in *Xenopus* oocytes. This could in principle be due to the requirement for a limiting factor, such as an obligatory β subunit. An example where this was indeed the case is the Ca^{2+} release-activated Ca^{2+} channel (CRAC) formed by Stim and Orai proteins. Stim1 and Orai1 were both identified as components of CRAC, but overexpression of neither of them did lead to substantial increases in CRAC currents (Feske et al., 2006; Liou et al., 2005; Roos et al., 2005; Vig et al., 2006). However, co-expression of Orai1 with Stim1 drastically increased currents (Mercer et al., 2006; Peinelt et al., 2006). It is now known that Stim1 forms the Ca^{2+} sensor of CRAC (Cahalan, 2009), while Orai proteins are the pore-forming subunits (Hou et al., 2012). Potential LRRC8 interaction partners could for example be identified by mass spectrometry screening approaches. Furthermore, the data obtained in our whole-genome siRNA screen may still contain hints which proteins may be involved in VRAC activation.

An alternative explanation for the lack of current increase upon LRRC8 overexpression could be that the LRRC8 subunit stoichiometry is the limiting factor. For instance, currents induced by recombinant expression of heteromeric acetylcholine receptors depended strongly on the expression ratio of the different subunits (Eertmoed et al., 1998). This hypothesis is compatible with the observed current suppression upon overexpression of LRRC8A in WT cells. Moreover, as the pore properties of VRACs depend on the subunit composition, it is also feasible that stoichiometry affects permeability or gating. As discussed in section 4.4.4, VRACs incorporating more LRRC8D subunits may exclusively conduct organic osmolytes, while other stoichiometries may give rise to halide-selective channels. However, expression ratios are difficult to control in plasmid-transfected mammalian cells. The *Xenopus* oocyte expression system in which the ratios of expressed protein can be finely tuned by adjusting the amounts of injected RNA could help to solve the question how different LRRC8 stoichiometries affect VRAC function. Alternatively, artificial LRRC8 concatemers could be constructed to fix the subunit stoichiometry. However, this approach may not be feasible as the N-terminus of LRRC8 proteins proved very sensitive to manipulations and

even the attachment of the relatively small GFP rendered resulting VRACs nonfunctional (unpublished observation).

Our limited understanding of the stoichiometry of LRRC8 subunit assembly is aggravated by the lack of definitive proof that LRRC8s form hexamers, a hypothesis which was based on the homology to pannexins. However, the assumption that pannexins actually form hexamers rests heavily on their similarity to connexins (Bruzzone et al., 2003) and few studies on Panx1 (Ambrosi et al., 2010; Boassa et al., 2007). There is also evidence that the Panx2 isoform does not form hexamers, but higher-order oligomers (Ambrosi et al., 2010; Bond and Naus, 2014). Thus, the oligomerization behavior of pannexins is far from clear and the limited similarity to pannexins alone is no convincing argument for a functional hexameric assembly of LRRC8s. The issue will have to be addressed experimentally, but the difficulties encountered by Syeda et al. (2016) when trying to estimate the size of LRRC8 complexes from biochemical assays illustrate how challenging this task may be. One method that might be suited to answer this pressing question is single-molecule fluorescence photobleaching. Whereas the method is difficult to apply to multimers containing more than five subunits (Ulbrich and Isacoff, 2007), it may be possible to tag only LRRC8A or one co-expressed subunit to clarify how many of these proteins contribute to VRACs. Alternatively, purified LRRC8 complexes could be imaged using cryo-electron microscopy (cryo-EM). With this method, it may be possible to gain insights into the oligomeric state even at low resolution, and protein tags attached to different LRRC8s could be used to elucidate their contribution to VRACs. The recent advances in applicability of cryo-EM to structural biology (Nogales, 2015) also make this technique an interesting alternative to crystallization for the determination of a high-resolution VRAC structure.

Another important topic in VRAC structure-function is its permeability profile. It seems counterintuitive that the channel is so selective for anions over cations, while also conducting comparably large charged and non-charged substrates. The special role of LRRC8D in the permeation of taurine and Pt-drugs makes this isoform especially interesting. Based on sequence comparison, it has been speculated that the LRRC8 ECL1 may contribute to the VRAC pore and that the longer ECL1 of LRRC8D leads to an increased pore diameter (Voets et al., 2015). This hypothesis is compatible with our finding that residues in this region determine $I_{Cl,vol}$ inactivation and selectivity. Chimeric approaches and a suitable assay for VRAC-dependent organic osmolyte or drug transport might allow identification of structural determinants of the differential selectivity conferred by LRRC8D and other isoforms, helping to further elucidate the properties of the VRAC pore. Furthermore, it now seems plausible that many other substances may

permeate specific VRACs. Additional studies are required to confirm previously proposed VRAC substrates such as ATP, bicarbonate or glutathione and to clarify if these are also transported in an isoform-specific manner. A screen for entirely new VRAC permeants among substances such as amino acids, metabolites or drugs may also be worthwhile as it might help to identify as of yet unknown physiological and pathophysiological roles of the channel.

Another pressing issue is the molecular mechanism of VRAC gating. As shown by Syeda et al. (2016), reduced ionic strength is an important trigger for the induction of channel activity, but the underlying mechanism remains to be elucidated. The bacterial glycine betaine transporter OpuA is also sensitive to ionic strength. In OpuA, an increase in ionic strength disrupts protein-phospholipid interactions, leading to a conformational change that renders the transporter active (Biemans-Oldehinkel et al., 2006; Poolman et al., 2004). This mechanism was inferred because the transport activity of reconstituted OpuA in liposomes depended strongly on the charge of phospholipid headgroups. Protein-phospholipid interactions are also involved in the gating of mechanosensitive $K_{2P}2.1$ channels (Chemin et al., 2005). It will have to be clarified if VRAC activation thresholds also depend on the lipid composition, e.g. using reconstituted channels in liposomes, which would allow direct control of the lipid environment. In addition to the activation by cell swelling, we could also show that VRAC is activated by pro-apoptotic stimuli such as Pt-drugs or staurosporine. Furthermore, several other isovolumic stimuli that activate $I_{Cl,vol}$ have been discussed and require confirmation (see section 1.2.3). The mechanisms through which such stimuli open VRACs are of high interest as well and could be addressed by chimeric approaches, possibly using the similar pannexins or connexins as negative controls.

When compared to the activation mechanism, the inactivation gating of VRAC is probably of lesser biological importance as it occurs at highly depolarized potentials which are not reached under physiological conditions. Nevertheless, the variable inactivation of differently composed VRACs is good evidence for the involvement of LRRC8 proteins in the channel pore. Moreover, as it was the only functional difference between differently composed VRACs that we could measure in patch clamp experiments, it proved a promising starting point to explore the structure-function relationship of the channel. Our work did not only reveal the structural determinants of differential inactivation within LRRC8 proteins, but also residues which are involved in the formation of the outer VRAC pore. While we speculate that inactivation may be due to a closure of the extracellular mouth of the VRAC pore, the exact mechanism still remains unclear and detailed structural information may be required to understand this complex process in more detail.

Although the genetic disruption of specific LRRC8 proteins is a great approach to illuminate the physiological roles of VRACs, there is still a need for specific VRAC inhibitors or activators, not only as research tools but also as possible leads for drug development. For instance, the role of LRRC8D in the uptake of chemotherapeutic drugs suggests that specific activation of LRRC8D-containing channels may be beneficial in the treatment of Pt-drug sensitive cancers. Indeed, we could show that cisplatin inhibition of $I_{Cl,vol}$ depended on the expression of LRRC8D, which proves the principle that differently composed VRACs can be specifically targeted pharmacologically. VRACs might become even more attractive as targets for drug development as soon as further isoform-specific pathophysiological roles emerge. The YFP-based assay that we used to identify the channel is also suited for a high-throughput pharmacological screen using drug libraries. In addition, YFP-expressing cell lines with disrupted *LRRC8* genes could be generated to identify isoform-specific VRAC modulators.

As already implied, a high-resolution structure of VRAC would be a major breakthrough which could be of great help in answering many of the questions discussed here. Large mammalian transmembrane protein complexes are among the biggest challenges in structural biology and the vast diversity of possible LRRC8 heteromers may add to the difficulty of the endeavor. However, recent developments in cryo-EM technology, which has proven especially well-suited for the structure determination of large membrane protein complexes (Nogales, 2015) warrant some optimism that we may well see a high-resolution structure of a LRRC8 channel in the near future.

5. MATERIAL AND METHODS

5.1. Material

5.1.1. Chemicals

All chemicals were purchased from Sigma, Fluka, Merck or Roth, if not otherwise stated.

5.1.2. Bacteria strains

Table 2 | *E. coli* strains

***E. coli* strain**	**Genotype**	**Application**
XL1-Blue	*recA1 endA1 gyrA96 thi-1 hsdR17 supE44 relA1 lac [F´ proAB lacIqZΔM15 Tn10 (Tet^r)]*	standard cloning
DH12S	*80dlacZ∆M15 mcrA ∆(mrr-hsdRMS-mcrBC) araD139 ∆(ara, leu)7697 ∆(lacX74 galU galK rpsL (Str^R) nupG recA1/F' proAB$^+$ lacI^{q}Z∆ M15*	standard cloning using electroporation (Kan^r)
ET-10	*∆(mcrA)183 ∆(mcrCBhsdSMRmrr)173 endA1 supE44 thi-1 recA1 gyrA96 relA1 lac Kan^r [F' proAB lacIqZ M15 Tn10 (Tet^r)]*	standard cloning using electroporation (Amp^r)

5.1.3. Cell lines

Table 3 | Cell lines

Cell line	**Origin**	**Karyotype**	**RRID**	**Reference**
HEK293	human embryonic kidney	hypo-triploid	CVCL_0045	(Graham et al., 1977)
HCT116	human colon carcinoma	diploid	CVCL_0291	(Brattain et al., 1981)
HeLa	human cervical adenocarcinoma	aneuploid	CVCL_0030	(Gey et al., 1952)
KBM7	human chronic myelogenous leukemia	near-haploid	CVCL_A426	(Andersson et al., 1987)
HAP1	human chronic myelogenous leukemia, derived from KBM7	haploid	CVCL_Y019	(Carette et al., 2011)
HL-60	human peripheral blood leukocytes	pseudodiploid	CVCL_0002	(Collins et al., 1977)

Table 4 | Guide Sequences for the generation of knockout cell lines with CRISPR/Cas

Target gene	**Construct no.**	**Guide sequence (5'→3')**	**Targeting strand**	**Target location in protein**
LRRC8A	1A	ggctgatgtagaaggacgccagg	−	aa 320–328 (beginning of TM4)
	3A	tgatgattgccgtcttcgggggg	+	aa 36–43 (in TM2)
	4A	tcctgcaatgattcgttccgggg	+	aa 64–71 (between TM1 and TM2)
LRRC8B	1B	tttttctcttaacgcctcaaagg	−	aa 346–353 (after TM4)
	2B	ggccacaaaatgctcgagcctgg	−	aa 147–354 (between TM2 and TM3)
LRRC8C	1C	atgctcatgatcggcgtgtttgg	+	aa 35–42 (in TM1)
LRRC8D	1D	gtggctctgagaggtatgtcagg	−	aa 107–114 (between TM1 and TM2)
LRRC8E	1E	gctggccgagtacctcaccgtgg	+	aa 27–34 (inTM1)

aa= amino acid; TM = transmembrane domain; PAM sequences are underlined

Table 5 | LRRC8 knockout cell lines

Cell line	Clone name	Construct*	Genetic modification	Protein modification
LRRC8A$^{-/-}$ (HEK293)	3E7	3A	a1: Δ21nt (t110-a130) a2: insertion of 1 nt (t after c123)	**A1**: ΔM37-G43 in TM1 (non- functional) **A2**: G42W-fs in TM1
	1F7	1A	a1: Δ9nt (a958-g966) a2: Δ2nt (c965-g966) a3: Δ23nt (a958-g980)	**A1**: ΔI320-A322 at start of TM4 (non-functional) **A2**: A322V-fs at start of TM4 **A3**: I320P-fs at start of TM4
LRRC8A$^{-/-}$ (HCT116)	3F8	3A	Δ2g out of 6g (g124-g129)	G43D-fs in TM1
	4B9	4A	a1: Δ32nt (c195-g226) a2: duplication of t206	**A1**: C65W-fs between TM1 and TM2 **A2**: R70P-fs between TM1 and TM2
	ZF9	ZFN	a1: Δ2nt (a508-c509) a2: insertion of 5nt (cacga after a511)	**A1**: T170E-fs between TM2 and TM3 **A2**: R171T-fs between TM2 and TM3
LRRC8B$^{-/-}$ (HCT116)	n2B-D3	2B	duplication of t446	E150R-fs after TM2
LRRC8C$^{-/-}$ (HCT116)	n1C-C2	1C	duplication of t119	F41V-fs in TM1
LRRC8D$^{-/-}$ (HCT116)	n1D-F11	1D	a1: Δ19nt (a325-t343) a2: duplication of a325	**D1**: P110L-fs between TM1 and TM2 **D2**: I109N-fs between TM1 and TM2
	n1D-B2	1D	duplication of a325	I109N-fs between TM1 and TM2
LRRC8E$^{-/-}$ (HCT116)	BCDE(WT)-F5	1E	duplication of a94	T32N-fs in TM1
	CE(WT)-B6	1E	duplication of a94	T32N-fs in TM1
LRRC8(D/E)$^{-/-}$ (HCT116)	nBCDE (WT)-G9	1D, 1E	*D*: duplication of a325	**D**: I109N-fs between TM1 and TM2
			E: duplication of a94	**E**: T32N-fs in TM1
	nBCDE (WT)-B3	1D, 1E	*D*: duplication of a325	**D**: I109N-fs between TM1 and TM2
			E: duplication of a94	**E**: T32N-fs in TM1
LRRC8(C/E)$^{-/-}$ (HCT116)	BCDE(WT)-F5+1C-D5	1C, 1E	*C*: a1: duplication of t119 a2: Δ5nt (c114-g118) and duplication of t119	**C1**: F41V-fs in TM1 **C2**: G39C-fs in TM1
			E: duplication of a94	**E**: T32N-fs in TM1
LRRC8(B/C/D)$^{-/-}$ (HCT116)	BCD-C5	2B, 1C, 1D	*B*: duplication of t446	**B:** E150R-fs after TM2
			C: duplication of t119	**C:** F41V-fs in TM1
			D: duplication of a325	**D:** I109N-fs between TM1 and TM2
LRRC8(B/D/E)$^{-/-}$ (HCT116)	BDE-B8	2B, 1D, 1E	*B*: duplication of t446	**B:** E150R-fs after TM2
			D: duplication of a325	**D:** I109N-fs between TM1 and TM2
			E: duplication of a94	**E:** T32N-fs in TM1
LRRC8(C/D/E)$^{-/-}$ (HCT116)	nBCDE(WT)-H8	1C, 1D, 1E	*C:* 78nt (from a66 onwards) incl. splice acceptor site replaced by 13 nt (net Δ65nt)	**C**: W23R-fs at start of TM1, before missing splice site
			D: a1: duplication of a325 a2: Δ11nt (g322-t332)	**D1**: I109N-fs between TM1 and TM2 **D2**: D108Q-fs between TM1 and TM2
			E: a1: duplication of a94 a2: Δ10nt (g87-c96)	**E1**: T32N-fs in TM1 **E2**: Y30W-fs in TM1
LRRC8(B/C/D/E)$^{-/-}$ (HCT116)	BCDE (WT2)-D2+2B-E8	2B,1C, 1D, 1E	*B:* a1: duplication of t446 a2: Δ2nt (c447-g448)	**B1**: E150R-fs after TM2 **B2**: E150A-fs after TM2
			C: duplication of t119	**C**: F41V-fs in TM1
			D: duplication of a325	**D**: I109N-fs between TM1 and TM2
			E: Δ2nt (t92-c93)	**E**: L31H-fs in TM1
LRRC8$^{-/-}$ (HCT116)	BC+DE (KO)D5+ 2B-G4	3A,2B, 1B§,1C, 1D, 1E	*A*: Δ2g out of 6g (g124-g129)	**A**: G43D-fs in TM1
			B: a1: duplication of t446 a2: Δ4nt (c447-g450)	**B1**: E150R-fs after TM2 **B2**: E150I-fs after TM2
			C: duplication of t119	**C**: F41V-fs in TM1
			D: duplication of a325	**D**: I109N-fs between TM1 and TM2
			E: duplication of a94	**E**: T32N-fs in TM1

a = allele (only given if alleles differed in modifications); fs = frameshift; nt = nucleotide; TM = transmembrane domain; ZFN = zinc-finger nuclease; Δ = deletion. Indicated nucleotide numbers give nucleotide position within the ORF.

* For targeted guide sequences, see Table 4.

§ Targeting with construct 1B in *LRRC8*$^{-/-}$ cell line resulted in a duplication of a1043 which would lead to A349G-fs after TM4. However, the mutations by the 2B targeting (given in Table 4) truncate LRRC8B already after TM2.

5.1.4. Sequencing and genotyping primers

Table 6 | Sequencing primers

Target	Location*	Orientation	No.#	Sequence
CMV	−220	forward	2	CAAAATGTCGTAACAACTCCG
LRRC8A	0	forward	10995	GCAGAATTCCATGATTCCGGTGACAGAGC
	400	forward	10997	GGCCTGCAGCAACTTCTG
	550	forward	13393	GAGGAGAGCGACCCCAAGC
	800	forward	10998	AGGTGATCAAGTTCATCC
	1200	forward	10999	GGACGCTGGACAAGCTCC
	1600	forward	11000	AACGCCTCAAGGTGCTGC
	2000	forward	13394	CTCACCTGCCTTAAGCTG
	2415	reverse	10996	CTTGGTACCTCAGGCCTGCTCCTTGTC
LRRC8C	400	reverse	11133	TCCTCATCCATACCCTG
	550	forward	13395	CTCAGAAGAAAAGGACAAC
	800	forward	11134	TTCCTAATCATCATTGC
	1200	forward	11135	TCCTGATAAACTGAGG
	1600	forward	11136	AAAATCCCTCAGGCAGTG
	1950	forward	13396	GCTAAAACTGTGGCATAACAG
LRRC8E	400	reverse	11141	CCCTGCACTGGTATGC
	550	forward	13397	GCTGCGGCCACCATAGTGG
	800	forward	11142	GCGACATCCTGTACACC
	1200	forward	11143	CGAGGTCAGCGAAAGCC
	1600	forward	11144	GGGAGCTGAAGCAGCTC
	1850	forward	13398	CAAGGACAACCACCTGCGCTC
GFP	680§	reverse	5775	CGTCCAGCTCGACCAGGATG

* Approximate annealing location within the ORF (in bp), start codon = 0
# Number of primer in internal oligo database of the Jentsch laboratory
§ With respect to the stop codon of the insert

Table 7 | Primers for genotyping of knockout cell lines

Target	No.*	Sequence	Product size
1A	10998	AGGTGATCAAGTTCATCC	311
	11200	GAAGGCGAAGTCGTTCTTGACGTCGG	
3A	10995	GCAGAATTCCATGATTCCGGTGACAGAGC	672
	11344	CTCGATCCGTGCCTTGGTCCGCTGCAGC	
4A	10998	AGGTGATCAAGTTCATCC	905
	11041	CAGCTTCTGCAGGTGCACG	
1B	11130	CAAAGTCATTTTGTTTGTGC	470
	11625	TGACTCCAAACCTGGCTGTG	
2B	12153	AGTACTCCTATATTGATGCC	545
	12155	TGACTCCAAACCTGGCTGTG	
1C	11004	TCGAGCGGCCGCCATGATTCCCGTGACAGAATTCC	469
	11627	GTATCAATGGTGCTGGAC	
1D	11006	GCAGAATTCCATGTTTACCCTTGCGG	489
	11628	TTAGAATACCACGGAAGG	
1E	10838	GCAGAATTCCATGATCCCAGTGGCCGAG	255
	11629	AGTGGGGCTCTGTCTTCA	
ZFN	10997	GGCCTGCAGCAACTTCTG	488
	11040	CAATGTCCACGGTGCAGTCC	

* Number of primer in internal oligo database of the Jentsch laboratory

5.1.5. Plasmids

Table 8 | Plasmids for heterologous expression in mammalian cells

Plasmid name	No.*	Insert#	Vector backbone	Description
LRRC8A	5500	NM_019594	pcDNA3.1/myc-His(-)B	Stop before myc/His, no tag
LRRC8B	5501	NM_015350	pcDNA3.1/myc-His(-)B	Stop before myc/His, no tag
LRRC8C	5502	NM_032270	pcDNA3.1/myc-His(-)B	Stop before myc/His, no tag
LRRC8D	5503	NM_018103	pcDNA3.1/myc-His(-)B	Stop before myc/His, no tag
LRRC8E	5504	NM_025061	pcDNA3.1/myc-His(-)B	Stop before myc/His, no tag
LRRC8A-myc	5651	NM_019594	pcDNA3.1/myc-His(-)B	No stop, C-terminal myc tag
LRRC8B-myc	5506	NM_015350	pcDNA3.1/myc-His(-)B	No stop, C-terminal myc tag
LRRC8C-myc	5507	NM_032270	pcDNA3.1/myc-His(-)B	No stop, C-terminal myc tag
LRRC8D-myc	5508	NM_018103	pcDNA3.1/myc-His(-)B	No stop, C-terminal myc tag
LRRC8E-myc	5509	NM_025061	pcDNA3.1/myc-His(-)B	No stop, C-terminal myc tag
LRRC8A-GFP	5518	NM_019594	pEGFP-N1	No stop, C-terminal GFP tag
LRRC8B-GFP	5519	NM_015350	pEGFP-N1	No stop, C-terminal GFP tag
LRRC8C-GFP	5520	NM_032270	pEGFP-N1	No stop, C-terminal GFP tag
LRRC8D-GFP	5521	NM_018103	pEGFP-N1	No stop, C-terminal GFP tag
LRRC8E-GFP	5570	NM_025061	pEGFP-N1	No stop, C-terminal GFP tag
GFP-LRRC8A	5514	NM_019594	pEGFP-C1	N-terminal GFP tag
GFP-LRRC8B	5568	NM_015350	pEGFP-C1	N-terminal GFP tag
GFP-LRRC8C	5569	NM_032270	pEGFP-C1	N-terminal GFP tag
GFP-LRRC8D	5515	NM_018103	pEGFP-C1	N-terminal GFP tag
GFP-LRRC8E	5516	NM_025061	pEGFP-C1	N-terminal GFP tag
LRRC8A-RFP	5524	NM_019594	pmRFP-N1	No stop, C-terminal RFP tag
$LRRC8A_{trunc}$-GFP	5526	NM_019594&	pEGFP-N1	No stop, C-terminal GFP tag, truncation at R719
GFP-LRRC8A -exHA	5536	NM_019594&	pEGFP-C1	N-terminal GFP tag, HA tag in ECL1
GFP-LRRC8A -ctHA	5538	NM_019594	pEGFP-C1	N-terminal GFP tag, C-terminal HA tag
LRRC8A-(N66A-N83A)-myc	5512	NM_019594&	pcDNA3.1/myc-His(-)B	No stop, C-terminal GFP tag, mutated glycosylation sites
GFP-ClC-1	3781	NM_000083	pEGFP-C1	N-terminal GFP tag

* Number of plasmid in internal plasmid database of the Jentsch laboratory
# RefSeq accession number of the DNA sequence
& original sequence altered

All mutants generated for the experiments presented in section 3.2 and in Ullrich et al. (2016) are listed in Table 9. Many more DNA constructs were generated in the course of the study, but have been omitted here for brevity. These plasmids have all been entered into the plasmid database of the Jentsch laboratory. More detailed information on all plasmids generated by Felizia Vosss, Tobias Stauber, Momsen Reincke, and myself in the course of our studies on VRAC can be found on the internal Jentsch laboratory server[2].

[2] *\\mdcstg4.mdc-berlin.net\AG_Jentsch\grpdata\shared data\VRAC_Cloning_Ephys* and *\\mdcstg4.mdc-berlin.net\AG_Jentsch\grpdata\shared data\VRAC-Ephys-Results-2016*

Table 9 | Mutant constructs generated for experiments presented in section 3.2

Construct*	No.#	Name	Mut. primers§	Template(s)#
Chimera 1, LRRC8E$^{1–42}$/LRRC8C$^{43–830}$	6492	CE-24-GFP	12828/29	5520, 5570
Chimera 2, LRRC8C$^{1–125}$/LRRC8E$^{117–796}$	6486	CE-14-GFP	12395/96	5520, 5570
Chimera 3, LRRC8E$^{1–84,117–796}$/LRRC8C$^{94–125}$	6500	CE-38-GFP	13047/48	5520, 5570
Chimera 4, LRRC8C$^{1–93,126–803}$/LRRC8E$^{85–116}$	6499	CE-37-GFP	13051/52	5520, 5570
LRRC8C(M96V)-GFP	5946	C-M96V-GFP	13197/98	5520
LRRC8C(T101N)-GFP	5943	C-T101N-GFP	13191/92	5520
LRRC8C(D102N)-GFP	5944	C-D102N-GFP	13193/94	5520
LRRC8C(T101N,D102N)-GFP	5945	C-TDNN-GFP	13195/96	5520
LRRC8C(M114L)-GFP	5947	C-M114L-GFP	13199/200	5520
LRRC8C(R118T)-GFP	5948	C-R118T-GFP	13201/02	5520
LRRC8E(N92T)-GFP	5937	E-N92T-GFP	13203/04	5570
LRRC8E(N93D)-GFP	5938	E-N93D-GFP	13205/06	5570
LRRC8E(N92T,N93D)-GFP	5939	E-NNTD-GFP	13207/08	5570
LRRC8A(Y99N,D100N)	6186	A-YDNN	13520/21	5500
LRRC8A(D100N)	6433	A-D100N	14347/48	5500
LRRC8A(D100A)	6430	A-D100A	14341/42	5500
LRRC8A(D100R)	6432	A-D100R	14345/46	5500
LRRC8A(D100K)	6431	A-D100K	14343/44	5500
LRRC8A(D100E)	6434	A-D100E	14349/50	5500
LRRC8E(N93A)-GFP	6463	E-N93A-GFP	14211/12	5570
LRRC8E(N93R)-GFP	6175	E-N93R-GFP	13510/11	5570
LRRC8E(N93K)-GFP	6174	E-N93K-GFP	13508/09	5570
LRRC8E(N93E)-GFP	6173	E-N93E-GFP	13506/07	5570
LRRC8A(K98A)	6435	A-K98A	13772/73	5500
LRRC8A(K98N)	6410	A-K98N	13882/83	5500
LRRC8A(K98R)	6421	A-K98R	14094/94	5500
LRRC8A(K98E)	6408	A-K98E	13878/79	5500

* As used in the results section of this thesis
§ Number of primer in internal oligo database of the Jentsch laboratory
# Number of plasmid in internal plasmid database of the Jentsch laboratory

5.1.6. Solutions for patch clamp experiments

The isotonic extracellular bath solution contained (in mM) 150 NaCl, 6 KCl, 1 $MgCl_2$, 1.5 $CaCl_2$, 10 glucose, and 10 HEPES, pH 7.4 with NaOH (320 mOsm). The hypotonic solution contained (in mM) 105 NaCl, 6 CsCl, 1 $MgCl_2$, 1.5 $CaCl_2$, 10 glucose, 10 HEPES, pH 7.4 with NaOH (240 mOsm). For anion selectivity experiments, NaCl was replaced by an equimolar amount of NaI, $NaNO_3$, NMDG-Cl or Na-D-gluconate.

The standard pipette solution contained (in mM) 40 CsCl, 100 Cs-methanesulfonate, 1 $MgCl_2$, 1.9 $CaCl_2$, 5 EGTA, 4 Na_2ATP, and 10 HEPES, pH 7.2 with CsOH (290 mOsm). The free Ca^{2+} concentration in this solution was calculated to be approximately 80 nM.

Osmolarities of all solutions were assessed with an Osmomat 030 freezing point osmometer (Gonotec) and adjusted with mannitol if necessary. Water used for these solutions was deionized, filtered and deionized again by a Milli-Q purifier (Merck Millipore). All solutions were sterile filtered after preparation through 0.20–0.22 µm filters. Bath solutions were stored at 4 °C and used up within 2 months. Pipette solutions were stored in 1 ml aliquots at −20 °C and freshly thawed on every experimental day. They were kept on ice during experiments to prevent degradation of ATP.

5.1.7. Antibodies

The following commercially available primary antibodies were used for experiments shown in this thesis: rabbit anti-myc (A-14, Santa Cruz Biotechnology), rabbit anti-GFP (A-11122, Life Technologies) for IP and chicken anti-GFP (1020, Aves Lab) for Western blot, mouse anti-α-tubulin (DM1A, Sigma), mouse anti-HA (HA.11, Covance). Secondary antibodies conjugated to AlexaFluor 488 or 546 (Molecular Probes) or to horseradish peroxidase (Jackson ImmunoResearch) were used for detection.

The lab-generated antibodies (Voss, 2015; Voss et al., 2014) used for the experiments shown in this thesis are listed in Table 10.

Table 10 | Lab-generated antibodies against LRRC8 proteins

Target protein	Target species*	No.#	Designation	Immunizing peptide	Peptide position
LRRC8A	**Human/mouse**	1339	mLRRC-8A-5a rb1	QRTKSRIEQGIVDRSE	intracellular loop
LRRC8B	Human/**mouse**	1345	mLRRC-8B-5b rb1	QSLPYPQPGLESPGIESPT	intracellular loop
LRRC8C	Human/**mouse**	1347	mLRRC-8C-ct rb2	EDALFETLPSDVREQMKAD	C-terminus
LRRC8D	Human/**mouse**	1348	mLRRC-8D-ct rb1	LEVKEALNQDVNVPFANGI	C-terminus
LRRC8E	Human/**mouse**	1351	mLRRC-8E-ct rb2	LYEGLPAEVREKMEEE	C-terminus

* The target species of the immunizing peptide are indicated in bold

Number of antibody in the internal antibody database of the Jentsch laboratory

5.2. Methods

5.2.1. Molecular biology techniques

5.2.1.1. Molecular cloning

All cloning followed adapted standard procedures described in detail elsewhere (Sambrook and Russell, 2001). DNA primers were designed by hand and ordered from Eurofins Genomics in 0.01 µmol amounts for cloning purposes. The entire ORF was sequenced for all cloned *LRRC8* genes or mutants and chimeras thereof presented in this thesis. For this, the Eurofins Genomics sequencing service was used. Standard sequencing primers for the investigated *LRRC8* genes and plasmid vectors are listed in Table 6. Sequence data was analyzed and cloning strategies were designed using the Lasergene software package (DNASTAR).

cDNAs encoding the human LRRC8 proteins were cloned from HEK293 or HeLa cDNA libraries using specific primers, or ordered from SourceBioscience. For recombinant expression, cDNAs were cloned into the pcDNA3.1 (Invitrogen) or pEGFP-N1/C1 plasmid vectors (Clontech, see Table 8) which were amplified in specialized *E. coli* strains (also see Table 2). Plasmid DNA was isolated from bacteria using the NucleoSpin Plasmid QuickPure Miniprep kit (Macherey-Nagel) or the PureLink HiPure Plasmid Filter Midiprep kit (Invitrogen) and dissolved in TE buffer (10 mM Tris-Cl, 1 mM EDTA, pH 7.5) for storage and further processing. The amount and purity of the isolated DNA were controlled with a Nanodrop ND-1000 spectro-photometer (PeqLab).

Mutants and chimeras were generated using PCR-based protocols, generally variations of the primer-extension technique. The high-fidelity DNA polymerases Phusion (Finnzymes) or PfuUltra II Fusion HS (Agilent) were used to ensure high processivity and to avoid introduction of unwanted mutations. Extraction of DNA fragments from plasmid vectors was done using specific recombinant restriction endonucleases ordered from New England Biolabs or Fermentas. Generally, restriction enzymes generating overhangs (‘sticky ends’) were preferred for easier ligation. DNA fragments were size-separated by electrophoresis in 1–3% agarose gels prepared with UltraPure agarose (Invitrogen) and TAE buffer (40 mM Tris, 40 mM acetic acid, 1 mM EDTA, pH 8.0). Purification of DNA from gels was done using the NucleoSpin Gel and PCR Clean-up kit (Macherey-Nagel). Ligation reactions were set up using recombinant T4 Ligase (Fermentas) and incubated over night at 4 °C. For transformation, bacteria were electroporated in a Gene Pulser electroporation device (BIO-RAD) in the presence of DNA. Bacteria were then allowed to recover in liquid LB medium (Sigma), before being plated on antibiotic-containing LB agar for selection of transformants. Clones were identified using specific restriction digests and subsequent sequencing.

5.2.1.2. Genome editing with CRISPR/Cas and zinc finger nucleases

The CRISPR/Cas system and a custom-designed zinc finger nuclease (ZFN) were used to disrupt *LRRC8* genes in cell lines. For CRISPR/Cas, targeting single guide RNAs (sgRNAs) were designed using the UCSC Genome Browser (Kent et al., 2002) and following instructions detailed in (Mali et al., 2013). Guide sequences are listed in Table 4. sgRNAs were cloned into the px330 expression vector which also encodes a codon-optimized SpCas9 enzyme (Cong et al., 2013). A *LRRC8A*-specific CompoZr Knockout ZFN kit was ordered from Sigma. The px330 plasmid or the ZFN plasmids were each transfected together with pEGFP-C1 into HEK293 or HCT116 cells. After 2–5 days, GFP-positive cells were FACS-sorted and subsequently raised as single clones. Genomic DNA was isolated from the resulting monoclonal cell lines using the Invisorb Spin Tissue Minikit (Invitek). PCR with primers listed in Table 7 was used to amplify modification sites, which were then analyzed by sequencing for introduced mutations. The final *LRRC8* knockout cell lines generated by genome editing are listed in Table 5, including the targeting constructs used, the genetic alterations identified by sequencing and the resulting mutations in the proteins. To check for the absence of protein, Western blots were performed in cases where specific antibodies were available (Voss, 2015). To generate cell lines in which several *LRRC8* genes were disrupted in parallel, the respective targeting plasmids were either transfected together or additional targeting was performed on verified knockouts. Genetically modified cell lines were generated by Felizia Voss and Tobias Stauber.

5.2.1.3. Quantitative real-time PCR

Quantitative real-time PCR (qRT-PCR) was performed by Felizia Voss as described elsewhere (Voss, 2015; Voss et al., 2014, see preface). Briefly, total RNA was isolated using the RNeasy Mini Kit (Quiagen) and digested with amplification grade DNase I (Invitrogen) before using Superscript II reverse transcriptase (Invitrogen) with random primers to generate cDNA. PCR reactions (20 µl) were set up with the Power SYBR Green PCR Master Mix (Applied Biosystems) and contained 0.2 µM of each primer and 0.4 µl cDNA. Table 11 lists the primers used for qRT-PCR experiments.

Table 11 | Primers used for qRT-PCR

Gene	No.[#]	Primer sequence (5'→3')	PCR product	Remarks
GAPDH	8076 8077	ACAGTCAGCCGCATCTTCT GTTAAAAGCAGCCCTGGTGA	127	internal standard
LRRC8A	11012 11013	GGGTTGAACCATGATTCCGGTGAC GAAGACGGCAATCATCAGCATGAC	133	-
LRRC8B	11284 11285	ACCTGGATGGCCCACAGGTAATAG ATGCTGGTCAACTGGAACCTCTGC	126	-
LRRC8C	11288 11289	ACAAGCCATGAGCAGCGAC GGAATCATGTTTCTCCGGGC	132	-
LRRC8D	11036 11037	ATGGAGGAGTGAAGTCTCCTGTCG CTTCCGCAAGGGTAAACATTCCTG	126	-
LRRC8E	11038 11039	ACCGTGGCCATGCTCATGATTG ATCTTGTCCTGTGTCACCTGGAG	62	-

[#] Number of primer in internal oligo database of the Jentsch laboratory

5.2.2. Biochemistry techniques and reagents

For protein expression assays, cells were harvested from the substrate by scraping and incubated in lysis buffer for 10 min on ice. The lysis buffer contained 150 mM NaCl, 1% NP-40, 0.5% sodium deoxycholate, 50 mM Tris-HCl, pH 7.5 with NaOH, 4 mM Pefabloc (Roth) and complete proteinase inhibitor (Roche). Lysates were pre-cleared by centrifugation at 14.000 rpm for 10 min at 4°C and again centrifuged at 30.000 rpm for 30 min at 4°C. Protein concentrations were determined by the Lowry method (Lowry et al., 1951). Equal protein amounts were separated by SDS-PAGE and analyzed by Western blot. SDS-Page was usually performed on 8% SDS-polyarcylamide gels using the Mini-PROTEAN 3 gel chamber system (Bio-Rad). The PageRuler Plus Protein Ladder (Fermentas) was used as molecular weight marker. For Western blots, the tank blotting system Mini Trans-Blot Electrophoretic Transfer Cell (Bio-Rad) was used. The transfer buffer contained 25 mM Tris-HCl, pH 8.2, 20% methanol and 200 mM glycine. Samples were blotted onto polyvinylidene difluoride (PVDF) membranes for 2–3 h at 4°C at a voltage of 84 mV.

Membranes were stained with Ponceau S (0.2% Ponceau S, 3% acetic acid) to check for equal protein loading and transfer, and subsequently blocked for at least 30 min using a blocking buffer containing TBS with 0.1% Tween 20 and 5% milk powder. Primary antibodies were then added and incubated overnight at 4°C in blocking buffer. Membranes were then washed 3 times with TBS supplemented with 0.1% Tween. Secondary antibodies coupled to horseradish peroxidase were applied in blocking buffer for 45 min. After three more washing steps, signals were visualized by chemiluminescence using SuperSignal West Pico or Femto (Pierce). Blots were photographed with a Chemi-Smart 5000 acquisition system controlled via the ChemiCapt 5000 software (PeqLab).

5.2.3. Immunocytochemistry

For immunocytochemistry experiments, different fixation methods were applied depending on the antibodies used. For stainings with the LRRC8A antibody, cells were fixed in pre-cooled methanol at −20°C for 10 min. For other antibodies, cells were fixed in 2% or 4% PFA in PBS for 15 min followed by a 5-min incubation with 30 mM glycine in PBS at room temperature. Cells were incubated for 1 h with each antibody in PBS containing 0.1% Triton X and 3% BSA. Images were acquired with a LSM510 inverted confocal microscope with a 63x oil-immersion objective (Zeiss) and processed using the ZEN software package (Zeiss). Immunocytochemistry experiments were conducted by Felizia Voss and Tobias Stauber.

5.2.4. Cell culture techniques and reagents

HEK293 and HeLa cells were cultured in Dulbecco's Modified Eagle Medium (DMEM, Pan Biotech). HCT116 cells were cultured in McCoy’s 5A medium (Pan Biotech). HL-60, KBM7 and HAP1 cells were cultured in Iscove's Modified Dulbecco's Medium (IMDM, Pan Biotech). Medium for all cell lines was supplemented with 10% (v/v %) fetal calf serum (FCS), 100 U/ml Penicillin and 0.1 mg/ml Streptomycin. Cells were grown on plastic tissue culture dishes (Greiner Bio-One) in tissue culture incubators maintaining 37 °C and 5% CO_2. Cells were split every 3–6 days. For splitting, adherent cells were washed with PBS, trypsinized, separated through vigorous trituration and transferred into fresh medium. For patch clamp experiments, cells were plated at low density onto glass coverslips (ø15 mm) coated with poly-L-lysine (Pan Biotech) or 0.1% gelatine in water. Transfection was generally performed just after plating. The Fugene HD (Promega) or Lipofectamine 2000 (Life Technologies) transfection reagents were used for HEK293 or HCT116 cells, respectively.

If two or more plasmids encoding LRRC8 proteins were transfected simultaneously, identical amounts were used. One of the transfected LRRC8 isoforms

was fused C-terminally to GFP. When LRRC8A was co-transfected with other LRRC8 isoforms only the latter carried GFP because plasma membrane fluorescence indicated co-expression with LRRC8A (see Figure 9).

5.2.5. Whole-cell patch clamp recording and data analysis

All experiments were performed at constant temperature of 20–22°C. Currents were recorded with an EPC-10 USB patch clamp amplifier and PatchMaster software (HEKA Elektronik). Patch pipettes had a resistance of 2–5 MΩ. Series resistance was compensated by 60–90% to minimize voltage errors. Currents were sampled at 5 kHz and low-pass filtered at 10 kHz. The holding potential was −30 mV. Cells with a membrane resistance below 800 MΩ or series resistance above 10 MΩ were discarded. The standard protocol for measuring the time course of $I_{Cl,vol}$ activation, applied every 15 s after membrane rupture, consisted of a 0.6-s-step to −80 mV followed by a 2.6-s-ramp from −100 to 100 mV. The read-out for $I_{Cl,vol}$ was the steady state whole-cell current at −80 mV normalized to the cell capacitance (current density). The voltage protocol, applied after complete activation of $I_{Cl,vol}$, consisted of 1-s or 2-s steps starting from −120 mV to 120 mV in 20-mV, 10-mV or 5-mV intervals preceded and followed by a 0.5-s-step to −80 mV every 5 s.

Relative anion permeabilities (P_X/P_{Cl}) were calculated from the shifts in reversal potential induced by perfusion with the anion substituted hypotonic salines using a modified Goldman-Hodgkin-Katz equation:

$$P_X \,/\, P_{Cl} \;=\; \frac{[Cl]_{hypo}\, e^{-\frac{\Delta E_{rev} F}{RT}} - [Cl]_{subst}}{[X]_{subst}}$$

where ΔE_{rev} is the shift in reversal potential, $[Cl]_{hypo}$ and $[Cl]_{subst}$ are the extracellular chloride concentrations in the normal and anion substituted hypotonic saline, and $[X]_{subst}$ is the concentration of the substituting anion. R is the gas constant, T is the absolute temperature, and F is the Faraday constant. Reversal potentials were only recorded in cells with appreciable $I_{Cl,vol}$ activation. Liquid junction potentials were measured for all solutions and corrected for in ion selectivity experiments.

The inactivation kinetics of $I_{Cl,vol}$ in WT cells could not be fitted appropriately by single- or double-exponential functions. Therefore, the fraction of remaining current was calculated by dividing the current amplitude at the end of the 2-s voltage step by the current amplitude 1.5 ms after the beginning of the voltage step (avoiding contamination by capacitive transients). The half inactivation time $t_{1/2}$ was determined as the time point where the inactivation reached half of the total inactivation after 2 s.

Time constants of inactivation (τ_i or $\tau_{inactivation}$) in overexpression experiments or knockout cell lines were obtained by approximating the current decay over 2 s versus time with an exponential function,

$$I = I_{ss} + I_i \, e^{\frac{-t}{\tau_i}}$$

where I_{ss} is the steady state current after inactivation and I_i is the inactivating current. Time constants of recovery from inactivation (τ_{slow} or τ_{fast}) were obtained fitting the recovering current versus time with a double-exponential function,

$$I = I_{max} + I_{slow} \, e^{\frac{-t}{\tau_{slow}}} + I_{fast} \, e^{\frac{-t}{\tau_{fast}}}$$

where I_{max} is the fully recovered current, and I_{slow} or I_{fast} are the currents recovered through the slow and fast components, respectively.

Data analysis and generation of figures was done using IgorPro (WaveMetrics) and GraphPad Prism 5 (GraphPad Software). Example current traces were low-pass-filtered at 2 kHz and reduced to a sampling rate of 1 kHz for clarity. Averaged data is presented as mean ± SEM if not stated otherwise. If significance levels are given, the test used for the calculation is mentioned in the corresponding figure legend. At least 5 cells per condition were measured on at least three different days if not stated otherwise; exact n-values are given in the figures.

6. REFERENCES

ABASCAL, F., AND ZARDOYA, R. (2012). LRRC8 proteins share a common ancestor with pannexins, and may form hexameric channels involved in cell-cell communication. *BioEssays : News and Reviews in Molecular, Cellular and Developmental Biology* **34**, 551–560.

ABDULLAEV, I.F., RUDKOUSKAYA, A., SCHOOLS, G.P., KIMELBERG, H.K., AND MONGIN, A.A. (2006). Pharmacological comparison of swelling-activated excitatory amino acid release and Cl^- currents in cultured rat astrocytes. *The Journal of Physiology* **572**, 677–689.

ACKERMAN, M.J., WICKMAN, K.D., AND CLAPHAM, D.E. (1994). Hypotonicity activates a native chloride current in Xenopus oocytes. *The Journal of General Physiology* **103**, 153–179.

ADOMAVICIENE, A., SMITH, K.J., GARNETT, H., AND TAMMARO, P. (2013). Putative pore-loops of TMEM16/anoctamin channels affect channel density in cell membranes. *The Journal of Physiology* **591**, 3487–3505.

AKITA, T., AND OKADA, Y. (2011). Regulation of bradykinin-induced activation of volume-sensitive outwardly rectifying anion channels by Ca^{2+} nanodomains in mouse astrocytes. *The Journal of Physiology* **589**, 3909–3927.

AKITA, T., AND OKADA, Y. (2014). Characteristics and roles of the volume-sensitive outwardly rectifying (VSOR) anion channel in the central nervous system. *Neuroscience* **275**, 211–231.

AKITA, T., FEDOROVICH, S. V., AND OKADA, Y. (2011). Ca^{2+} nanodomain-mediated component of swelling-induced volume-sensitive outwardly rectifying anion current triggered by autocrine action of ATP in mouse astrocytes. *Cellular Physiology and Biochemistry* **28**, 1181–1190.

ALEKSANDROV, A.A., ALEKSANDROV, L.A., AND RIORDAN, J.R. (2007). CFTR (ABCC7) is a hydrolyzable-ligand-gated channel. *Pflügers Archiv : European Journal of Physiology* **453**, 693–702.

ALMAÇA, J., TIAN, Y., ALDEHNI, F., OUSINGSAWAT, J., KONGSUPHOL, P., ROCK, J.R., HARFE, B.D., SCHREIBER, R., AND KUNZELMANN, K. (2009). TMEM16 proteins produce volume-regulated chloride currents that are reduced in mice lacking TMEM16A. *The Journal of Biological Chemistry* **284**, 28571–28578.

AMBROSI, C., GASSMANN, O., PRANSKEVICH, J.N., BOASSA, D., SMOCK, A., WANG, J., DAHL, G., STEINEM, C., AND SOSINSKY, G.E. (2010). Pannexin1 and Pannexin2 channels show quaternary similarities to connexons and different oligomerization numbers from each other. *The Journal of Biological Chemistry* **285**, 24420–24431.

ANDERSON, R.G.W. (1998). The caveolae membrane system. *Annual Review of Biochemistry* **67**, 199–225.

ANDERSON, J.W., JIRSCH, J.D., AND FEDIDA, D. (1995). Cation regulation of anion current activated by cell swelling in two types of human epithelial cancer cells. *The Journal of Physiology* **483**, 549–557.

ANDERSSON, B.S., BERAN, M., PATHAK, S., GOODACRE, A., BARLOGIE, B., AND MCCREDIE, K.B. (1987). Ph-positive chronic myeloid leukemia with near-haploid conversion in vivo and establishment of a continuously growing cell line with similar cytogenetic pattern. *Cancer Genetics and Cytogenetics* **24**, 335–343.

ANDO-AKATSUKA, Y., ABDULLAEV, I., LEE, E., OKADA, Y., AND SABIROV, R. (2002). Down-regulation of volume-sensitive Cl^- channels by CFTR is mediated by the second nucleotide-binding domain. *Pflügers Archiv European Journal of Physiology* **445**, 177–186.

ARREOLA, J., MELVIN, J.E., AND BEGENISICH, T. (1995). Volume-activated chloride channels in rat parotid acinar cells. *The Journal of Physiology* **484**, 677–687.

ARREOLA, J., BEGENISICH, T., NEHRKE, K., NGUYEN, H.-V., PARK, K., RICHARDSON, L., YANG, B., SCHUTTE, B.C., LAMB, F.S., AND MELVIN, J.E. (2002). Secretion and cell volume regulation by salivary acinar cells from mice lacking expression of the Clcn3 Cl^- channel gene. *The Journal of Physiology* **545**, 207–216.

ASHCROFT, F.M., AND RORSMAN, P. (1989). Electrophysiology of the pancreatic beta-cell. *Progress in Biophysics and Molecular Biology* **54**, 87–143.

BAO, L., LOCOVEI, S., AND DAHL, G. (2004). Pannexin membrane channels are mechanosensitive conduits for ATP. *FEBS Letters* **572**, 65–68.

BARAKAT, A.I., LEAVER, E. V, PAPPONE, P.A., AND DAVIES, P.F. (1999). A flow-activated chloride-selective membrane current in vascular endothelial cells. *Circulation Research* **85**, 820–828.

BARBE, M.T., MONYER, H., AND BRUZZONE, R. (2006). Cell-cell communication beyond connexins: the pannexin channels. *Physiology (Bethesda, Md.)* **21**, 103–114.

BENFENATI, V., CAPRINI, M., NICCHIA, G.P., ROSSI, A., DOVIZIO, M., CERVETTO, C., NOBILE, M., AND FERRONI, S. Carbenoxolone inhibits volume-regulated anion conductance in cultured rat cortical astroglia. *Channels (Austin, Tex.)* **3**, 323–336.

BERNDTSSON, M., HÄGG, M., PANARETAKIS, T., HAVELKA, A.M., SHOSHAN, M.C., AND LINDER, S. (2007). Acute apoptosis by cisplatin requires induction of reactive oxygen species but is not associated with damage to nuclear DNA. *International Journal of Cancer. Journal International Du Cancer* **120**, 175–180.

BEST, L. (2005). Glucose-induced electrical activity in rat pancreatic beta-cells: dependence on intracellular chloride concentration. *The Journal of Physiology* **568**, 137–144.

BEST, L., SHEADER, E.A., AND BROWN, P.D. (1996). A volume-activated anion conductance in insulin-secreting cells. *Pflügers Archiv European Journal of Physiology* **431**, 363–370.

BEST, L., BROWN, P.D., SENER, A., AND MALAISSE, W.J. (2010). Electrical activity in pancreatic islet cells: The VRAC hypothesis. *Islets* **2**, 59–64.

BIEMANS-OLDEHINKEL, E., MAHMOOD, N.A.B.N., AND POOLMAN, B. (2006). A sensor for intracellular ionic strength. *Proceedings of the National Academy of Sciences* **103**, 10624–10629.

BLUM, A.E., WALSH, B.C., AND DUBYAK, G.R. (2010). Extracellular osmolarity modulates G protein-coupled receptor-dependent ATP release from 1321N1 astrocytoma cells. *American Journal of Physiology. Cell Physiology* **298**, C386-96.

BOASSA, D., AMBROSI, C., QIU, F., DAHL, G., GAIETTA, G., AND SOSINSKY, G. (2007). Pannexin1 Channels Contain a Glycosylation Site That Targets the Hexamer to the Plasma Membrane. *Journal of Biological Chemistry* **282**, 31733–31743.

BOESE, S.H., WEHNER, F., AND KINNE, R.K. (1996a). Taurine permeation through swelling-activated anion conductance in rat IMCD cells in primary culture. *The American Journal of Physiology* **271**, F498-507.

BOESE, S.H., KINNE, R.K., AND WEHNER, F. (1996b). Single-channel properties of swelling-activated anion conductance in rat inner medullary collecting duct cells. *The American Journal of Physiology* **271**, F1224-33.

BOND, S.R., AND NAUS, C.C. (2014). The pannexins: past and present. *Frontiers in Physiology* **5**, 58.

BOOM, A., LYBAERT, P., POLLET, J.-F., JACOBS, P., JIJAKLI, H., GOLSTEIN, P.E., SENER, A., MALAISSE, W.J., AND BEAUWENS, R. (2007). Expression and localization of cystic fibrosis transmembrane conductance regulator in the rat endocrine pancreas. *Endocrine* **32**, 197–205.

BORSANI, G., RUGARLI, E.I., TAGLIALATELA, M., WONG, C., AND BALLABIO, A. (1995). Characterization of a human and murine gene (CLCN3) sharing similarities to voltage-gated chloride channels and to a yeast integral membrane protein. *Genomics* **27**, 131–141.

BORST, P., BORST, J., AND SMETS, L.A. (2001). Does resistance to apoptosis affect clinical response to antitumor drugs? *Drug Resistance Updates : Reviews and Commentaries in Antimicrobial and Anticancer Chemotherapy* **4**, 129–131.

BORTNER, C.D., AND CIDLOWSKI, J.A. (1998). A necessary role for cell shrinkage in apoptosis. *Biochemical Pharmacology* **56**, 1549–1559.

BOTCHKIN, L.M., AND MATTHEWS, G. (1993). Chloride current activated by swelling in retinal pigment epithelium cells. *The American Journal of Physiology* **265**, C1037-45.

BOURQUE, C.W., AND OLIET, S.H. (1997). Osmoreceptors in the central nervous system. *Annual Review of Physiology* **59**, 601–619.

BOWENS, N.H., DOHARE, P., KUO, Y.-H., AND MONGIN, A.A. (2013). DCPIB, the proposed selective blocker of volume-regulated anion channels, inhibits several glutamate transport pathways in glial cells. *Molecular Pharmacology* **83**, 22–32.

BRATTAIN, M.G., FINE, W.D., KHALED, F.M., THOMPSON, J., AND BRATTAIN, D.E. (1981). Heterogeneity of malignant cells from a human colonic carcinoma. *Cancer Research* **41**, 1751–1756.

BRAUN, A.P., AND SCHULMAN, H. (1996). Distinct voltage-dependent gating behaviours of a swelling-activated chloride current in human epithelial cells. *The Journal of Physiology* **495**, 743–753.

BRÈS, V., HURBIN, A., DUVOID, A., ORCEL, H., MOOS, F.C., RABIÉ, A., AND HUSSY, N. (2000). Pharmacological characterization of volume-sensitive, taurine permeable anion channels in rat supraoptic glial cells. *British Journal of Pharmacology* **130**, 1976–1982.

BROWE, D.M., AND BAUMGARTEN, C.M. (2003). Stretch of beta 1 integrin activates an outwardly rectifying chloride current via FAK and Src in rabbit ventricular myocytes. *The Journal of General Physiology* **122**, 689–702.

BROWE, D.M., AND BAUMGARTEN, C.M. (2004). Angiotensin II (AT1) Receptors and NADPH Oxidase Regulate Cl^- Current Elicited by 1 Integrin Stretch in Rabbit Ventricular Myocytes. *The Journal of General Physiology* **124**, 273–287.

BROWE, D.M., AND BAUMGARTEN, C.M. (2006). EGFR kinase regulates volume-sensitive chloride current elicited by integrin stretch via PI-3K and NADPH oxidase in ventricular myocytes. *The Journal of General Physiology* **127**, 237–251.

BRUZZONE, R., HORMUZDI, S.G., BARBE, M.T., HERB, A., AND MONYER, H. (2003). Pannexins, a family of gap junction proteins expressed in brain. *Proceedings of the National Academy of Sciences of the United States of America* **100**, 13644–13649.

BRUZZONE, R., BARBE, M.T., JAKOB, N.J., AND MONYER, H. (2005). Pharmacological properties of homomeric and heteromeric pannexin hemichannels expressed in Xenopus oocytes. *Journal of Neurochemistry* **92**, 1033–1043.

BRYAN-SISNEROS, A., SABANOV, V., THOROED, S.M., AND DOROSHENKO, P. (2000). Dual role of ATP in supporting volume-regulated chloride channels in mouse fibroblasts. *Biochimica et Biophysica Acta* **1468**, 63–72.

BURG, M.B. (2002). Response of renal inner medullary epithelial cells to osmotic stress. *Comparative Biochemistry and Physiology. Part A, Molecular & Integrative Physiology* **133**, 661–666.

BURNSTOCK, G. (2008). Purinergic signalling and disorders of the central nervous system. *Nature Reviews. Drug Discovery* **7**, 575–590.

BUROW, P., KLAPPERSTÜCK, M., AND MARKWARDT, F. (2015). Activation of ATP secretion via volume-regulated anion channels by sphingosine-1-phosphate in RAW macrophages. *Pflügers Archiv : European Journal of Physiology* **467**, 1215–1226.

BUYSE, G., VOETS, T., TYTGAT, J., DE GREEF, C., DROOGMANS, G., NILIUS, B., AND EGGERMONT, J. (1997). Expression of human pI_{Cln} and ClC-6 in Xenopus oocytes induces an identical endogenous chloride conductance. *The Journal of Biological Chemistry* **272**, 3615–3621.

BYFIELD, F.J., ARANDA-ESPINOZA, H., ROMANENKO, V.G., ROTHBLAT, G.H., AND LEVITAN, I. (2004). Cholesterol depletion increases membrane stiffness of aortic endothelial cells. *Biophysical Journal* **87**, 3336–3343.

BYFIELD, F.J., HOFFMAN, B.D., ROMANENKO, V.G., FANG, Y., CROCKER, J.C., AND LEVITAN, I. (2006). Evidence for the role of cell stiffness in modulation of volume-regulated anion channels. *Acta Physiologica (Oxford, England)* **187**, 285–294.

CAHALAN, M.D. (2009). STIMulating store-operated Ca^{2+} entry. *Nature Cell Biology* **11**, 669–677.

CAHALAN, M.D., AND LEWIS, R.S. (1988). Role of potassium and chloride channels in volume regulation by T lymphocytes. *Society of General Physiologists Series* **43**, 281–301.

CAI, S., ZHANG, T., ZHANG, D., QIU, G., AND LIU, Y. (2015). Volume-sensitive chloride channels are involved in cisplatin treatment of osteosarcoma. *Molecular Medicine Reports* **11**, 2465–2470.

CANNON, C.L., BASAVAPPA, S., AND STRANGE, K. (1998). Intracellular ionic strength regulates the volume sensitivity of a swelling-activated anion channel. *The American Journal of Physiology* **275**, C416-22.

CARETTE, J.E., RAABEN, M., WONG, A.C., HERBERT, A.S., OBERNOSTERER, G., MULHERKAR, N., KUEHNE, A.I., KRANZUSCH, P.J., GRIFFIN, A.M., RUTHEL, G., DAL CIN, P., DYE, J.M., WHELAN, S.P., CHANDRAN, K., AND BRUMMELKAMP, T.R. (2011). Ebola virus entry requires the cholesterol transporter Niemann-Pick C1. *Nature* **477**, 340–343.

CARTON, I., TROUET, D., HERMANS, D., BARTH, H., AKTORIES, K., DROOGMANS, G., JORGENSEN, N.K., HOFFMANN, E.K., NILIUS, B., AND EGGERMONT, J. (2002). RhoA exerts a permissive effect on volume-regulated anion channels in vascular endothelial cells. *American Journal of Physiology. Cell Physiology* **283**, C115-25.

CATTERALL, W.A. (2012). Voltage-gated sodium channels at 60: structure, function and pathophysiology. *The Journal of Physiology* **590**, 2577–2589.

CHARI, A., GOLAS, M.M., KLINGENHÄGER, M., NEUENKIRCHEN, N., SANDER, B., ENGLBRECHT, C., SICKMANN, A., STARK, H., AND FISCHER, U. (2008). An assembly chaperone collaborates with the SMN complex to generate spliceosomal SnRNPs. *Cell* **135**, 497–509.

CHEKENI, F.B., ELLIOTT, M.R., SANDILOS, J.K., WALK, S.F., KINCHEN, J.M., LAZAROWSKI, E.R., ARMSTRONG, A.J., PENUELA, S., LAIRD, D.W., SALVESEN, G.S., ISAKSON, B.E., BAYLISS, D.A., AND RAVICHANDRAN, K.S. (2010). Pannexin 1 channels mediate "find-me" signal release and membrane permeability during apoptosis. *Nature* **467**, 863–867.

CHEMIN, J., PATEL, A.J., DUPRAT, F., LAURITZEN, I., LAZDUNSKI, M., HONORÉ, E., ARONHEIM, A., BANG, H., KIM, Y., KIM, D., BAUKROWITZ, T., SCHULTE, U., OLIVER, D., HERLITZE, S., KRAUTER, T., TUCKER, S., RUPPERSBERG, J., FAKLER, B., BERG, A., ET AL. (2005). A phospholipid sensor controls mechanogating of the K^+ channel TREK-1. *The EMBO Journal* **24**, 44–53.

CHEN, L.X., ZHU, L.Y., JACOB, T.J.C., AND WANG, L.W. (2007). Roles of volume-activated Cl^- currents and regulatory volume decrease in the cell cycle and proliferation in nasopharyngeal carcinoma cells. *Cell Proliferation* **40**, 253–267.

CHIEN, L.-T., AND HARTZELL, H.C. (2007). Drosophila bestrophin-1 chloride current is dually regulated by calcium and cell volume. *The Journal of General Physiology* **130**, 513–524.

CHIEN, L.-T., AND HARTZELL, H.C. (2008). Rescue of volume-regulated anion current by bestrophin mutants with altered charge selectivity. *The Journal of General Physiology* **132**, 537–546.

CHIEN, L.-T., ZHANG, Z.-R., AND HARTZELL, H.C. (2006). Single Cl^- channels activated by Ca^{2+} in Drosophila S2 cells are mediated by bestrophins. *The Journal of General Physiology* **128**, 247–259.

COCA-PRADOS, M., ANGUÍTA, J., CHALFANT, M.L., AND CIVAN, M.M. (1995). PKC-sensitive Cl^- channels associated with ciliary epithelial homologue of pI_{Cln}. *The American Journal of Physiology* **268**, C572-9.

COLLINS, S.J., GALLO, R.C., AND GALLAGHER, R.E. (1977). Continuous growth and differentiation of human myeloid leukaemic cells in suspension culture. *Nature* **270**, 347–349.

CONG, L., RAN, F.A., COX, D., LIN, S., BARRETTO, R., HABIB, N., HSU, P.D., WU, X., JIANG, W., MARRAFFINI, L.A., AND ZHANG, F. (2013). Multiplex genome engineering using CRISPR/Cas systems. *Science (New York, N.Y.)* **339**, 819–823.

CONNORS, B.W. (2012). Tales of a dirty drug: carbenoxolone, gap junctions, and seizures. *Epilepsy Currents / American Epilepsy Society* **12**, 66–68.

CUELLO, L.G., JOGINI, V., CORTES, D.M., AND PEROZO, E. (2010). Structural mechanism of C-type inactivation in K^+ channels. *Nature* **466**, 203–208.

D'ANGLEMONT DE TASSIGNY, A., SOUKTANI, R., HENRY, P., GHALEH, B., AND BERDEAUX, A. (2004). Volume-sensitive chloride channels ($I_{Cl,vol}$) mediate doxorubicin-induced apoptosis through apoptotic volume decrease in cardiomyocytes. *Fundamental & Clinical Pharmacology* **18**, 531–538.

D'ANGLEMONT DE TASSIGNY, A., BERDEAUX, A., SOUKTANI, R., HENRY, P., AND GHALEH, B. (2008). The volume-sensitive chloride channel inhibitors prevent both contractile dysfunction and apoptosis induced by doxorubicin through PI_3kinase, Akt and Erk 1/2. *European Journal of Heart Failure* **10**, 39–46.

DANBOLT, N.C. (2001). Glutamate uptake. *Progress in Neurobiology* **65**, 1–105.

DARBY, M., KUZMISKI, J.B., PANENKA, W., FEIGHAN, D., AND MACVICAR, B.A. (2003). ATP released from astrocytes during swelling activates chloride channels. *Journal of Neurophysiology* **89**, 1870–1877.

DASCAL, N. (1987). The use of Xenopus oocytes for the study of ion channels. *CRC Critical Reviews in Biochemistry* **22**, 317–387.

DECHER, N., LANG, H.J., NILIUS, B., BRÜGGEMANN, A., BUSCH, A.E., AND STEINMEYER, K. (2001). DCPIB is a novel selective blocker of $I_{(Cl,swell)}$ and prevents swelling-induced shortening of guinea-pig atrial action potential duration. *British Journal of Pharmacology* **134**, 1467–1479.

DELEUZE, C., DUVOID, A., AND HUSSY, N. (1998). Properties and glial origin of osmotic-dependent release of taurine from the rat supraoptic nucleus. *The Journal of Physiology* **507**, 463–471.

DICK, G.M., ROSSOW, C.F., SMIRNOV, S., HOROWITZ, B., AND SANDERS, K.M. (2001). Tamoxifen activates smooth muscle BK channels through the regulatory beta 1 subunit. *The Journal of Biological Chemistry* **276**, 34594–34599.

DOLAN, J., WALSHE, K., ALSBURY, S., HOKAMP, K., O'KEEFFE, S., OKAFUJI, T., MILLER, S.F.C., TEAR, G., AND MITCHELL, K.J. (2007). The extracellular leucine-rich repeat superfamily; a comparative survey and analysis of evolutionary relationships and expression patterns. *BMC Genomics* **8**, 320.

DOROSHENKO, P. (1991). Second messengers mediating activation of chloride current by intracellular GTP gamma S in bovine chromaffin cells. *The Journal of Physiology* **436**, 725–738.

DOROSHENKO, P., AND NEHER, E. (1992). Volume-sensitive chloride conductance in bovine chromaffin cell membrane. *The Journal of Physiology* **449**, 197–218.

DOROSHENKO, P., SABANOV, V., AND DOROSHENKO, N. (2001). Cell cycle-related changes in regulatory volume decrease and volume-sensitive chloride conductance in mouse fibroblasts. *Journal of Cellular Physiology* **187**, 65–72.

DROOGMANS, G., PRENEN, J., EGGERMONT, J., VOETS, T., AND NILIUS, B. (1998). Voltage-dependent block of endothelial volume-regulated anion channels by calix[4]arenes. *Am J Physiol Cell Physiol* **275**, C646-652.

DROOGMANS, G., MAERTENS, C., PRENEN, J., AND NILIUS, B. (1999). Sulphonic acid derivatives as probes of pore properties of volume-regulated anion channels in endothelial cells. *British Journal of Pharmacology* **128**, 35–40.

DUAN, D., HUME, J.R., AND NATTEL, S. (1997a). Evidence that outwardly rectifying Cl^- channels underlie volume-regulated Cl^- currents in heart. *Circulation Research* **80**, 103–113.

DUAN, D., WINTER, C., COWLEY, S., HUME, J.R., AND HOROWITZ, B. (1997b). Molecular identification of a volume-regulated chloride channel. *Nature* **390**, 417–421.

DUBOIS, J.-M., AND ROUZAIRE-DUBOIS, B. (2004). The influence of cell volume changes on tumour cell proliferation. *European Biophysics Journal : EBJ* **33**, 227–232.

DUCHARME, G., NEWELL, E.W., PINTO, C., AND SCHLICHTER, L.C. (2007). Small-conductance Cl^- channels contribute to volume regulation and phagocytosis in microglia. *The European Journal of Neuroscience* **26**, 2119–2130.

EERTMOED, A.L., VALLEJO, Y.F., AND GREEN, W.N. (1998). Transient expression of heteromeric ion channels. *Methods in Enzymology* **293**, 564–585.

EHRING, G.R., OSIPCHUK, Y. V, AND CAHALAN, M.D. (1994). Swelling-activated chloride channels in multidrug-sensitive and -resistant cells. *The Journal of General Physiology* **104**, 1129–1161.

EISENMAN, G. (1961). On the elementary atomic origin of equilibrium ionic specificity. In Symposium on Membrane Transport and Metabolism, pp. 163–179.

ELLIOTT, M.R., CHEKENI, F.B., TRAMPONT, P.C., LAZAROWSKI, E.R., KADL, A., WALK, S.F., PARK, D., WOODSON, R.I., OSTANKOVICH, M., SHARMA, P., LYSIAK, J.J., HARDEN, T.K., LEITINGER, N., AND RAVICHANDRAN, K.S. (2009). Nucleotides released by apoptotic cells act as a find-me signal to promote phagocytic clearance. *Nature* **461**, 282–286.

ELLIS, R.J. (2001). Macromolecular crowding: obvious but underappreciated. *Trends in Biochemical Sciences* **26**, 597–604.

ENKHBAYAR, P., KAMIYA, M., OSAKI, M., MATSUMOTO, T., AND MATSUSHIMA, N. (2004). Structural principles of leucine-rich repeat (LRR) proteins. *Proteins* **54**, 394–403.

FAN, H.T., MORISHIMA, S., KIDA, H., AND OKADA, Y. (2001). Phloretin differentially inhibits volume-sensitive and cyclic AMP-activated, but not Ca-activated, Cl^- channels. *British Journal of Pharmacology* **133**, 1096–1106.

FATHERAZI, S., IZUTSU, K.T., WELLNER, R.B., AND BELTON, C.M. (1994). Hypotonically activated chloride current in HSG cells. *The Journal of Membrane Biology* **142**, 181–193.

FAYAD, W., BRNJIC, S., BERGLIND, D., BLIXT, S., SHOSHAN, M.C., BERNDTSSON, M., OLOFSSON, M.H., AND LINDER, S. (2009). Restriction of cisplatin induction of acute apoptosis to a subpopulation of cells in a three-dimensional carcinoma culture model. *International Journal of Cancer. Journal International Du Cancer* **125**, 2450–2455.

FESKE, S., GWACK, Y., PRAKRIYA, M., SRIKANTH, S., PUPPEL, S.-H., TANASA, B., HOGAN, P.G., LEWIS, R.S., DALY, M., AND RAO, A. (2006). A mutation in Orai1 causes immune deficiency by abrogating CRAC channel function. *Nature* **441**, 179–185.

FEUSTEL, P.J., JIN, Y., AND KIMELBERG, H.K. (2004). Volume-regulated anion channels are the predominant contributors to release of excitatory amino acids in the ischemic cortical penumbra. *Stroke; a Journal of Cerebral Circulation* **35**, 1164–1168.

FIÉVET, B., GABILLAT, N., BORGESE, F., AND MOTAIS, R. (1995). Expression of band 3 anion exchanger induces chloride current and taurine transport: structure-function analysis. *The EMBO Journal* **14**, 5158–5169.

FISCHER, S.J., BENSON, L.M., FAUQ, A., NAYLOR, S., AND WINDEBANK, A.J. (2008). Cisplatin and dimethyl sulfoxide react to form an adducted compound with reduced cytotoxicity and neurotoxicity. *Neurotoxicology* **29**, 444–452.

FISCHMEISTER, R., AND HARTZELL, H.C. (2005). Volume sensitivity of the bestrophin family of chloride channels. *The Journal of Physiology* **562**, 477–491.

FISHER, S.K., CHEEMA, T.A., FOSTER, D.J., AND HEACOCK, A.M. (2008). Volume-dependent osmolyte efflux from neural tissues: regulation by G-protein-coupled receptors. *Journal of Neurochemistry* **106**, 1998–2014.

FISHER, S.K., HEACOCK, A.M., KEEP, R.F., AND FOSTER, D.J. (2010). Receptor regulation of osmolyte homeostasis in neural cells. *The Journal of Physiology* **588**, 3355–3364.

FLICEK, P., AMODE, M.R., BARRELL, D., BEAL, K., BRENT, S., CHEN, Y., CLAPHAM, P., COATES, G., FAIRLEY, S., FITZGERALD, S., GORDON, L., HENDRIX, M., HOURLIER, T., JOHNSON, N., KÄHÄRI, A., KEEFE, D., KEENAN, S., KINSELLA, R., KOKOCINSKI, F., ET AL. (2011). Ensembl 2011. *Nucleic Acids Research* **39**, D800-6.

FRANCO, R., PANAYIOTIDIS, M.I., AND DE LA PAZ, L.D.O. (2008). Autocrine signaling involved in cell volume regulation: the role of released transmitters and plasma membrane receptors. *Journal of Cellular Physiology* **216**, 14–28.

FRIEDRICH, T., BREIDERHOFF, T., AND JENTSCH, T.J. (1999). Mutational analysis demonstrates that ClC-4 and ClC-5 directly mediate plasma membrane currents. *The Journal of Biological Chemistry* **274**, 896–902.

FUJII, T., TAKAHASHI, Y., TAKESHIMA, H., SAITOH, C., SHIMIZU, T., TAKEGUCHI, N., AND SAKAI, H. (2015). Inhibition of gastric H^+,K^+-ATPase by 4-(2-butyl-6,7-dichloro-2-cyclopentylindan-1-on-5-yl)oxybutyric acid (DCPIB), an inhibitor of volume-regulated anion channel. *European Journal of Pharmacology* **765**, 34–41.

GATELY, D.P., AND HOWELL, S.B. (1993). Cellular accumulation of the anticancer agent cisplatin: a review. *British Journal of Cancer* **67**, 1171–1176.

GAY, N.J., SYMMONS, M.F., GANGLOFF, M., AND BRYANT, C.E. (2014). Assembly and localization of Toll-like receptor signalling complexes. *Nature Reviews Immunology* **14**, 546–558.

GEY, G.O., COFFMANN, W.D., AND KUBICEK, M.T. (1952). Tissue culture studies of the proliferative capacity of cervical carcinoma and normal epithelium. *Cancer Research* **12**, 264–265.

GILL, D.R., HYDE, S.C., HIGGINS, C.F., VALVERDE, M.A., MINTENIG, G.M., AND SEPÚLVEDA, F. V (1992). Separation of drug transport and chloride channel functions of the human multidrug resistance P-glycoprotein. *Cell* **71**, 23–32.

GOLDSTEIN, L., AND BRILL, S.R. (1991). Volume-activated taurine efflux from skate erythrocytes: possible band 3 involvement. *The American Journal of Physiology* **260**, R1014-20.

GOLDSTEIN, L., BRILL, S.R., AND FREUND, E. V. (1990). Activation of taurine efflux in hypotonically stressed elasmobranch cells: Inhibition by stilbene disulfonates. *Journal of Experimental Zoology* **254**, 114–118.

GONG, W., XU, H., SHIMIZU, T., MORISHIMA, S., TANABE, S., TACHIBE, T., UCHIDA, S., SASAKI, S., AND OKADA, Y. (2004). ClC-3-independent, PKC-dependent activity of volume-sensitive Cl channel in mouse ventricular cardiomyocytes. *Cellular Physiology and Biochemistry : International Journal of Experimental Cellular Physiology, Biochemistry, and Pharmacology* **14**, 213–224.

GOSLING, M., SMITH, J.W., AND POYNER, D.R. (1995). Characterization of a volume-sensitive chloride current in rat osteoblast-like (ROS 17/2.8) cells. *The Journal of Physiology* **485**, 671–682.

GOSLING, M., POYNER, D.R., AND SMITH, J.W. (1996). Effects of arachidonic acid upon the volume-sensitive chloride current in rat osteoblast-like (ROS 17/2.8) cells. *The Journal of Physiology* **493**, 613–623.

GRAF, J., RUPNIK, M., ZUPANCIC, G., AND ZOREC, R. (1995). Osmotic swelling of hepatocytes increases membrane conductance but not membrane capacitance. *Biophysical Journal* **68**, 1359–1363.

GRAHAM, F.L., SMILEY, J., RUSSELL, W.C., AND NAIRN, R. (1977). Characteristics of a human cell line transformed by DNA from human adenovirus type 5. *The Journal of General Virology* **36**, 59–74.

DE GREEF, C., VAN DER HEYDEN, S., VIANA, F., EGGERMONT, J., DE BRUIJN, E.A., RAEYMAEKERS, L., DROOGMANS, G., AND NILIUS, B. (1995a). Lack of correlation between mdr-1 expression and volume-activation of cloride-currents in rat colon cancer cells. *Pflügers Archiv : European Journal of Physiology* **430**, 296–298.

DE GREEF, C., SEHRER, J., VIANA, F., VAN ACKER, K., EGGERMONT, J., MERTENS, L., RAEYMAEKERS, L., DROOGMANS, G., AND NILIUS, B. (1995b). Volume-activated chloride currents are not correlated with P-glycoprotein expression. *The Biochemical Journal* **307**, 713–718.

GRINSTEIN, S., AND FOSKETT, J.K. (1990). Ionic mechanisms of cell volume regulation in leukocytes. *Annual Review of Physiology* **52**, 399–414.

GRINSTEIN, S., CLARKE, C.A., DUPRE, A., AND ROTHSTEIN, A. (1982). Volume-induced increase of anion permeability in human lymphocytes. *The Journal of General Physiology* **80**, 801–823.

GROULX, N., BOUDREAULT, F., ORLOV, S.N., AND GRYGORCZYK, R. (2006). Membrane reserves and hypotonic cell swelling. *The Journal of Membrane Biology* **214**, 43–56.

GRUBB, S., POULSEN, K.A., JUUL, C.A., KYED, T., KLAUSEN, T.K., LARSEN, E.H., AND HOFFMANN, E.K. (2013). TMEM16F (Anoctamin 6), an anion channel of delayed Ca^{2+} activation. *The Journal of General Physiology* **141**, 585–600.

GRÜNDER, S., THIEMANN, A., PUSCH, M., AND JENTSCH, T.J. (1992). Regions involved in the opening of CIC-2 chloride channel by voltage and cell volume. *Nature* **360**, 759–762.

GUO, J.H., CHEN, H., RUAN, Y.C., ZHANG, X.L., ZHANG, X.H., FOK, K.L., TSANG, L.L., YU, M.K., HUANG, W.Q., SUN, X., CHUNG, Y.W., JIANG, X., SOHMA, Y., AND CHAN, H.C. (2014). Glucose-induced electrical activities and insulin secretion in pancreatic islet β-cells are modulated by CFTR. *Nature Communications* **5**, 4420.

GUZMAN, R.E., GRIESCHAT, M., FAHLKE, C., AND ALEKOV, A.K. (2013). ClC-3 is an intracellular chloride/proton exchanger with large voltage-dependent nonlinear capacitance. *ACS Chemical Neuroscience* **4**, 994–1003.

HABELA, C.W., AND SONTHEIMER, H. (2007). Cytoplasmic volume condensation is an integral part of mitosis. *Cell Cycle (Georgetown, Tex.)* **6**, 1613–1620.

HAGIWARA, N., MASUDA, H., SHODA, M., AND IRISAWA, H. (1992). Stretch-activated anion currents of rabbit cardiac myocytes. *The Journal of Physiology* **456**, 285–302.

HALL, J.A., KIRK, J., POTTS, J.R., RAE, C., AND KIRK, K. (1996). Anion channel blockers inhibit swelling-activated anion, cation, and nonelectrolyte transport in HeLa cells. *The American Journal of Physiology* **271**, C579-88.

HARRIGAN, T.J., ABDULLAEV, I.F., JOURD'HEUIL, D., AND MONGIN, A.A. (2008). Activation of microglia with zymosan promotes excitatory amino acid release via volume-regulated anion channels: the role of NADPH oxidases. *Journal of Neurochemistry* **106**, 2449–2462.

HARTZELL, H.C., QU, Z., YU, K., XIAO, Q., AND CHIEN, L.-T. (2008). Molecular physiology of bestrophins: multifunctional membrane proteins linked to best disease and other retinopathies. *Physiological Reviews* **88**, 639–672.

HARVEY, V.L., SAUL, M.W., GARNER, C., AND MCDONALD, R.L. (2010). A role for the volume regulated anion channel in volume regulation in the murine CNS cell line, CAD. *Acta Physiologica (Oxford, England)* **198**, 159–168.

HAYASHI, T., NOZAKI, Y., NISHIZUKA, M., IKAWA, M., OSADA, S., AND IMAGAWA, M. (2011). Factor for adipocyte differentiation 158 gene disruption prevents the body weight gain and insulin resistance induced by a high-fat diet. *Biological & Pharmaceutical Bulletin* **34**, 1257–1263.

HAZAMA, A., AND OKADA, Y. (1988). Ca^{2+} sensitivity of volume-regulatory K^+ and Cl^- channels in cultured human epithelial cells. *The Journal of Physiology* **402**, 687–702.

HEINKE, S., RASKIN, G., DE SMET, P., DROOGMANS, G., VAN DRIESSCHE, W., AND NILIUS, B. (1997). Simultaneous measurement of membrane capacitance and whole cell currents during cell swelling in macrovascular endothelium. *Cellular Physiology and Biochemistry* **7**, 19–24.

HÉLIX, N., STRØBAEK, D., DAHL, B.H., AND CHRISTOPHERSEN, P. (2003). Inhibition of the endogenous volume-regulated anion channel (VRAC) in HEK293 cells by acidic di-aryl-ureas. *The Journal of Membrane Biology* **196**, 83–94.

HERNÁNDEZ-CARBALLO, C.Y., DE SANTIAGO-CASTILLO, J.A., ROSALES-SAAVEDRA, T., PÉREZ-CORNEJO, P., AND ARREOLA, J. (2010). Control of volume-sensitive chloride channel inactivation by the coupled action of intracellular chloride and extracellular protons. *Pflügers Archiv : European Journal of Physiology* **460**, 633–644.

HISADOME, K., KOYAMA, T., KIMURA, C., DROOGMANS, G., ITO, Y., AND OIKE, M. (2002). Volume-regulated anion channels serve as an auto/paracrine nucleotide release pathway in aortic endothelial cells. *The Journal of General Physiology* **119**, 511–520.

HODSON, M.E. (1992). Diabetes mellitus and cystic fibrosis. *Baillière's Clinical Endocrinology and Metabolism* **6**, 797–805.

HOFFMANN, E. (1978). Regulation of cell volume by selective changes in the leak permeabilities of Ehrlich ascites tumor cells. *Alfred Benzon Symposium*.

HOFFMANN, E.K., LAMBERT, I.H., AND PEDERSEN, S.F. (2009). Physiology of cell volume regulation in vertebrates. *Physiological Reviews* **89**, 193–277.

HOFFMANN, E.K., SØRENSEN, B.H., SAUTER, D.P.R., AND LAMBERT, I.H. (2015). Role of volume-regulated and calcium-activated anion channels in cell volume homeostasis, cancer and drug resistance. *Channels (Austin, Tex.)* **9**, 1–17.

HOSHI, T., ZAGOTTA, W.N., AND ALDRICH, R.W. (1990). Biophysical and molecular mechanisms of Shaker potassium channel inactivation. *Science (New York, N.Y.)* **250**, 533–538.

HOSHI, T., ZAGOTTA, W.N., AND ALDRICH, R.W. (1991). Two types of inactivation in Shaker K^+ channels: effects of alterations in the carboxy-terminal region. *Neuron* **7**, 547–556.

HOU, X., PEDI, L., DIVER, M.M., AND LONG, S.B. (2012). Crystal structure of the calcium release-activated calcium channel Orai. *Science (New York, N.Y.)* **338**, 1308–1313.

HUANG, F., WONG, X., AND JAN, L.Y. (2012). International Union of Basic and Clinical Pharmacology. LXXXV: calcium-activated chloride channels. *Pharmacological Reviews* **64**, 1–15.

HUSSY, N., DELEUZE, C., PANTALONI, A., DESARMÉNIEN, M.G., AND MOOS, F. (1997). Agonist action of taurine on glycine receptors in rat supraoptic magnocellular neurones: possible role in osmoregulation. *The Journal of Physiology* **502**, 609–621.

HYZINSKI-GARCÍA, M.C., RUDKOUSKAYA, A., AND MONGIN, A.A. (2014). LRRC8A protein is indispensable for swelling-activated and ATP-induced release of excitatory amino acids in rat astrocytes. *The Journal of Physiology* **592**, 4855–4862.

ICHIKAWA, M., OKAMURA-OHO, Y., SHIMOKAWA, K., KONDO, S., NAKAMURA, S., YOKOTA, H., HIMENO, R., LESCH, K.-P., AND HAYASHIZAKI, Y. (2008). Expression analysis for inverted effects of serotonin transporter inactivation. *Biochemical and Biophysical Research Communications* **368**, 43–49.

IDZKO, M., FERRARI, D., AND ELTZSCHIG, H.K. (2014). Nucleotide signalling during inflammation. *Nature* **509**, 310–317.

INOUE, H., AND OKADA, Y. (2007). Roles of volume-sensitive chloride channel in excitotoxic neuronal injury. *The Journal of Neuroscience : The Official Journal of the Society for Neuroscience* **27**, 1445–1455.

INOUE, H., MORI, S.-I., MORISHIMA, S., AND OKADA, Y. (2005). Volume-sensitive chloride channels in mouse cortical neurons: characterization and role in volume regulation. *The European Journal of Neuroscience* **21**, 1648–1658.

ISE, T., SHIMIZU, T., LEE, E.L., INOUE, H., KOHNO, K., AND OKADA, Y. (2005). Roles of volume-sensitive Cl^- channel in cisplatin-induced apoptosis in human epidermoid cancer cells. *The Journal of Membrane Biology* **205**, 139–145.

IWASA, K., TASAKI, I., AND GIBBONS, R.C. (1980). Swelling of nerve fibers associated with action potentials. *Science (New York, N.Y.)* **210**, 338–339.

JACKSON, P.S., AND STRANGE, K. (1993). Volume-sensitive anion channels mediate swelling-activated inositol and taurine efflux. *The American Journal of Physiology* **265**, C1489-500.

JACKSON, P.S., AND STRANGE, K. (1995a). Characterization of the voltage-dependent properties of a volume-sensitive anion conductance. *The Journal of General Physiology* **105**, 661–676.

JACKSON, P.S., AND STRANGE, K. (1995b). Single-channel properties of a volume-sensitive anion conductance. Current activation occurs by abrupt switching of closed channels to an open state. *The Journal of General Physiology* **105**, 643–660.

JACKSON, P.S., MORRISON, R., AND STRANGE, K. (1994). The volume-sensitive organic osmolyte-anion channel VSOAC is regulated by nonhydrolytic ATP binding. *The American Journal of Physiology* **267**, C1203-9.

JACKSON, P.S., CHURCHWELL, K., BALLATORI, N., BOYER, J.L., AND STRANGE, K. (1996). Swelling-activated anion conductance in skate hepatocytes: regulation by cell Cl^- and ATP. *The American Journal of Physiology* **270**, C57-66.

JENTSCH, T.J. (2008). CLC Chloride Channels and Transporters: From Genes to Protein Structure, Pathology and Physiology. *Critical Reviews in Biochemistry and Molecular Biology* **43**, 3–36.

JENTSCH, T.J. (2015). Discovery of CLC transport proteins: cloning, structure, function and pathophysiology. *The Journal of Physiology* **593**, 4091–4109.

JENTSCH, T.J., GÜNTHER, W., PUSCH, M., AND SCHWAPPACH, B. (1995). Properties of voltage-gated chloride channels of the ClC gene family. *The Journal of Physiology* **482**, 19S–25S.

JENTSCH, T.J., STEIN, V., WEINREICH, F., AND ZDEBIK, A.A. (2002). Molecular structure and physiological function of chloride channels. *Physiological Reviews* **82**, 503–568.

JIAO, J.-D., XU, C.-Q., YUE, P., DONG, D.-L., LI, Z., DU, Z.-M., AND YANG, B.-F. (2006). Volume-sensitive outwardly rectifying chloride channels are involved in oxidative stress-induced apoptosis of mesangial cells. *Biochemical and Biophysical Research Communications* **340**, 277–285.

JUSZCZAK, G.R., AND SWIERGIEL, A.H. (2009). Properties of gap junction blockers and their behavioural, cognitive and electrophysiological effects: animal and human studies. *Progress in Neuro-Psychopharmacology & Biological Psychiatry* **33**, 181–198.

JUUL, C.A., GRUBB, S., POULSEN, K.A., KYED, T., HASHEM, N., LAMBERT, I.H., LARSEN, E.H., AND HOFFMANN, E.K. (2014). Anoctamin 6 differs from VRAC and VSOAC but is involved in apoptosis and supports volume regulation in the presence of Ca^{2+}. *Pflügers Archiv : European Journal of Physiology* **466**, 1899–1910.

KACZMAREK, L.K., AND BLUMENTHAL, E.M. (1997). Properties and regulation of the minK potassium channel protein. *Physiological Reviews* **77**, 627–641.

KAWASAKI, M., UCHIDA, S., MONKAWA, T., MIYAWAKI, A., MIKOSHIBA, K., MARUMO, F., AND SASAKI, S. (1994). Cloning and expression of a protein kinase C-regulated chloride channel abundantly expressed in rat brain neuronal cells. *Neuron* **12**, 597–604.

KAWASAKI, M., SUZUKI, M., UCHIDA, S., SASAKI, S., AND MARUMO, F. (1995). Stable and functional expression of the CIC-3 chloride channel in somatic cell lines. *Neuron* **14**, 1285–1291.

KENAGY, R.D., MIN, S.-K., MULVIHILL, E., AND CLOWES, A.W. (2011). A link between smooth muscle cell death and extracellular matrix degradation during vascular atrophy. *Journal of Vascular Surgery* **54**, 182–191.

KENT, W.J., SUGNET, C.W., FUREY, T.S., ROSKIN, K.M., PRINGLE, T.H., ZAHLER, A.M., AND HAUSSLER, A. D. (2002). The Human Genome Browser at UCSC. *Genome Research* **12**, 996–1006.

KIMELBERG, H.K. (2005). Astrocytic swelling in cerebral ischemia as a possible cause of injury and target for therapy. *Glia* **50**, 389–397.

KINARD, T.A., AND SATIN, L.S. (1995). An ATP-sensitive Cl^- channel current that is activated by cell swelling, cAMP, and glyburide in insulin-secreting cells. *Diabetes* **44**, 1461–1466.

KIRK, K., AND KIRK, J. (1993). Volume-regulatory taurine release from a human lung cancer cell line. Evidence for amino acid transport via a volume-activated chloride channel. *FEBS Letters* **336**, 153–158.

KIRK, K., AND STRANGE, K. (1998). Functional properties and physiological roles of organic solute channels. *Annual Review of Physiology* **60**, 719–739.

KITANO, T., HAZAMA, A., SUGIYAMA, H., AND OKADA, Y. (1992). Volume-sensitivity of ion channel currents in B-lineage cells. *Cell Structure & Function* **176**, 489.

KLAUSEN, T.K., HOUGAARD, C., HOFFMANN, E.K., AND PEDERSEN, S.F. (2006). Cholesterol modulates the volume-regulated anion current in Ehrlich-Lettre ascites cells via effects on Rho and F-actin. *American Journal of Physiology. Cell Physiology* **291**, C757-71.

KLAUSEN, T.K., BERGDAHL, A., HOUGAARD, C., CHRISTOPHERSEN, P., PEDERSEN, S.F., AND HOFFMANN, E.K. (2007). Cell cycle-dependent activity of the volume- and Ca^{2+}-activated anion currents in Ehrlich lettre ascites cells. *Journal of Cellular Physiology* **210**, 831–842.

KOBE, B., AND DEISENHOFER, J. (1993). Crystal structure of porcine ribonuclease inhibitor, a protein with leucine-rich repeats. *Nature* **366**, 751–756.

KOBE, B., AND DEISENHOFER, J. (1994). The leucine-rich repeat: a versatile binding motif. *Trends in Biochemical Sciences* **19**, 415–421.

KOBE, B., AND DEISENHOFER, J. (1995). A structural basis of the interactions between leucine-rich repeats and protein ligands. *Nature* **374**, 183–186.

KOBE, B., AND KAJAVA, A. V (2001). The leucine-rich repeat as a protein recognition motif. *Current Opinion in Structural Biology* **11**, 725–732.

KOYAMA, T., OIKE, M., AND ITO, Y. (2001). Involvement of Rho-kinase and tyrosine kinase in hypotonic stress-induced ATP release in bovine aortic endothelial cells. *The Journal of Physiology* **532**, 759–769.

KRAPIVINSKY, G.B., ACKERMAN, M.J., GORDON, E.A., KRAPIVINSKY, L.D., AND CLAPHAM, D.E. (1994). Molecular characterization of a swelling-induced chloride conductance regulatory protein, pI_{Cln}. *Cell* **76**, 439–448.

KRONENGOLD, J., TREXLER, E.B., BUKAUSKAS, F.F., BARGIELLO, T.A., AND VERSELIS, V.K. (2003). Single-channel SCAM identifies pore-lining residues in the first extracellular loop and first transmembrane domains of Cx46 hemichannels. *The Journal of General Physiology* **122**, 389–405.

KUBO, M., AND OKADA, Y. (1992). Volume-regulatory Cl^- channel currents in cultured human epithelial cells. *The Journal of Physiology* **456**, 351–371.

KUBOTA, K., KIM, J.Y., SAWADA, A., TOKIMASA, S., FUJISAKI, H., MATSUDA-HASHII, Y., OZONO, K., AND HARA, J. (2004). LRRC8 involved in B cell development belongs to a novel family of leucine-rich repeat proteins. *FEBS Letters* **564**, 147–152.

KUMAR, L., CHOU, J., YEE, C.S.K., BORZUTZKY, A., VOLLMANN, E.H., VON ANDRIAN, U.H., PARK, S.-Y., HOLLANDER, G., MANIS, J.P., POLIANI, P.L., AND GEHA, R.S. (2014). Leucine-rich repeat containing 8A (LRRC8A) is essential for T lymphocyte development and function. *The Journal of Experimental Medicine* **211**, 929–942.

KUNZELMANN, K. (2015). TMEM16, LRRC8A, bestrophin: chloride channels controlled by Ca^{2+} and cell volume. *Trends in Biochemical Sciences* **40**, 535–543.

DE LA FUENTE, R., NAMKUNG, W., MILLS, A., AND VERKMAN, A.S. (2008). Small-molecule screen identifies inhibitors of a human intestinal calcium-activated chloride channel. *Molecular Pharmacology* **73**, 758–768.

LAMBERT, I.H., AND HOFFMANN, E.K. (1994). Cell swelling activates separate taurine and chloride channels in Ehrlich mouse ascites tumor cells. *The Journal of Membrane Biology* **142**, 289–298.

LANG, F., RITTER, M., GAMPER, N., HUBER, S., FILLON, S., TANNEUR, V., LEPPLE-WIENHUES, A., SZABO, I., AND GULBINS, E. (2000). Cell volume in the regulation of cell proliferation and apoptotic cell death. *Cellular Physiology and Biochemistry : International Journal of Experimental Cellular Physiology, Biochemistry, and Pharmacology* **10**, 417–428.

LANG, F., FÖLLER, M., LANG, K., LANG, P., RITTER, M., VERENINOV, A., SZABO, I., HUBER, S.M., AND GULBINS, E. (2007). Cell volume regulatory ion channels in cell proliferation and cell death. *Methods in Enzymology* **428**, 209–225.

LAURITZEN, L., HOFFMANN, E.K., HANSEN, H.S., AND JENSEN, B. (1993). Dietary n-3 and n-6 fatty acids are equipotent in stimulating volume regulation in Ehrlich ascites tumor cells. *The American Journal of Physiology* **264**, C109-17.

LEANEY, J.L., MARSH, S.J., AND BROWN, D.A. (1997). A swelling-activated chloride current in rat sympathetic neurones. *The Journal of Physiology* **501**, 555–564.

LEE, C.C., CARETTE, J.E., BRUMMELKAMP, T.R., AND PLOEGH, H.L. (2013). A reporter screen in a human haploid cell line identifies CYLD as a constitutive inhibitor of NF-κB. *PloS One* **8**, e70339.

LEE, C.C., FREINKMAN, E., SABATINI, D.M., AND PLOEGH, H.L. (2014). The protein synthesis inhibitor blasticidin s enters mammalian cells via leucine-rich repeat-containing protein 8D. *The Journal of Biological Chemistry* **289**, 17124–17131.

LEE, E.L., SHIMIZU, T., ISE, T., NUMATA, T., KOHNO, K., AND OKADA, Y. (2007). Impaired activity of volume-sensitive Cl^- channel is involved in cisplatin resistance of cancer cells. *Journal of Cellular Physiology* **211**, 513–521.

LEHEN'KYI, V., SHAPOVALOV, G., SKRYMA, R., AND PREVARSKAYA, N. (2011). Ion channnels and transporters in cancer. 5. Ion channels in control of cancer and cell apoptosis. *American Journal of Physiology. Cell Physiology* **301**, C1281-9.

LEPPLE-WIENHUES, A., SZABÒ, I., LAUN, T., KABA, N.K., GULBINS, E., AND LANG, F. (1998). The tyrosine kinase p56lck mediates activation of swelling-induced chloride channels in lymphocytes. *The Journal of Cell Biology* **141**, 281–286.

LEVITAN, I., AND GARBER, S.S. (1995). Voltage-dependent inactivation of volume-regulated Cl^- current in human T84 colonic and B-cell myeloma cell lines. *Pflügers Archiv : European Journal of Physiology* **431**, 297–299.

LEVITAN, I., CHRISTIAN, A.E., TULENKO, T.N., AND ROTHBLAT, G.H. (2000). Membrane cholesterol content modulates activation of volume-regulated anion current in bovine endothelial cells. *The Journal of General Physiology* **115**, 405–416.

LEWIS, R.S., ROSS, P.E., AND CAHALAN, M.D. (1993). Chloride channels activated by osmotic stress in T lymphocytes. *The Journal of General Physiology* **101**, 801–826.

LIOU, J., KIM, M.L., DO HEO, W., JONES, J.T., MYERS, J.W., FERRELL, J.E., AND MEYER, T. (2005). STIM is a Ca^{2+} sensor essential for Ca^{2+}-store-depletion-triggered Ca^{2+} influx. *Current Biology* **15**, 1235–1241.

LIU, H.-T., AKITA, T., SHIMIZU, T., SABIROV, R.Z., AND OKADA, Y. (2009). Bradykinin-induced astrocyte-neuron signalling: glutamate release is mediated by ROS-activated volume-sensitive outwardly rectifying anion channels. *The Journal of Physiology* **587**, 2197–2209.

LOHMAN, A.W., AND ISAKSON, B.E. (2014). Differentiating connexin hemichannels and pannexin channels in cellular ATP release. *FEBS Letters* **588**, 1379–1388.

LOHMAN, A.W., BILLAUD, M., AND ISAKSON, B.E. (2012). Mechanisms of ATP release and signalling in the blood vessel wall. *Cardiovascular Research* **95**, 269–280.

LOWRY, O.H., ROSEBROUGH, N.J., FARR, A.L., AND RANDALL, R.J. (1951). Protein measurement with the Folin phenol reagent. *The Journal of Biological Chemistry* **193**, 265–275.

LUNDBAEK, J.A., BIRN, P., HANSEN, A.J., SØGAARD, R., NIELSEN, C., GIRSHMAN, J., BRUNO, M.J., TAPE, S.E., EGEBJERG, J., GREATHOUSE, D. V, MATTICE, G.L., KOEPPE, R.E., AND ANDERSEN, O.S. (2004). Regulation of sodium channel function by bilayer elasticity: the importance of hydrophobic coupling. Effects of Micelle-forming amphiphiles and cholesterol. *The Journal of General Physiology* **123**, 599–621.

MA, Z., SIEBERT, A.P., CHEUNG, K.-H., LEE, R.J., JOHNSON, B., COHEN, A.S., VINGTDEUX, V., MARAMBAUD, P., AND FOSKETT, J.K. (2012). Calcium homeostasis modulator 1 (CALHM1) is the pore-forming subunit of an ion channel that mediates extracellular Ca^{2+} regulation of neuronal excitability. *Proceedings of the National Academy of Sciences of the United States of America* **109**, E1963-71.

MACVICAR, B.A., FEIGHAN, D., BROWN, A., AND RANSOM, B. (2002). Intrinsic optical signals in the rat optic nerve: role for K^+ uptake via NKCC1 and swelling of astrocytes. *Glia* **37**, 114–123.

MAEDA, S., NAKAGAWA, S., SUGA, M., YAMASHITA, E., OSHIMA, A., FUJIYOSHI, Y., AND TSUKIHARA, T. (2009). Structure of the connexin 26 gap junction channel at 3.5 A resolution. *Nature* **458**, 597–602.

MAENO, E., ISHIZAKI, Y., KANASEKI, T., HAZAMA, A., AND OKADA, Y. (2000). Normotonic cell shrinkage because of disordered volume regulation is an early prerequisite to apoptosis. *Proceedings of the National Academy of Sciences of the United States of America* **97**, 9487–9492.

MAERTENS, C., WEI, L., VOETS, T., DROOGMANS, G., AND NILIUS, B. (1999). Block by fluoxetine of volume-regulated anion channels. *British Journal of Pharmacology* **126**, 508–514.

MAKARA, J.K., RAPPERT, A., MATTHIAS, K., STEINHÄUSER, C., SPÄT, A., AND KETTENMANN, H. (2003). Astrocytes from mouse brain slices express ClC-2-mediated Cl^- currents regulated during development and after injury. *Molecular and Cellular Neurosciences* **23**, 521–530.

MALI, P., YANG, L., ESVELT, K.M., AACH, J., GUELL, M., DICARLO, J.E., NORVILLE, J.E., AND CHURCH, G.M. (2013). RNA-guided human genome engineering via Cas9. *Science (New York, N.Y.)* **339**, 823–826.

MANOLOPOULOS, V.G., VOETS, T., DECLERCQ, P.E., DROOGMANS, G., AND NILIUS, B. (1997a). Swelling-activated efflux of taurine and other organic osmolytes in endothelial cells. *The American Journal of Physiology* **273**, C214-22.

MANOLOPOULOS, V.G., DROOGMANS, G., AND NILIUS, B. (1997b). Hypotonicity and thrombin activate taurine efflux in BC3H1 and C2C12 myoblasts that is down regulated during differentiation. *Biochemical and Biophysical Research Communications* **232**, 74–79.

MANOLOPOULOS, V.G., LIEKENS, S., KOOLWIJK, P., VOETS, T., PETERS, E., DROOGMANS, G., LELKES, P.I., DE CLERCQ, E., AND NILIUS, B. (2000). Inhibition of angiogenesis by blockers of volume-regulated anion channels. *General Pharmacology* **34**, 107–116.

MAO, J., WANG, L., FAN, A., WANG, J., XU, B., JACOB, T.J.C., AND CHEN, L. (2007). Blockage of volume-activated chloride channels inhibits migration of nasopharyngeal carcinoma cells. *Cellular Physiology and Biochemistry : International Journal of Experimental Cellular Physiology, Biochemistry, and Pharmacology* **19**, 249–258.

MASTERS, J.R. (2002). HeLa cells 50 years on: the good, the bad and the ugly. *Nature Reviews. Cancer* **2**, 315–319.

MCDONALD, T. V, NGHIEM, P.T., GARDNER, P., AND MARTENS, C.L. (1992). Human lymphocytes transcribe the cystic fibrosis transmembrane conductance regulator gene and exhibit CF-defective cAMP-regulated chloride current. *The Journal of Biological Chemistry* **267**, 3242–3248.

MERCER, J.C., DEHAVEN, W.I., SMYTH, J.T., WEDEL, B., BOYLES, R.R., BIRD, G.S., AND PUTNEY, J.W. (2006). Large store-operated calcium selective currents due to co-expression of Orai1 or Orai2 with the intracellular calcium sensor, Stim1. *The Journal of Biological Chemistry* **281**, 24979–24990.

MEYER, K., AND KORBMACHER, C. (1996). Cell swelling activates ATP-dependent voltage-gated chloride channels in M-1 mouse cortical collecting duct cells. *The Journal of General Physiology* **108**, 177–193.

MICHEA, L., FERGUSON, D.R., PETERS, E.M., ANDREWS, P.M., KIRBY, M.R., AND BURG, M.B. (2000). Cell cycle delay and apoptosis are induced by high salt and urea in renal medullary cells. *American Journal of Physiology. Renal Physiology* **278**, F209-18.

MILENKOVIC, A., BRANDL, C., MILENKOVIC, V.M., JENDRYKE, T., SIRIANANT, L., WANITCHAKOOL, P., ZIMMERMANN, S., REIFF, C.M., HORLING, F., SCHREWE, H., SCHREIBER, R., KUNZELMANN, K., WETZEL, C.H., AND WEBER, B.H.F. (2015). Bestrophin 1 is indispensable for volume regulation in human retinal pigment epithelium cells. *Proceedings of the National Academy of Sciences of the United States of America* **112**, E2630-9.

MIN, X.-J., LI, H., HOU, S.-C., HE, W., LIU, J., HU, B., AND WANG, J. (2011). Dysfunction of volume-sensitive chloride channels contributes to cisplatin resistance in human lung adenocarcinoma cells. *Experimental Biology and Medicine (Maywood, N.J.)* **236**, 483–491.

MINIERI, L., PIVONKOVA, H., CAPRINI, M., HARANTOVA, L., ANDEROVA, M., AND FERRONI, S. (2013). The inhibitor of volume-regulated anion channels DCPIB activates TREK potassium channels in cultured astrocytes. *British Journal of Pharmacology* **168**, 1240–1254.

MINTENIG, G.M., VALVERDE, M.A., SEPULVEDA, F. V, GILL, D.R., HYDE, S.C., KIRK, J., AND HIGGINS, C.F. (1993). Specific inhibitors distinguish the chloride channel and drug transporter functions associated with the human multidrug resistance P-glycoprotein. *Receptors & Channels* **1**, 305–313.

MITCHELL, C.H., ZHANG, J.J., WANG, L., AND JACOB, T.J. (1997). Volume-sensitive chloride current in pigmented ciliary epithelial cells: role of phospholipases. *The American Journal of Physiology* **272**, C212-22.

MIWA, A., UEDA, K., AND OKADA, Y. (1997). Protein kinase C-independent correlation between P-glycoprotein expression and volume sensitivity of Cl^- channel. *The Journal of Membrane Biology* **157**, 63–69.

MONGIN, A.A. (2007). Disruption of ionic and cell volume homeostasis in cerebral ischemia: The perfect storm. *Pathophysiology : The Official Journal of the International Society for Pathophysiology / ISP* **14**, 183–193.

MONGIN, A.A., AND KIMELBERG, H.K. (2005). ATP regulates anion channel-mediated organic osmolyte release from cultured rat astrocytes via multiple Ca^{2+}-sensitive mechanisms. *American Journal of Physiology. Cell Physiology* **288**, C204-13.

MORIN, X.K., BOND, T.D., LOO, T.W., CLARKE, D.M., AND BEAR, C.E. (1995). Failure of P-glycoprotein (MDR1) expressed in Xenopus oocytes to produce swelling-activated chloride channel activity. *The Journal of Physiology* **486**, 707–714.

MORISHIMA, S., SHIMIZU, T., KIDA, H., AND OKADA, Y. (2000). Volume expansion sensitivity of swelling-activated Cl^- channel in human epithelial cells. *The Japanese Journal of Physiology* **50**, 277–280.

MOSER, T., CHOW, R.H., AND NEHER, E. (1995). Swelling-induced catecholamine secretion recorded from single chromaffin cells. *Pflügers Archiv : European Journal of Physiology* **431**, 196–203.

NAKAO, M., ONO, K., FUJISAWA, S., AND IIJIMA, T. (1999). Mechanical stress-induced Ca^{2+} entry and Cl^- current in cultured human aortic endothelial cells. *The American Journal of Physiology* **276**, C238-49.

NAMKUNG, W., PHUAN, P.-W., AND VERKMAN, A.S. (2011). TMEM16A inhibitors reveal TMEM16A as a minor component of calcium-activated chloride channel conductance in airway and intestinal epithelial cells. *The Journal of Biological Chemistry* **286**, 2365–2374.

NICHOL, J.A., AND HUTTER, O.F. (1996). Tensile strength and dilatational elasticity of giant sarcolemmal vesicles shed from rabbit muscle. *The Journal of Physiology* **493**, 187–198.

NIETSCH, H.H., ROE, M.W., FIEKERS, J.F., MOORE, A.L., AND LIDOFSKY, S.D. (2000). Activation of potassium and chloride channels by tumor necrosis factor alpha. Role in liver cell death. *The Journal of Biological Chemistry* **275**, 20556–20561.

NILIUS, B. (2004). Is the Volume-Regulated Anion Channel VRAC a “Water-Permeable” Channel? *Neurochemical Research* **29**, 3–8.

NILIUS, B., AND DROOGMANS, G. (2001). Ion channels and their functional role in vascular endothelium. *Physiological Reviews* **81**, 1415–1459.

NILIUS, B., AND DROOGMANS, G. (2003). Amazing chloride channels: an overview. *Acta Physiologica Scandinavica* **177**, 119–147.

NILIUS, B., OIKE, M., ZAHRADNIK, I., AND DROOGMANS, G. (1994a). Activation of a Cl^- current by hypotonic volume increase in human endothelial cells. *The Journal of General Physiology* **103**, 787–805.

NILIUS, B., SEHRER, J., AND DROOGMANS, G. (1994b). Permeation properties and modulation of volume-activated Cl^--currents in human endothelial cells. *British Journal of Pharmacology* **112**, 1049–1056.

NILIUS, B., SEHRER, J., VIANA, F., DE GREEF, C., RAEYMAEKERS, L., EGGERMONT, J., AND DROOGMANS, G. (1994c). Volume-activated Cl^- currents in different mammalian non-excitable cell types. *Pflügers Archiv : European Journal of Physiology* **428**, 364–371.

NILIUS, B., GERKE, V., PRENEN, J., SZÜCS, G., HEINKE, S., WEBER, K., AND DROOGMANS, G. (1996). Annexin II modulates volume-activated chloride currents in vascular endothelial cells. *The Journal of Biological Chemistry* **271**, 30631–30636.

NILIUS, B., EGGERMONT, J., VOETS, T., BUYSE, G., MANOLOPOULOS, V., AND DROOGMANS, G. (1997). Properties of volume-regulated anion channels in mammalian cells. *Progress in Biophysics and Molecular Biology* **68**, 69–119.

NILIUS, B., PRENEN, J., AND DROOGMANS, G. (1998). Modulation of volume-regulated anion channels by extra- and intracellular pH. *Pflügers Archiv : European Journal of Physiology* **436**, 742–748.

NILIUS, B., VOETS, T., EGGERMONT, J., AND DROOGMANS, G. (1999a). VRAC: A multifunctional volume-regulated anion channel in vascular endothelium. In Chloride Channels, (Isis Medical Media Ltd, Oxford), pp. 47–64.

NILIUS, B., VOETS, T., PRENEN, J., BARTH, H., AKTORIES, K., KAIBUCHI, K., DROOGMANS, G., AND EGGERMONT, J. (1999b). Role of Rho and Rho kinase in the activation of volume-regulated anion channels in bovine endothelial cells. *The Journal of Physiology* **516**, 67–74.

NILIUS, B., PRENEN, J., WALSH, M.P., CARTON, I., BOLLEN, M., DROOGMANS, G., AND EGGERMONT, J. (2000). Myosin light chain phosphorylation-dependent modulation of volume-regulated anion channels in macrovascular endothelium. *FEBS Letters* **466**, 346–350.

NILIUS, B., PRENEN, J., WISSENBACH, U., BÖDDING, M., AND DROOGMANS, G. (2001). Differential activation of the volume-sensitive cation channel TRP12 (OTRPC4) and volume-regulated anion currents in HEK-293 cells. *Pflügers Archiv : European Journal of Physiology* **443**, 227–233.

NODA, M., SHIMIZU, S., TANABE, T., TAKAI, T., KAYANO, T., IKEDA, T., TAKAHASHI, H., NAKAYAMA, H., KANAOKA, Y., MINAMINO, N., KANGAWA, K., MATSUO, H., RAFTERY, M.A., HIROSE, T., INAYAMA, S., HAYASHIDA, H., MIYATA, T., AND NUMA, S. (1984). Primary structure of Electrophorus electricus sodium channel deduced from cDNA sequence. *Nature* **312**, 121–127.

NOGALES, E. (2015). The development of cryo-EM into a mainstream structural biology technique. *Nature Methods* **13**, 24–27.

OIKE, M., DROOGMANS, G., AND NILIUS, B. (1994). The volume-activated chloride current in human endothelial cells depends on intracellular ATP. *Pflügers Archiv : European Journal of Physiology* **427**, 184–186.

OIKI, S., KUBO, M., AND OKADA, Y. (1994). Mg^{2+} and ATP-dependence of volume-sensitive Cl^- channels in human epithelial cells. *The Japanese Journal of Physiology* **44**, S77-9.

OKADA, Y. (1997). Volume expansion-sensing outward-rectifier Cl^- channel: fresh start to the molecular identity and volume sensor. *The American Journal of Physiology* **273**, C755–C789.

OKADA, Y., AND MAENO, E. (2001). Apoptosis, cell volume regulation and volume-regulatory chloride channels. *Comparative Biochemistry and Physiology. Part A, Molecular & Integrative Physiology* **130**, 377–383.

OKADA, Y., PETERSEN, C.C.H., KUBO, M., MORISHIMA, S., AND TOMINAGA, M. (1994). Osmotic Swelling Activates Intermediate-Conductance Cl^- Channels in Human Intestinal Epithelial Cells. *The Japanese Journal of Physiology* **44**, 403–409.

OKADA, Y., MAENO, E., SHIMIZU, T., DEZAKI, K., WANG, J., AND MORISHIMA, S. (2001). Receptor-mediated control of regulatory volume decrease (RVD) and apoptotic volume decrease (AVD). *The Journal of Physiology* **532**, 3–16.

OKADA, Y., SHIMIZU, T., MAENO, E., TANABE, S., WANG, X., AND TAKAHASHI, N. (2006). Volume-sensitive chloride channels involved in apoptotic volume decrease and cell death. *The Journal of Membrane Biology* **209**, 21–29.

PAPAGEORGIOU, A.C., SHAPIRO, R., AND ACHARYA, K.R. (1997). Molecular recognition of human angiogenin by placental ribonuclease inhibitor - an X-ray crystallographic study at 2.0 A resolution. *The EMBO Journal* **16**, 5162–5177.

PAPPAS, C.A., AND RITCHIE, J.M. (1998). Effect of specific ion channel blockers on cultured Schwann cell proliferation. *Glia* **22**, 113–120.

PAULMICHL, M., LI, Y., WICKMAN, K., ACKERMAN, M., PERALTA, E., AND CLAPHAM, D. (1992). New mammalian chloride channel identified by expression cloning. *Nature* **356**, 238–241.

PAULMICHL, M., GSCHWENTNER, M., WÖLL, E., SCHMARDA, A., RITTER, M., KANIN, G., ELLEMUNTER, H., WAITZ, W., AND DEETJEN, P. (1993). Insight into the Structure-Function Relation of Chloride Channels. *Cellular Physiology and Biochemistry* **3**, 374–387.

PEDEMONTE, N., AND GALIETTA, L.J. V (2014). Structure and function of TMEM16 proteins (anoctamins). *Physiological Reviews* **94**, 419–459.

PEDERSEN, S.F., PRENEN, J., DROOGMANS, G., HOFFMANN, E.K., AND NILIUS, B. (1998). Separate swelling- and Ca^{2+}-activated anion currents in Ehrlich ascites tumor cells. *The Journal of Membrane Biology* **163**, 97–110.

PEDERSEN, S.F., HOFFMANN, E.K., AND MILLS, J.W. (2001). The cytoskeleton and cell volume regulation. *Comparative Biochemistry and Physiology. Part A, Molecular & Integrative Physiology* **130**, 385–399.

PEDERSEN, S.F., BEISNER, K.H., HOUGAARD, C., WILLUMSEN, B.M., LAMBERT, I.H., AND HOFFMANN, E.K. (2002). Rho family GTP binding proteins are involved in the regulatory volume decrease process in NIH3T3 mouse fibroblasts. *The Journal of Physiology* **541**, 779–796.

PEDERSEN, S.F., HOFFMANN, E.K., AND NOVAK, I. (2013). Cell volume regulation in epithelial physiology and cancer. *Frontiers in Physiology* **4**.

PEDERSEN, S.F., KLAUSEN, T.K., AND NILIUS, B. (2015). The identification of a volume-regulated anion channel: an amazing Odyssey. *Acta Physiologica (Oxford, England)* **213**, 868–881.

PEINELT, C., VIG, M., KOOMOA, D.L., BECK, A., NADLER, M.J.S., KOBLAN-HUBERSON, M., LIS, A., FLEIG, A., PENNER, R., AND KINET, J.-P. (2006). Amplification of CRAC current by STIM1 and CRACM1 (Orai1). *Nature Cell Biology* **8**, 771–773.

PENDERGRASS, W.R., ANGELLO, J.C., KIRSCHNER, M.D., AND NORWOOD, T.H. (1991). The relationship between the rate of entry into S phase, concentration of DNA polymerase alpha, and cell volume in human diploid fibroblast-like monokaryon cells. *Experimental Cell Research* **192**, 418–425.

PENUELA, S., GEHI, R., AND LAIRD, D.W. (2013). The biochemistry and function of pannexin channels. *Biochimica et Biophysica Acta* **1828**, 15–22.

PIEPOLI, A., PALMIERI, O., MAGLIETTA, R., PANZA, A., CATTANEO, E., LATIANO, A., LACZKO, E., GENTILE, A., CARELLA, M., MAZZOCCOLI, G., ANCONA, N., MARRA, G., AND ANDRIULLI, A. (2012). The expression of leucine-rich repeat gene family members in colorectal cancer. *Experimental Biology and Medicine (Maywood, N.J.)* **237**, 1123–1128.

PIFFERI, S., DIBATTISTA, M., AND MENINI, A. (2009). TMEM16B induces chloride currents activated by calcium in mammalian cells. *Pflügers Archiv : European Journal of Physiology* **458**, 1023–1038.

PLANELLS-CASES, R., LUTTER, D., GUYADER, C., GERHARDS, N.M., ULLRICH, F., ELGER, D.A., KUCUKOSMANOGLU, A., XU, G., VOSS, F.K., REINCKE, S.M., STAUBER, T., BLOMEN, V.A., VIS, D.J., WESSELS, L.F., BRUMMELKAMP, T.R., BORST, P., ROTTENBERG, S., AND JENTSCH, T.J. (2015). Subunit composition of VRAC channels determines substrate specificity and cellular resistance to Pt-based anti-cancer drugs. *The EMBO Journal* **34**, 2993–3008.

POOLMAN, B., SPITZER, J.J., AND WOOD, J.M. (2004). Bacterial osmosensing: roles of membrane structure and electrostatics in lipid–protein and protein–protein interactions. *Biochimica et Biophysica Acta (BBA) - Biomembranes* **1666**, 88–104.

PORCELLI, A.M., GHELLI, A., ZANNA, C., VALENTE, P., FERRONI, S., AND RUGOLO, M. (2003). Staurosporine induces apoptotic volume decrease (AVD) in ECV304 cells. *Annals of the New York Academy of Sciences* **1010**, 342–346.

PORCELLI, A.M., GHELLI, A., ZANNA, C., VALENTE, P., FERRONI, S., AND RUGOLO, M. (2004). Apoptosis induced by staurosporine in ECV304 cells requires cell shrinkage and upregulation of Cl^- conductance. *Cell Death and Differentiation* **11**, 655–662.

POULSEN, K.A., ANDERSEN, E.C., HANSEN, C.F., KLAUSEN, T.K., HOUGAARD, C., LAMBERT, I.H., AND HOFFMANN, E.K. (2010). Deregulation of apoptotic volume decrease and ionic movements in multidrug-resistant tumor cells: role of chloride channels. *American Journal of Physiology. Cell Physiology* **298**, C14-25.

PRAGER-KHOUTORSKY, M., KHOUTORSKY, A., AND BOURQUE, C.W. (2014). Unique interweaved microtubule scaffold mediates osmosensory transduction via physical interaction with TRPV1. *Neuron* **83**, 866–878.

PU, W.T., KRAPIVINSKY, G.B., KRAPIVINSKY, L., AND CLAPHAM, D.E. (1999). pI_{Cln} inhibits snRNP biogenesis by binding core spliceosomal proteins. *Molecular and Cellular Biology* **19**, 4113–4120.

QIU, F., WANG, J., AND DAHL, G. (2012). Alanine substitution scanning of pannexin1 reveals amino acid residues mediating ATP sensitivity. *Purinergic Signalling* **8**, 81–90.

QIU, Z., DUBIN, A.E.E., MATHUR, J., TU, B., REDDY, K., MIRAGLIA, L.J.J., REINHARDT, J., ORTH, A.P.P., AND PATAPOUTIAN, A. (2014). SWELL1, a plasma membrane protein, is an essential component of volume-regulated anion channel. *Cell* **157**, 447–458.

QU, Z., WEI, R.W., MANN, W., AND HARTZELL, H.C. (2003). Two bestrophins cloned from Xenopus laevis oocytes express Ca^{2+}-activated Cl^- currents. *The Journal of Biological Chemistry* **278**, 49563–49572.

RANSOM, C.B., O'NEAL, J.T., AND SONTHEIMER, H. (2001). Volume-activated chloride currents contribute to the resting conductance and invasive migration of human glioma cells. *The Journal of Neuroscience : The Official Journal of the Society for Neuroscience* **21**, 7674–7683.

RETTIG, J., HEINEMANN, S.H., WUNDER, F., LORRA, C., PARCEJ, D.N., DOLLY, J.O., AND PONGS, O. (1994). Inactivation properties of voltage-gated K^+ channels altered by presence of beta-subunit. *Nature* **369**, 289–294.

ROMANENKO, V.G., DAVIES, P.F., AND LEVITAN, I. (2002). Dual effect of fluid shear stress on volume-regulated anion current in bovine aortic endothelial cells. *American Journal of Physiology. Cell Physiology* **282**, C708-18.

ROMANENKO, V.G., ROTHBLAT, G.H., AND LEVITAN, I. (2004). Sensitivity of volume-regulated anion current to cholesterol structural analogues. *The Journal of General Physiology* **123**, 77–87.

ROOS, J., DIGREGORIO, P.J., YEROMIN, A. V., OHLSEN, K., LIOUDYNO, M., ZHANG, S., SAFRINA, O., KOZAK, J.A., WAGNER, S.L., CAHALAN, M.D., VELIÇELEBI, G., AND STAUDERMAN, K.A. (2005). STIM1, an essential and conserved component of store-operated Ca^{2+} channel function. *The Journal of Cell Biology* **169**, 435–445.

ROSÁRIO, L.M., BARBOSA, R.M., ANTUNES, C.M., BALDEIRAS, I.E., SILVA, A.M., TOMÉ, A.R., AND SANTOS, R.M. (2008). Regulation by glucose of oscillatory electrical activity and 5-HT/insulin release from single mouse pancreatic islets in absence of functional K_{ATP} channels. *Endocrine Journal* **55**, 639–650.

ROSELL, A., VILALTA, A., GARCÍA-BERROCOSO, T., FERNÁNDEZ-CADENAS, I., DOMINGUES-MONTANARI, S., CUADRADO, E., DELGADO, P., RIBÓ, M., MARTÍNEZ-SÁEZ, E., ORTEGA-AZNAR, A., AND MONTANER, J. (2011). Brain perihematoma genomic profile following spontaneous human intracerebral hemorrhage. *PloS One* **6**, e16750.

ROSS, P.E., GARBER, S.S., AND CAHALAN, M.D. (1994). Membrane chloride conductance and capacitance in Jurkat T lymphocytes during osmotic swelling. *Biophysical Journal* **66**, 169–178.

ROUZAIRE-DUBOIS, B., MILANDRI, J.B., BOSTEL, S., AND DUBOIS, J.M. (2000). Control of cell proliferation by cell volume alterations in rat C6 glioma cells. *Pflügers Archiv : European Journal of Physiology* **440**, 881–888.

ROUZAIRE-DUBOIS, B., O'REGAN, S., AND DUBOIS, J.-M. (2005). Cell size-dependent and independent proliferation of rodent neuroblastoma x glioma cells. *Journal of Cellular Physiology* **203**, 243–250.

ROY, G. (1995). Amino acid current through anion channels in cultured human glial cells. *The Journal of Membrane Biology* **147**, 35–44.

SABIROV, R.Z., PRENEN, J., TOMITA, T., DROOGMANS, G., AND NILIUS, B. (2000). Reduction of ionic strength activates single volume-regulated anion channels (VRAC) in endothelial cells. *Pflügers Archiv : European Journal of Physiology* **439**, 315–320.

SABIROV, R.Z., KURBANNAZAROVA, R.S., MELANOVA, N.R., AND OKADA, Y. (2013). Volume-sensitive anion channels mediate osmosensitive glutathione release from rat thymocytes. *PloS One* **8**, e55646.

SABIROV, R.Z., MERZLYAK, P.G., ISLAM, M.R., OKADA, T., AND OKADA, Y. (2016). The properties, functions, and pathophysiology of maxi-anion channels. *Pflügers Archiv : European Journal of Physiology* **468**, 405–420.

SADOSHIMA, J., QIU, Z., MORGAN, J.P., AND IZUMO, S. (1996). Tyrosine kinase activation is an immediate and essential step in hypotonic cell swelling-induced ERK activation and c-fos gene expression in cardiac myocytes. *The EMBO Journal* **15**, 5535–5546.

SAMBROOK, J., AND RUSSELL, D.W. (2001). Molecular cloning: a laboratory manual (CSHL Press).

SÁNCHEZ-OLEA, R., FULLER, C., BENOS, D., AND PASANTES-MORALES, H. (1995). Volume-associated osmolyte fluxes in cell lines with or without the anion exchanger. *The American Journal of Physiology* **269**, C1280-6.

SÁNCHEZ-OLEA, R., MORALES, M., GARCÍA, O., AND PASANTES-MORALES, H. (1996). Cl channel blockers inhibit the volume-activated efflux of Cl and taurine in cultured neurons. *The American Journal of Physiology* **270**, C1703-8.

SATO, K., NUMATA, T., SAITO, T., UETA, Y., AND OKADA, Y. (2011). V receptor-mediated autocrine role of somatodendritic release of AVP in rat vasopressin neurons under hypo-osmotic conditions. *Science Signaling* **4**, pl14.

SAUTER, D.R.P., NOVAK, I., PEDERSEN, S.F., LARSEN, E.H., AND HOFFMANN, E.K. (2015). ANO1 (TMEM16A) in pancreatic ductal adenocarcinoma (PDAC). *Pflügers Archiv : European Journal of Physiology* **467**, 1495–1508.

SAWADA, A., TAKIHARA, Y., KIM, J.Y., MATSUDA-HASHII, Y., TOKIMASA, S., FUJISAKI, H., KUBOTA, K., ENDO, H., ONODERA, T., OHTA, H., OZONO, K., AND HARA, J. (2003). A congenital mutation of the novel gene LRRC8 causes agammaglobulinemia in humans. *The Journal of Clinical Investigation* **112**, 1707–1713.

SCHLICHTER, L.C., MERTENS, T., AND LIU, B. (2011). Swelling activated Cl- channels in microglia: Biophysics, pharmacology and role in glutamate release. *Channels (Austin, Tex.)* **5**, 128–137.

SCHNEIDER, L., KLAUSEN, T.K., STOCK, C., MALLY, S., CHRISTENSEN, S.T., PEDERSEN, S.F., HOFFMANN, E.K., AND SCHWAB, A. (2008). H-ras transformation sensitizes volume-activated anion channels and increases migratory activity of NIH3T3 fibroblasts. *Pflügers Archiv : European Journal of Physiology* **455**, 1055–1062.

SCHROEDER, B.C., CHENG, T., JAN, Y.N., AND JAN, L.Y. (2008). Expression cloning of TMEM16A as a calcium-activated chloride channel subunit. *Cell* **134**, 1019–1029.

SCHUMACHER, P.A., SAKELLAROPOULOS, G., PHIPPS, D.J., AND SCHLICHTER, L.C. (1995). Small-conductance chloride channels in human peripheral T lymphocytes. *The Journal of Membrane Biology* **145**, 217–232.

SCHUMANN, M.A., GARDNER, P., AND RAFFIN, T.A. (1993). Recombinant human tumor necrosis factor alpha induces calcium oscillation and calcium-activated chloride current in human neutrophils. The role of calcium/calmodulin-dependent protein kinase. *The Journal of Biological Chemistry* **268**, 2134–2140.

SCHWAB, A., FABIAN, A., HANLEY, P.J., AND STOCK, C. (2012). Role of ion channels and transporters in cell migration. *Physiological Reviews* **92**, 1865–1913.

SEKI, Y., FEUSTEL, P.J., KELLER, R.W., TRANMER, B.I., AND KIMELBERG, H.K. (1999). Inhibition of ischemia-induced glutamate release in rat striatum by dihydrokinate and an anion channel blocker. *Stroke; a Journal of Cerebral Circulation* **30**, 433–440.

SHARIF NAEINI, R., WITTY, M.-F., SÉGUÉLA, P., AND BOURQUE, C.W. (2006). An N-terminal variant of Trpv1 channel is required for osmosensory transduction. *Nature Neuroscience* **9**, 93–98.

SHEN, M.R., DROOGMANS, G., EGGERMONT, J., VOETS, T., ELLORY, J.C., AND NILIUS, B. (2000). Differential expression of volume-regulated anion channels during cell cycle progression of human cervical cancer cells. *The Journal of Physiology* **529 Pt 2**, 385–394.

SHENNAN, D.B. (2008). Swelling-induced taurine transport: relationship with chloride channels, anion-exchangers and other swelling-activated transport pathways. *Cellular Physiology and Biochemistry : International Journal of Experimental Cellular Physiology, Biochemistry, and Pharmacology* **21**, 15–28.

SHENNAN, D.B., MCNEILLIE, S.A., AND CURRAN, D.E. (1994). The effect of a hyposmotic shock on amino acid efflux from lactating rat mammary tissue: stimulation of taurine and glycine efflux via a pathway distinct from anion exchange and volume-activated anion channels. *Experimental Physiology* **79**, 797–808.

SHEPPARD, D.N., AND WELSH, M.J. (1999). Structure and Function of the CFTR Chloride Channel. *Physiol Rev* **79**, S23-45.

SHIMIZU, T., NUMATA, T., AND OKADA, Y. (2004). A role of reactive oxygen species in apoptotic activation of volume-sensitive Cl^- channel. *Proceedings of the National Academy of Sciences of the United States of America* **101**, 6770–6773.

SHIMIZU, T., LEE, E.L., ISE, T., AND OKADA, Y. (2008). Volume-sensitive Cl^- channel as a regulator of acquired cisplatin resistance. *Anticancer Research* **28**, 75–83.

SHIMIZU, T., IEHARA, T., SATO, K., FUJII, T., SAKAI, H., AND OKADA, Y. (2013). TMEM16F is a component of a Ca^{2+}-activated Cl^- channel but not a volume-sensitive outwardly rectifying Cl^- channel. *American Journal of Physiology. Cell Physiology* **304**, C748-59.

SIEBERT, A.P., MA, Z., GREVET, J.D., DEMURO, A., PARKER, I., AND FOSKETT, J.K. (2013). Structural and functional similarities of calcium homeostasis modulator 1 (CALHM1) ion channel with connexins, pannexins, and innexins. *The Journal of Biological Chemistry* **288**, 6140–6153.

SMITHERMAN, K.A., AND SONTHEIMER, H. (2001). Inhibition of glial Na^+ and K^+ currents by tamoxifen. *The Journal of Membrane Biology* **181**, 125–135.

SMITS, G., AND KAJAVA, A. V (2004). LRRC8 extracellular domain is composed of 17 leucine-rich repeats. *Molecular Immunology* **41**, 561–562.

SOLC, C.K., AND WINE, J.J. (1991). Swelling-induced and depolarization-induced C1-channels in normal and cystic fibrosis epithelial cells. *The American Journal of Physiology* **261**, C658-74.

SOROCEANU, L., MANNING, T.J., AND SONTHEIMER, H. (1999). Modulation of glioma cell migration and invasion using Cl^- and K^+ ion channel blockers. *The Journal of Neuroscience : The Official Journal of the Society for Neuroscience* **19**, 5942–5954.

SOROTA, S. (1995). Tyrosine protein kinase inhibitors prevent activation of cardiac swelling-induced chloride current. *Pflügers Archiv : European Journal of Physiology* **431**, 178–185.

STEINMEYER, K., SCHWAPPACH, B., BENS, M., VANDEWALLE, A., AND JENTSCH, T.J. (1995). Cloning and functional expression of rat CLC-5, a chloride channel related to kidney disease. *The Journal of Biological Chemistry* **270**, 31172–31177.

STOBRAWA, S.M., BREIDERHOFF, T., TAKAMORI, S., ENGEL, D., SCHWEIZER, M., ZDEBIK, A.A., BÖSL, M.R., RUETHER, K., JAHN, H., DRAGUHN, A., JAHN, R., AND JENTSCH, T.J. (2001). Disruption of ClC-3, a chloride channel expressed on synaptic vesicles, leads to a loss of the hippocampus. *Neuron* **29**, 185–196.

STODDARD, J.S., STEINBACH, J.H., AND SIMCHOWITZ, L. (1993). Whole cell Cl^- currents in human neutrophils induced by cell swelling. *The American Journal of Physiology* **265**, C156-65.

STOTZ, S.C., AND CLAPHAM, D.E. (2012). Anion-sensitive fluorophore identifies the Drosophila swell-activated chloride channel in a genome-wide RNA interference screen. *PloS One* **7**, e46865.

STRANGE, K., AND JACKSON, P.S. (1995). Swelling-activated organic osmolyte efflux: a new role for anion channels. *Kidney International* **48**, 994–1003.

STRANGE, K., EMMA, F., AND JACKSON, P.S. (1996). Cellular and molecular physiology of volume-sensitive anion channels. *The American Journal of Physiology* **270**, C711-30.

STUTZIN, A., TORRES, R., OPORTO, M., PACHECO, P., EGUIGUREN, A.L., CID, L.P., AND SEPÚLVEDA, F. V (1999). Separate taurine and chloride efflux pathways activated during regulatory volume decrease. *The American Journal of Physiology* **277**, C392-402.

SUH, S.H., VENNEKENS, R., MANOLOPOULOS, V.G., FREICHEL, M., SCHWEIG, U., PRENEN, J., FLOCKERZI, V., DROOGMANS, G., AND NILIUS, B. (1999). Characterisation of explanted endothelial cells from mouse aorta: electrophysiology and Ca^{2+} signalling. *Pflügers Archiv : European Journal of Physiology* **438**, 612–620.

SUN, H., TSUNENARI, T., YAU, K.-W., AND NATHANS, J. (2002). The vitelliform macular dystrophy protein defines a new family of chloride channels. *Proceedings of the National Academy of Sciences of the United States of America* **99**, 4008–4013.

SUZUKI, J., UMEDA, M., SIMS, P.J., AND NAGATA, S. (2010). Calcium-dependent phospholipid scrambling by TMEM16F. *Nature* **468**, 834–838.

SYEDA, R., QIU, Z., DUBIN, A.E., MURTHY, S.E., FLORENDO, M.N., MASON, D.E., MATHUR, J., CAHALAN, S.M., PETERS, E.C., MONTAL, M., AND PATAPOUTIAN, A. (2016). LRRC8 Proteins Form Volume-Regulated Anion Channels that Sense Ionic Strength. *Cell* **164**, 499–511.

SZOLLOSI, A., NENQUIN, M., AGUILAR-BRYAN, L., BRYAN, J., AND HENQUIN, J.-C. (2007). Glucose stimulates Ca^{2+} influx and insulin secretion in 2-week-old beta-cells lacking ATP-sensitive K^+ channels. *The Journal of Biological Chemistry* **282**, 1747–1756.

SZÜCS, G., BUYSE, G., EGGERMONT, J., DROOGMANS, G., AND NILIUS, B. (1996a). Characterization of volume-activated chloride currents in endothelial cells from bovine pulmonary artery. *The Journal of Membrane Biology* **149**, 189–197.

SZÜCS, G., HEINKE, S., DROOGMANS, G., AND NILIUS, B. (1996b). Activation of the volume-sensitive chloride current in vascular endothelial cells requires a permissive intracellular Ca^{2+} concentration. *Pflügers Archiv : European Journal of Physiology* **431**, 467–469.

SZÜCS, G., HEINKE, S., DE GREEF, C., RAEYMAEKERS, L., EGGERMONT, J., DROOGMANS, G., AND NILIUS, B. (1996c). The volume-activated chloride current in endothelial cells from bovine pulmonary artery is not modulated by phosphorylation. *Pflügers Archiv : European Journal of Physiology* **431**, 540–548.

TAKANO, T., KANG, J., JAISWAL, J.K., SIMON, S.M., LIN, J.H.-C., YU, Y., LI, Y., YANG, J., DIENEL, G., ZIELKE, H.R., AND NEDERGAARD, M. (2005). Receptor-mediated glutamate release from volume sensitive channels in astrocytes. *Proceedings of the National Academy of Sciences of the United States of America* **102**, 16466–16471.

TERNOVSKY, V.I., OKADA, Y., AND SABIROV, R.Z. (2004). Sizing the pore of the volume-sensitive anion channel by differential polymer partitioning. *FEBS Letters* **576**, 433–436.

THIEMANN, A., GRÜNDER, S., PUSCH, M., AND JENTSCH, T.J. (1992). A chloride channel widely expressed in epithelial and non-epithelial cells. *Nature* **356**, 57–60.

TILLY, B.C., VAN DEN BERGHE, N., TERTOOLEN, L.G., EDIXHOVEN, M.J., AND DE JONGE, H.R. (1993). Protein tyrosine phosphorylation is involved in osmoregulation of ionic conductances. *The Journal of Biological Chemistry* **268**, 19919–19922.

TOMINAGA, K., KONDO, C., KAGATA, T., HISHIDA, T., NISHIZUKA, M., AND IMAGAWA, M. (2004). The novel gene fad158, having a transmembrane domain and leucine-rich repeat, stimulates adipocyte differentiation. *The Journal of Biological Chemistry* **279**, 34840–34848.

TOMINAGA, M., TOMINAGA, T., MIWA, A., AND OKADA, Y. (1995). Volume-sensitive chloride channel activity does not depend on endogenous P-glycoprotein. *The Journal of Biological Chemistry* **270**, 27887–27893.

TREXLER, E.B., BUKAUSKAS, F.F., KRONENGOLD, J., BARGIELLO, T.A., AND VERSELIS, V.K. (2000). The first extracellular loop domain is a major determinant of charge selectivity in connexin46 channels. *Biophysical Journal* **79**, 3036–3051.

TROUET, D., NILIUS, B., JACOBS, A., REMACLE, C., DROOGMANS, G., AND EGGERMONT, J. (1999). Caveolin-1 modulates the activity of the volume-regulated chloride channel. *The Journal of Physiology* **520**, 113–119.

TROUET, D., HERMANS, D., DROOGMANS, G., NILIUS, B., AND EGGERMONT, J. (2001a). Inhibition of volume-regulated anion channels by dominant-negative caveolin-1. *Biochemical and Biophysical Research Communications* **284**, 461–465.

TROUET, D., CARTON, I., HERMANS, D., DROOGMANS, G., NILIUS, B., AND EGGERMONT, J. (2001b). Inhibition of VRAC by c-Src tyrosine kinase targeted to caveolae is mediated by the Src homology domains. *American Journal of Physiology. Cell Physiology* **281**, C248-56.

TSUMURA, T., OIKI, S., UEDA, S., OKUMA, M., AND OKADA, Y. (1996). Sensitivity of volume-sensitive Cl^- conductance in human epithelial cells to extracellular nucleotides. *The American Journal of Physiology* **271**, C1872-8.

TSUNENARI, T., SUN, H., WILLIAMS, J., CAHILL, H., SMALLWOOD, P., YAU, K.-W., AND NATHANS, J. (2003). Structure-function analysis of the bestrophin family of anion channels. *The Journal of Biological Chemistry* **278**, 41114–41125.

TZOUNOPOULOS, T., MAYLIE, J., AND ADELMAN, J.P. (1995). Induction of endogenous channels by high levels of heterologous membrane proteins in Xenopus oocytes. *Biophysical Journal* **69**, 904–908.

ULBRICH, M.H., AND ISACOFF, E.Y. (2007). Subunit counting in membrane-bound proteins. *Nature Methods* **4**, 319.

ULLRICH, F., REINCKE, S.M., VOSS, F.K., STAUBER, T., AND JENTSCH, T.J. (2016). Inactivation and Anion Selectivity of Volume-regulated Anion Channels (VRACs) Depend on C-terminal Residues of the First Extracellular Loop. *The Journal of Biological Chemistry* **291**, 17040–17048.

UNIPROT CONSORTIUM, T.U. (2015). UniProt: a hub for protein information. *Nucleic Acids Research* **43**, D204-12.

VALVERDE, M.A., DÍAZ, M., SEPÚLVEDA, F. V, GILL, D.R., HYDE, S.C., AND HIGGINS, C.F. (1992). Volume-regulated chloride channels associated with the human multidrug-resistance P-glycoprotein. *Nature* **355**, 830–833.

VALVERDE, M.A., MINTENIG, G.M., AND SEPÚLVEDA, F. V (1993). Differential effects of tamoxifen and I^- on three distinguishable chloride currents activated in T84 intestinal cells. *Pflügers Archiv : European Journal of Physiology* **425**, 552–554.

VANDENBERG, J.I., YOSHIDA, A., KIRK, K., AND POWELL, T. (1994). Swelling-activated and isoprenaline-activated chloride currents in guinea pig cardiac myocytes have distinct electrophysiology and pharmacology. *The Journal of General Physiology* **104**, 997–1017.

VARELA, D., SIMON, F., RIVEROS, A., JØRGENSEN, F., AND STUTZIN, A. (2004). NAD(P)H oxidase-derived H_2O_2 signals chloride channel activation in cell volume regulation and cell proliferation. *The Journal of Biological Chemistry* **279**, 13301–13304.

VARELA, D., SIMON, F., OLIVERO, P., ARMISÉN, R., LEIVA-SALCEDO, E., JØRGENSEN, F., SALA, F., AND STUTZIN, A. (2007). Activation of H_2O_2-induced VSOR Cl^- currents in HTC cells require phospholipase Cgamma1 phosphorylation and Ca^{2+} mobilisation. *Cellular Physiology and Biochemistry : International Journal of Experimental Cellular Physiology, Biochemistry, and Pharmacology* **20**, 773–780.

VERDON, B., WINPENNY, J.P., WHITFIELD, K.J., ARGENT, B.E., AND GRAY, M.A. (1995). Volume-activated chloride currents in pancreatic duct cells. *The Journal of Membrane Biology* **147**, 173–183.

VERKHRATSKY, A., MATTEOLI, M., PARPURA, V., MOTHET, J.-P., ZOREC, R., ANDREWS, N., CHAKRABARTI, S., ARCIENEGA, I., BRUNET, J., BLOCH, J., BADAUT, J., ARIMA, H., YAMAMOTO, N., SOBUE, K., UMENISHI, F., TADA, T., KATSUYA, H., ASAI, K., BAIETTI, M., ET AL. (2016). Astrocytes as secretory cells of the central nervous system: idiosyncrasies of vesicular secretion. *The EMBO Journal* **35**, 239–257.

VERKMAN, A.S. (2011). Aquaporins at a glance. *Journal of Cell Science* **124**, 2107–2112.

VIG, M., PEINELT, C., BECK, A., KOOMOA, D.L., RABAH, D., KOBLAN-HUBERSON, M., KRAFT, S., TURNER, H., FLEIG, A., PENNER, R., AND KINET, J.-P. (2006). CRACM1 is a plasma membrane protein essential for store-operated Ca^{2+} entry. *Science (New York, N.Y.)* **312**, 1220–1223.

VOETS, T., SZÜCS, G., DROOGMANS, G., AND NILIUS, B. (1995). Blockers of volume-activated Cl^- currents inhibit endothelial cell proliferation. *Pflügers Archiv : European Journal of Physiology* **431**, 132–134.

VOETS, T., DROOGMANS, G., AND NILIUS, B. (1996a). Potent block of volume-activated chloride currents in endothelial cells by the uncharged form of quinine and quinidine. *British Journal of Pharmacology* **118**, 1869–1871.

VOETS, T., BUYSE, G., TYTGAT, J., DROOGMANS, G., EGGERMONT, J., AND NILIUS, B. (1996b). The chloride current induced by expression of the protein pICln in Xenopus oocytes differs from the endogenous volume-sensitive chloride current. *The Journal of Physiology* **495**, 441–447.

VOETS, T., DROOGMANS, G., AND NILIUS, B. (1997a). Modulation of voltage-dependent properties of a swelling-activated Cl^- current. *The Journal of General Physiology* **110**, 313–325.

VOETS, T., WEI, L., DE SMET, P., VAN DRIESSCHE, W., EGGERMONT, J., DROOGMANS, G., AND NILIUS, B. (1997b). Downregulation of volume-activated Cl^- currents during muscle differentiation. *The American Journal of Physiology* **272**, C667-74.

VOETS, T., MANOLOPOULOS, V., EGGERMONT, J., ELLORY, C., DROOGMANS, G., AND NILIUS, B. (1998). Regulation of a swelling-activated chloride current in bovine endothelium by protein tyrosine phosphorylation and G proteins. *The Journal of Physiology* **506**, 341–352.

VOETS, T., DROOGMANS, G., RASKIN, G., EGGERMONT, J., AND NILIUS, B. (1999). Reduced intracellular ionic strength as the initial trigger for activation of endothelial volume-regulated anion channels. *Proceedings of the National Academy of Sciences of the United States of America* **96**, 5298–5303.

VOETS, T., NILIUS, B., AND VENNEKENS, R. (2015). VRACs swallow platinum drugs. *The EMBO Journal* **34**, 2985–2987.

VOSS, F.K. (2015). Molecular identification of the volume-regulated anion channel VRAC by a genome-wide siRNA screen (Doctoral dissertation).

VOSS, F.K., ULLRICH, F., MÜNCH, J., LAZAROW, K., LUTTER, D., MAH, N., ANDRADE-NAVARRO, M.A., VON KRIES, J.P., STAUBER, T., AND JENTSCH, T.J. (2014). Identification of LRRC8 heteromers as an essential component of the volume-regulated anion channel VRAC. *Science (New York, N.Y.)* **344**, 634–638.

WANG, J., AND DAHL, G. (2010). SCAM analysis of Panx1 suggests a peculiar pore structure. *The Journal of General Physiology* **136**, 515–527.

WANG, G.-X., MCCRUDDEN, C., DAI, Y.-P., HOROWITZ, B., HUME, J.R., AND YAMBOLIEV, I.A. (2004). Hypotonic activation of volume-sensitive outwardly rectifying chloride channels in cultured PASMCs is modulated by SGK. *American Journal of Physiology. Heart and Circulatory Physiology* **287**, H533-44.

WANG, Y., ROMAN, R., LIDOFSKY, S.D., AND FITZ, J.G. (1996). Autocrine signaling through ATP release represents a novel mechanism for cell volume regulation. *Proceedings of the National Academy of Sciences of the United States of America* **93**, 12020–12025.

WEYLANDT, K.H., VALVERDE, M.A., NOBLES, M., RAGUZ, S., AMEY, J.S., DIAZ, M., NASTRUCCI, C., HIGGINS, C.F., AND SARDINI, A. (2001). Human ClC-3 is not the swelling-activated chloride channel involved in cell volume regulation. *The Journal of Biological Chemistry* **276**, 17461–17467.

WONDERGEM, R., GONG, W., MONEN, S.H., DOOLEY, S.N., GONCE, J.L., CONNER, T.D., HOUSER, M., ECAY, T.W., AND FERSLEW, K.E. (2001). Blocking swelling-activated chloride current inhibits mouse liver cell proliferation. *The Journal of Physiology* **532**, 661–672.

WORRELL, R.T., BUTT, A.G., CLIFF, W.H., AND FRIZZELL, R.A. (1989). A volume-sensitive chloride conductance in human colonic cell line T84. *The American Journal of Physiology* **256**, C1111-9.

WU, J., ZHANG, J.J., KOPPEL, H., AND JACOB, T.J. (1996). P-glycoprotein regulates a volume-activated chloride current in bovine non-pigmented ciliary epithelial cells. *The Journal of Physiology* **491**, 743–755.

YANG, H., KIM, A., DAVID, T., PALMER, D., JIN, T., TIEN, J., HUANG, F., CHENG, T., COUGHLIN, S.R., JAN, Y.N., AND JAN, L.Y. (2012). TMEM16F forms a Ca^{2+}-activated cation channel required for lipid scrambling in platelets during blood coagulation. *Cell* **151**, 111–122.

YE, Z.-C., OBERHEIM, N., KETTENMANN, H., AND RANSOM, B.R. (2009). Pharmacological “cross-inhibition” of connexin hemichannels and swelling activated anion channels. *Glia* **57**, 258–269.

YU, K., WHITLOCK, J.M., LEE, K., ORTLUND, E.A., CUI, Y.Y., AND HARTZELL, H.C. (2015). Identification of a lipid scrambling domain in ANO6/TMEM16F. *eLife* **4**, e06901.

ZHANG, J.J., AND JACOB, T.J. (1996). Volume regulation in the bovine lens and cataract. The involvement of chloride channels. *The Journal of Clinical Investigation* **97**, 971–978.

ZHANG, J.J., AND JACOB, T.J. (1997). Three different Cl^- channels in the bovine ciliary epithelium activated by hypotonic stress. *The Journal of Physiology* **499**, 379–389.

ZHANG, H., CAO, H.J., KIMELBERG, H.K., AND ZHOU, M. (2011). Volume regulated anion channel currents of rat hippocampal neurons and their contribution to oxygen-and-glucose deprivation induced neuronal death. *PloS One* **6**, e16803.

ZHANG, J., RASMUSSON, R.L., HALL, S.K., AND LIEBERMAN, M. (1993). A chloride current associated with swelling of cultured chick heart cells. *The Journal of Physiology* **472**, 801–820.

ZHANG, J.J., JACOB, T.J., VALVERDE, M.A., HARDY, S.P., MINTENIG, G.M., SEPÚLVEDA, F. V, GILL, D.R., HYDE, S.C., TREZISE, A.E., AND HIGGINS, C.F. (1994). Tamoxifen blocks chloride channels. A possible mechanism for cataract formation. *The Journal of Clinical Investigation* **94**, 1690–1697.

ZHANG, Y., ZHANG, H., FEUSTEL, P.J., AND KIMELBERG, H.K. (2008). DCPIB, a specific inhibitor of volume regulated anion channels (VRACs), reduces infarct size in MCAo and the release of glutamate in the ischemic cortical penumbra. *Experimental Neurology* **210**, 514–520.

ZIEGELHOEFFER, T., SCHOLZ, D., FRIEDRICH, C., HELISCH, A., WAGNER, S., FERNANDEZ, B., AND SCHAPER, W. (2003). Inhibition of collateral artery growth by mibefradil: possible role of volume-regulated chloride channels. *Endothelium : Journal of Endothelial Cell Research* **10**, 237–246.

ZOU, Y., AKAZAWA, H., QIN, Y., SANO, M., TAKANO, H., MINAMINO, T., MAKITA, N., IWANAGA, K., ZHU, W., KUDOH, S., TOKO, H., TAMURA, K., KIHARA, M., NAGAI, T., FUKAMIZU, A., UMEMURA, S., IIRI, T., FUJITA, T., AND KOMURO, I. (2004). Mechanical stress activates angiotensin II type 1 receptor without the involvement of angiotensin II. *Nature Cell Biology* **6**, 499–506.

7. PUBLICATIONS

LUTTER, D., ULLRICH, F., LUECK, J.C., KEMPA, S., AND JENTSCH, T.J. Selective transport of neurotransmitters and -modulators by distinct volume-regulated LRRC8 anion channels. *Manuscript under review.*

LEIPOLD, E., ULLRICH, F., THIELE, M., TIETZE, A.A., TERLAU, H., IMHOF, D., AND HEINEMANN, S.H. (2017). Subtype-specific block of voltage-gated K^+ channels by μ-conopeptides. *Biochem. Biophys. Res. Commun.*, *in press*.

ULLRICH, F., REINCKE, S.M., VOSS, F.K., STAUBER, T., AND JENTSCH, T.J. (2016). Inactivation and Anion Selectivity of Volume-regulated Anion Channels (VRACs) Depend on C-terminal Residues of the First Extracellular Loop. *J. Biol. Chem.* **291**, 17040–17048.

JENTSCH, T.J., LUTTER, D., PLANELLS-CASES, R., ULLRICH, F., AND VOSS, F.K. (2016). VRAC: molecular identification as LRRC8 heteromers with differential functions. *Pflügers Arch.* **468**, 385–393.

TIAN, Y., ULLRICH, F., XU, R., HEINEMANN, S.H., HOU, S., AND HOSHI, T. (2015). Two distinct effects of PIP_2 underlie auxiliary subunit-dependent modulation of Slo1 BK channels. *J. Gen. Physiol.* **145**, 331–343.

PLANELLS-CASES, R., LUTTER, D., GUYADER, C., GERHARDS, N.M., ULLRICH, F., ELGER, D.A., KUCUKOSMANOGLU, A., XU, G., VOSS, F.K., REINCKE, S.M., STAUBER, T., BLOMEN, V.A., VIS, D.J., WESSELS, L.F., BRUMMELKAMP, T.R., BORST, P., ROTTENBERG, S., AND JENTSCH, T.J. (2015). Subunit composition of VRAC channels determines substrate specificity and cellular resistance to Pt-based anti-cancer drugs. *EMBO J.* **34**, 2993–3008.

VOSS, F.K., ULLRICH, F., MÜNCH, J., LAZAROW, K., LUTTER, D., MAH, N., ANDRADE-NAVARRO, M.A., VON KRIES, J.P., STAUBER, T., AND JENTSCH, T.J. (2014). Identification of LRRC8 heteromers as an essential component of the volume-regulated anion channel VRAC. *Science* **344**, 634–638.

LUDWIG, C.F., ULLRICH, F., LEISLE, L., STAUBER, T., AND JENTSCH, T.J. (2013). Common Gating of Both CLC Transporter Subunits Underlies Voltage-dependent Activation of the $2Cl^-/1H^+$ Exchanger ClC-7/Ostm1. *J. Biol. Chem.* **288**, 28611–28619.

TIETZE, A.A., TIETZE, D., OHLENSCHLÄGER, O., LEIPOLD, E., ULLRICH, F., KÜHL, T., MISCHO, A., BUNTKOWSKY, G., GÖRLACH, M., HEINEMANN, S.H., AND IMHOF, D. (2012). Structurally diverse μ-conotoxin PIIIA isomers block sodium channel $Na_V1.4$. *Angew. Chemie - Int. Ed.* **51**, 4058–4061.

8. ACKNOWLEDGMENTS

I would like to express my gratitude to Thomas Jentsch for granting me the privilege of working in his excellently equipped laboratory and for always having an open door when I needed advice. His unconditional support and constant interest in my work have been of great help.

I also thank all my current and former colleagues from the Jentsch laboratory for technical help, stimulating discussions, and the great working environment. Special thanks go to the original 'VRAC team' for making this possible and for sharing a truly unforgettable publication experience: Felizia Voss, Tobias Stauber, and Jonas Münch. I am also specially obliged to Momsen Reincke for his essential contributions to the gating project, and to Rosa Planells and Darius Lutter for allowing me to contribute to their fruitful projects.

Finally, I would like to thank my family in Jena and in Berlin for all the support.